Dissertation

submitted to the

Combined Faculty of Natural Sciences and Mathematics

of the Ruperto Carola University Heidelberg, Germany

for the degree of

Doctor of Natural Sciences

Presented by

M. Sc. Anja Bufe

born in: Spaichingen, Germany

Oral examination: 29.06.2022

The roles of Wnt signaling during mitosis

Referees:

Dr. Sergio Pérez Acebrón

Prof. Dr. Thomas Holstein

Zusammenfassung

Der Wnt-Signalweg ist sowohl für die embryonale Muster- und Gewebebildung in der Entwicklung als auch die Aufrechterhaltung von Geweben im adulten Organismus essenziell. Durch die Expression von β-catenin-Zielgenen steuert der kanonische Wnt-Signalweg das Zellzyklus-Fortschreiten in der G1/S-Phase, sowie die Selbsterneuerung und Differenzierung von Stammzellen. Der Wnt-Signalweg hat, abgesehen von seinen transkriptionalen, auch posttranslationale Funktionen während der Mitose. Die Misregulation des Signalwegs führt zu schweren mitotischen Defekten, wie beispielsweise der fehlerhaften Anordnung oder ungleichmäßigen Verteilung von Chromosomen, was Aneuploidien hervorrufen kann.

Das Ziel dieser Arbeit war es, neue Zielproteine des Wnt-Signalwegs, welche den Ablauf der Mitose gewährleisten, sowie deren molekulare Mechanismen, zu identifizieren, um die Entstehung mitotischer Defekte aufgrund von Anomalien im Signalweg erklären zu können.

Zum einen konnte ich hierbei zeigen, dass das mitotische Kinesin KIF2A von der Wnt-Komponente DVL rekrutiert wird. DVL transportiert KIF2A an die mitotischen Spindelpole, wo dieses die Dynamiken von Mikrotubuli an deren Minusenden reguliert um die korrekte Anordnung der Chromosomen vor Beginn der Anaphase, in somatischen sowie pluripotenten Stammzellen, sicherzustellen. Dieser Prozess wird durch die Phosphorylierung von KIF2A an Serin 100 und der Interaktion mit PLK1 unterstützt, was beides durch die Aktivierung des Wnt-Signalwegs und die Bildung von LRP6-Signalosomen begünstigt wird.

Zum anderen konnte ich einen über die S-Phase vermittelten Mechanismus des Wnt-Signalwegs, welcher die Segregation von Chromosomen während der Anaphase in pluripotenten Stammzellen sicherstellt, verifizieren. Hierbei stützen meine Daten die Hypothese, dass der Wnt-Signalweg zur fehlerfreien DNA-Replikation in der S-Phase beiträgt, was wiederum die Länge von Mikrotubuli an deren Plusenden reguliert und die gleichmäßige Verteilung von Chromosomen während der Mitose ermöglicht.

Die Validierung beider Mechanismen in pluripotenten Stammzellen hebt deren Relevanz für das Verständnis von Defekten in der Entwicklung, der Degeneration von Geweben sowie der Entstehung von Krebs, welche häufig durch chromosomale Instabilität charakterisiert ist, hervor. Zudem wurde KIF2A ebenfalls in der Interphase von DVL rekrutiert, was darauf hinweist, dass die Wnt-vermittelte Regulierung von KIF2A auch eine Rolle in Prozessen jenseits der Mitose spielen könnte, beispielsweise in der Ziliogenese oder Neurogenese.

Insgesamt konnte ich in meiner Arbeit zwei neue Wnt-abhängige Mechanismen identifizieren, welche direkt in der Mitose oder indirekt über die S-Phase die Dynamiken von Mikrotubuli, an deren Minus- beziehungsweise Plusenden, regulieren um den korrekten Ablauf der Mitose, die Erhaltung von Euploidie und potenziell weitere postmitotische Prozesse zu gewährleisten.

Abstract

Wnt signaling is crucial for embryonic patterning, the formation of tissues during development, and tissue maintenance in the adult organism. The canonical Wnt pathway induces the transcription of β-catenin target genes, thereby controlling cell cycle progression during G1/S phase, stem cell self-renewal, and stem cell differentiation. However, besides its transcriptional roles, it emerged that Wnt signaling also takes post-translational functions during mitosis. Accordingly, a misregulation of the pathway causes severe mitotic defects, such as chromosome misalignments and chromosome segregation errors, which can ultimately lead to aneuploidy.

In this work, I aimed to identify targets of Wnt signaling, which safeguard the correct progression through mitosis, and characterize the underlying molecular mechanisms to explain the emergence of mitotic defects upon Wnt disturbance.

First, I revealed that the mitotic kinesin KIF2A is recruited by the Wnt component DVL. DVL localizes KIF2A to the mitotic spindle poles, where it regulates microtubule minus-end dynamics to ensure chromosome alignment before anaphase, both in somatic cells and pluripotent stem cells. This process is supported by the phosphorylation of KIF2A at serine 100 and the interaction with PLK1, which is positively regulated by active Wnt signaling and LRP6 signalosome formation.

Second, I verified an S phase-dependent mechanism of Wnt signaling, ensuring the equal segregation of chromosomes in pluripotent stem cells during anaphase. At this, I hypothesize that Wnt signaling contributes to the error-free replication of DNA in S phase, which mediates microtubule plus-end assembly in mitosis, and thereby facilitates faithful chromosome segregation.

The validation of both mechanisms in pluripotent stem cells emphasizes their relevance for the understanding of developmental defects, tissue degeneration, and cancer progression, which is often characterized by chromosomal instability. Besides, KIF2A was recruited by DVL also in interphase, indicating that the Wnt-mediated regulation of KIF2A may contribute to processes beyond mitosis, namely ciliogenesis and neurogenesis.

Taken together, in my work, I revealed two novel Wnt-dependent mechanisms, which function directly in mitosis or through S phase to control microtubule minus- or plus-end dynamics respectively, ensuring the faithful progression through mitosis, preservation of euploidy, and possibly further post-mitotic processes.

Table of contents

List of schemes and figures

List of tables

List of common abbreviations

Abbreviation	Meaning
APC	Adenomatous polyposis coli
APS	Ammonium persulphate
ATCC	American Type Culture Collection
BIO	6-bromoindirubin-3'-oxime (GSK3 inhibitor)
CCND	Cyclin D
CCNE	Cyclin E
CCNY	Cyclin Y
CDC	Cell division cycle
CDK	Cyclin-dependent kinase
CK1α/ε/γ	Casein kinase 1 alpha/epsilon/gamma
CM	Conditioned medium
CTCF	Corrected total cell fluorescence
DAPI	4′,6-diamidino-2-phenylindole
DKK1	Dickkopf-related protein 1 (LRP inhibitor)
DME	Dimethylenastron
DMEM	Dulbecco's Modified Eagle's Medium
DPBS	Dulbecco's phosphate-buffered saline
DTT	Dithiothreitol
DVL	Dishevelled
e.g.	For example
EDTA	Ethylenediaminetetraacetic acid
EGFP	Enhanced green fluorescent protein
ESC	Embryonic stem cell
FBS	Fetal bovine serum
FZD	Frizzled
GSK3β	Glycogen synthase kinase 3 beta
h	Hours
HCl	Hydrochloric acid
HEK293T	Human Embryonic Kidney 293T
HeLa	Henrietta Lacks
HEPES	4-(2-hydroxyethyl)-1-piperazineethanesulfonic acid

hiPSC	Human induced pluripotent stem cell
IF	Immunofluorescence
IP	Immunoprecipitation
LRP	Low-density lipoprotein receptor-related protein
min	Minutes
MS	Mass spectrometry
MT	Microtubule
MYC	C-Myc
NaCl	Sodium chloride
NP40	Nonidet-P40
ns	Not significant
nTERT	Human telomerase reverse transcriptase
PCR	Polymerase chain reaction
PLA	Proximity ligation assay
RPE1	Retinal pigment epithelial 1
rpm	Revolutions per minute
RT	Room temperature
SD	Standard deviation
SDS	Sodium dodecyl sulfate
SILAC	Stable isotope labelling by amino acids in cell culture
siRNA	Small interfering RNA
TBS	Tris-buffered saline
TBST	Tris-buffered saline with Tween-20
TCF/LEF	T-cell factor/lymphoid enhancer factor
UHPLC	Ultra high performance liquid chromatography
WNT	Wnt family member
β-TrCP	Beta-transducin repeat containing E3 ubiquitin protein ligase

1. Introduction

1.1 Wnt signaling

1.1.1 Wnt proteins and their underlying signaling cascades

Wnt proteins constitute a family of growth factors, also called morphogens, guiding a variety of processes both during development and adulthood, which include the proliferation of cells, determination of cell polarity and fate, as well as the formation and maintenance of tissues[1-3]. The origins of Wnt signaling arose with early metazoans and the pathway is highly conserved in the animal kingdom, being present in multiple phyla including sponges, cnidaria, arthropoda and chordata[4-7]. To date, 12 WNT gene families have been described. The number of WNT genes is highly species-dependent, varying from only 5 WNT genes in nematodes to 19 WNTs in mammals[8]. Once a Wnt protein binds to its receptor on a receiving cell, it can induce various signaling cascades, which are traditionally classified into canonical (β-catenin-dependent) and non-canonical (β-catenin-independent) Wnt signaling, which will be described in more detail below. In previous studies, certain WNTs have been associated with one pathway or the other. In particular, WNT1, WNT3A and WNT8 were categorized as canonical/β-catenin-inducing WNTs, whereas WNT5A and WNT11 were linked to non-canonical/β-catenin-independent Wnt signaling[9-11]. Though, in contrast to the previous assumption that the different Wnt pathways are largely separated from each other, some Wnt ligands and pathway components, including WNT5A, frizzled (FZD) and dishevelled (DVL), are shared and act in both canonical and non-canonical Wnt signaling, often antagonizing the opposite pathway[10-14]. Besides, more than 15 different WNT receptors and co-receptors have been identified, which are bound by multiple WNTs and induce distinct downstream cascades[15,16]. For instance, WNT5A can activate non-canonical Wnt signaling by binding to the receptors FZD2 and tyrosine kinase-like orphan receptor 2 (ROR2), whereas its binding to FZD4 promotes β-catenin-dependent signaling[10,17,18]. Therefore, not only the presence of Wnt ligands, but also the receptor context is determining for the evoked effects[15].

1.1.1.1 Canonical Wnt signaling

The canonical Wnt pathway, which is also termed Wnt/β-catenin pathway, regulates cell proliferation and differentiation during development[2,19].

In the absence of a canonical Wnt ligand, the so-called “destruction complex”, consisting of axis inhibition protein (AXIN), glycogen synthase kinase 3 beta (GSK3β), adenomatous polyposis coli (APC) and casein kinase 1 alpha (CK1α), is formed[20-22]. The two kinases of the destruction complex, CK1α and GSK3β, phosphorylate β-catenin successively, leading to its

recognition and ubiquitination by beta-transducin repeat containing E3 ubiquitin protein ligase (β-TrCP), which mediates its proteasomal degradation and prevents the transcription of β-catenin-dependent target genes[22,23].

In contrast, upon active canonical Wnt signaling, the degradation of β-catenin is prevented. The binding of a canonical Wnt ligand to the cysteine-rich domain (CRD) of a canonical FZD receptor[24] and the extra-cellular domain (ECD) of the co-receptor low-density lipoprotein receptor-related protein 5 or 6 (LRP5/6)[25] triggers the recruitment of DVL[6,26] and polymerization of LRP. The Pro-Pro-Pro-Ser/Thr-Pro (PPPS/TP) motif in the cytoplasmic tail of LRP is phosphorylated by GSK3β on a serine or threonine, which primes LRP to be phosphorylated by the kinase casein kinase 1 gamma (CK1γ) at the neighboring serine (PPPSPxS/T)[27,28]. Cyclin-dependent kinase 14 (CDK14/PFTAIRE) in association with cyclin Y (CCNY) supports these phosphorylations by additionally phosphorylating LRP6 and priming it to respond to a Wnt ligand[29]. The phosphorylation of LRP leads to the recruitment of AXIN by LRP and DVL and thereby inhibition of the destruction complex, preventing GSK3β-mediated phosphorylation and degradation of target proteins[20-22]. At this, the destruction complex is inhibited on the one hand by the direct binding of LRP[30] and on the other hand by the induction of signalosome formation and caveolin-mediated endocytosis in multivesicular bodies[31-35]. As a consequence, β-catenin accumulates in the cytoplasm and translocates to the nucleus, where it binds to transcription factors of the T-cell factor/lymphoid enhancer factor (TCF/LEF) family[36,37]. Binding of β-catenin removes the transcription inhibitor groucho, which is normally bound to TCF, and thereby induces the expression of Wnt target genes, such as *AXIN2*, *MYC* and *CCND1*[38-41] (Scheme 1).

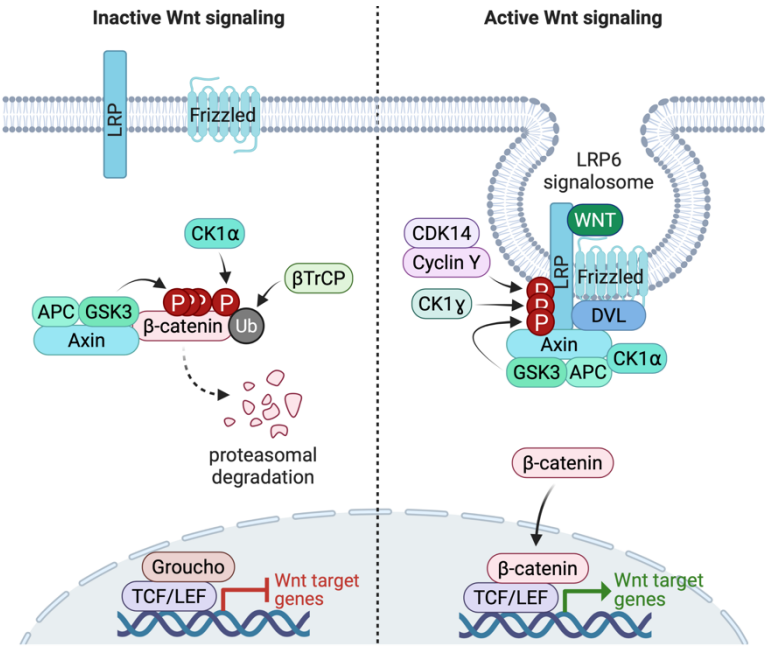

Scheme 1. Canonical Wnt signaling pathway. When Wnt signaling is inactive (left side) β-catenin is bound by the cytoplasmic destruction complex, consisting of adenomatous polyposis coli (APC), axis inhibition protein (AXIN), glycogen synthase kinase 3 beta (GSK3β) and casein kinase 1 alpha (CK1α), and targeted for proteasomal degradation via GSK3β and CK1α phosphorylations followed by ubiquitination by beta-transducin repeat containing E3 ubiquitin protein ligase (βTrCP). At the same time, the transcription of target genes is inhibited by groucho, which interacts with T-cell factor/lymphoid enhancer factor (TCF/LEF) transcription factors. The binding of a canonical Wnt ligand to its receptor frizzled and co-receptor low-density lipoprotein receptor-related proteins 5 or 6 (LRP5/6) (right) induces the phosphorylation of LRP5/6 on multiple sites, which promotes the recruitment of dishevelled (DVL) and the destruction complex to the plasma membrane. A multiprotein complex, termed LRP6 signalosome, is formed and internalized by endocytosis, inactivating the destruction complex. As a result, β-catenin accumulates in the cytoplasm, translocates to the nucleus, removes the inhibitor groucho and induces the TCF/LEF-mediated transcription of Wnt target genes. P = phosphorylation, Ub = ubiquitination, CDK14 = cyclin-dependent kinase 14, CK1γ = casein kinase 1 gamma.

The activity of the canonical Wnt pathway is adjusted by a variety of secreted proteins, which can bind to Wnt ligands or receptors to support either their activation or inhibition and were reviewed in detail by Cruciat and Niehrs (2013)[42]. Within the frame of this work, I would like to mention only the Wnt inhibitor dickkopf-related protein 1 (DKK1), which was used in this study. DKK1 antagonizes canonical Wnt signaling on the one hand by binding directly to the Wnt co-receptors LRP5/6, preventing the interaction of Wnt ligands with LRP[43,44]. On the other hand, DKKs bind to the transmembrane receptor kringle-containing transmembrane protein 1 or 2

(KREMEN1/2), which induces the clathrin-mediated endocytosis of LRP, thereby removing the receptors and preventing Wnt activation[45,46].

1.1.1.1.1 WNT/STOP signaling

The transcription factor β-catenin has been postulated as the main target of GSK3β and thereby main readout of the canonical Wnt pathway for a long time[23]. However, the kinase GSK3β phosphorylates and induces the degradation of many more proteins apart from β-catenin[32,47-50]. Consistently, activation of Wnt signaling stabilizes these GSK3 targets, a process which is termed Wnt-dependent stabilization of proteins (WNT/STOP)[49]. The GSK3-regulated proteins contribute to a variety of cellular processes, including transcriptional regulation, cell signaling and cytoskeletal organization, thereby mediating microtubule assembly, cell sizing, cell cycle progression, sperm maturation, neurogenesis and ribosome biogenesis[32,47-55]. Furthermore, Wnt/STOP signaling was shown to peak during mitosis, leading to the downregulation of GSK3-mediated protein degradation and stabilization of distinct mitotic proteins before cell division[29,49,50,56]. The increase in WNT/STOP activities is supported by two modes of actions, namely I) the phosphorylation of the PPPSP motif of LRP6 by the G2/M cyclin CCNY and CDK14, which primes LRP6 to be phosphorylated by CK1γ and thereby increases its competence to respond to a Wnt ligand[29], and II) the stabilization of LRP6-signalosomes by B-cell CLL/lymphoma 9 (BCL9), which inhibits clathrin-mediated-endocytosis and is positively regulated by cyclin-dependent kinase 1 (CDK1)[56].

1.1.1.2 Non-canonical Wnt signaling

Apart from activating canonical Wnt signaling, which results in the accumulation of β-catenin[1], Wnt ligands can also activate Wnt branches independent of β-catenin, referred to as non-canonical Wnt pathways. The best characterized non-canonical Wnt branches are the planar cell polarity (Wnt/PCP) and the Wnt/calcium (Wnt/Ca^{2+}) pathway, which regulate cell polarity, orientation, migration and extrusions as well as convergent extension (reviewed in [3] and [57]).

B-catenin-independent Wnt pathways are induced by the binding of a non-canonical Wnt ligand to a FZD receptor and/or a co-receptor of the receptor tyrosine kinase family, such as tyrosine kinase-like orphan receptor 2 (ROR2) or receptor tyrosine kinase (RYK)[15]. The activation of the receptors triggers, similarly as in canonical Wnt signaling, the recruitment of DVL[58,59], but instead of stabilizing β-catenin, the pathways induce downstream cascades that activate e.g. cell division cycle 42 (CDC42), the c-Jun N-terminal kinase (JNK) pathway, rho-associated coiled-coil kinase (ROCK) signaling or calcium (Ca^{2+}) release, which induces actin cytoskeleton reorganization or the transcription of non-canonical Wnt target genes[18,58-62].

1.1.2 Regulation and interconnection of Wnt signaling pathways

As described above, canonical and non-canonical Wnt pathways share distinct components, namely FZD receptors and DVL proteins, and hence may compete for these proteins and restrict each other[10,13,26,58,59,63]. Supporting this idea, it has been shown that all known DVL proteins are capable of inducing the phosphorylation and activation of the canonical co-receptor LRP6 and non-canonical receptor ROR1 in response to WNT3A and WNT5A respectively[14]. Besides, the two pathways antagonize each other directly. For instance, the non-canonical Wnt ligand WNT5A and the downstream effectors PKC and CAMKII have been shown to negatively regulate canonical Wnt signaling[11,12,64]. In particular, WNT5A can, in addition to its binding to ROR1/2 and FZD2, associate with LRP5 and FZD2 to inhibit the binding of a canonical Wnt ligand (e.g. WNT1 or WNT3A) to its receptors[11,13,64].

However, apart from the reciprocal regulation of the pathways, the signaling cascades also regulate themselves by positive and negative feedback loops. By way of example, the canonical Wnt target brachyury was shown to activate the expression of *wnt3a* and *wnt8a* in zebrafish, thereby inducing as a positive feedback[65]. As opposed to this, many β-catenin target genes comprise negative regulators of Wnt signaling, such as *AXIN2* or *DKK1*, and hence represent negative feedback loops[40,66,67].

1.1.3 Roles and functions of Wnt signaling

1.1.3.1 Wnt signaling in stem cell regulation during development and tissue homeostasis

During embryonic development as well as in adulthood canonical and non-canonical Wnt signaling fulfill essential functions in driving the proliferation, specification, polarity, and migration of cells to guide the establishment and maintenance of tissues[3,16,19].

In this process, non-canonical Wnt/PCP signaling regulates the polarization and morphogenesis of cells, thereby establishing asymmetries, which facilitate directed cell divisions, cell migration, cell intercalation and cell extensions[68-70]. In line with this, Wnt/PCP signaling is a driver of convergent extension, a process enabling gastrulation, neurulation and the formation of other organs[71-73].

In contrast, the canonical Wnt pathway plays a key role in the establishment of the anterior-posterior axis during embryogenesis and cell fate specification during the building and maintenance of tissues[19,44,74,75]. Active Wnt signaling promotes the self-renewal of pluripotent embryonic stem cells through β-catenin by supporting the expression of the pluripotency factors OCT3/4, REX1, SOX2 and NANOG[76-78]. Correspondingly, the interference with Wnt signaling decreases the self-renewing capacity of pluripotent stem cells, leads to the shift from

a naïve to primed state and supports differentiation[78-81]. Likewise, it has been proposed for adult stem cells that GSK3β and β-catenin/TCF-induced transcription represent a master switch, deciding on stem cell proliferation and self-renewal versus differentiation[82]. Supporting this notion, localized Wnt signals evoke directed, asymmetric cell divisions in embryonic and adult stem cells[83,84]. In detail, upon presentation of a Wnt stimulus, Wnt components distribute asymmetrically within the cell and orient their axis towards the Wnt source, generating a pluripotent daughter cell close to the Wnt source and a distal differentiated daughter cell during cell division[83,84]. This mechanism is important for the generation and homeostasis of tissues. Correspondingly, Wnt signaling represents a key signaling pathway in various stem cell niches and enables the constant renewal of highly regenerative tissues, such as the skin, liver or intestine[19]. By way of example, the colon harbors a highly proliferative leucine-rich repeat-containing G-protein coupled receptor 5 (LGR5)-positive stem cell compartment in its crypts, which is maintained by active Wnt signaling[82,85-89]. The crypt stem cells can differentiate into various cell types that migrate along the villi, where they reside as non-proliferative cells, which correlates with a Wnt gradient peaking at the crypts and decreasing towards the lumen and villi[82,85,87,88]. Hence, impaired Wnt signaling interferes with the tissue architecture and causes the disruption of the intestinal crypt-villi structure[87,92]. Under normal conditions, the activity of Wnt signaling is further enhanced in the presence of R-spondins (RSPOs)[90,91]. RSPOs bind to the LGR5 receptors on the stem cells and thereby support FZD-LRP5/6 complex formation and Wnt signaling[85,86,90,91].

Owing to their dependency on Wnt signaling, *ex vivo* intestinal organoids emerged as a powerful tool to study Wnt signaling in the context of adult stem cell self-renewal, tissue homeostasis, regeneration, and cancer[85,89]. In contrast, the characteristics of pluripotent stem cells were traditionally examined in embryonic stem cells (ESCs), which need to be extracted from embryos and are therefore subject to ethical concerns and limited availability[93]. Providing an alternative model, in 2006 K. Takahashi and S. Yamanaka established so-called “induced pluripotent stem cells (iPSCs)”, which were generated from adult fibroblasts by introducing the four pluripotency factors OCT3/4, SOX2, MYC, and KLF4, and yield the potential to be differentiated into cells of all three germ layers[94]. The reprogramming of somatic cells into iPSCs and their pluripotent nature is also supported by active canonical Wnt signaling[95].

However, contrasting the promotion of self-renewal and pluripotency in most cells[76-82,95], conflicting functions of the canonical Wnt pathway have been observed in the development of distinct tissues. For instance, during cardiogenesis, Wnt signaling promotes cardiac differentiation in an early developmental stage of ESCs, while it inhibits differentiation and heart formation in later stages[96-98]. Similarly, Wnt signaling regulates the self-renewal of

neuronal progenitor cells (NPCs), but was noticed to also induce NPC differentiation, during neurogenesis[99-101]. The factors leading to the various outputs of Wnt signaling are still under exploration, however it was hypothesized that the effects may depend on the developmental stage, presence of Wnt ligands, Wnt receptors and possibly other external signals, which induce differential signaling cascades[51,98,99,102].

In correlation with its pro-proliferative functions, Wnt signaling also takes important roles in cell cycle progression, namely the G1-to-S transition and mitosis[103], which will be discussed in detail after introducing the process of cell cycle progression and mitosis itself (section 1.3). Correspondingly, the misregulation of Wnt signaling can lead to excessive cell proliferation and has been associated with cancer and other diseases[1]. Particularly, the irregular expression of *MYC* (e.g. upon loss or mutation of *APC*, *AXIN2*, *GSK3B* or *CTNNB1*) has been shown to promote cell proliferation and tumorigenesis[1,39,82]. Conversely, mutations in the Wnt co-receptor LRP were associated with degenerative genetic diseases, such as osteoporosis or coronary artery disease[104,105].

1.1.3.2 Wnt signaling in ciliogenesis

In addition to the regulation of development and tissue maintenance, Wnt signaling also guides cilia formation[106-108]. Cilia are microtubule-based structures, that grow from the surface of almost all vertebrate cells, are involved in the sensing and transmission of signals, and can be motile or non-motile[109]. Non-motile or primary cilia appear usually once per cell and are assembled from basal bodies during G0/G1 phase, while they are disassembled at G2 phase prior to the entry into mitosis[110]. Defects in ciliogenesis or cilia functions are associated with ciliopathies and cancer in a variety of organs (reviewed in [109,111]). Both β-catenin-dependent and -independent Wnt pathways are involved in the regulation of primary ciliogenesis. The activation of canonical Wnt signaling (e.g. by WNT3A) was reported to induce primary cilia assembly by phosphorylating and accumulating β-catenin at the centrosomes via a novel branch of Wnt signaling[106]. In contrast, activation of non-canonical Wnt signaling (e.g. by WNT5A) supports cilia disassembly via the phosphorylation and binding of DVL to polo-like kinase 1 (PLK1), which induces human enhancer of filamentation 1 (HEF1 or NEDD9) and Aurora A activation[107]. Consistently, the Wnt/PCP component VANGL2 was reported to interact with phospho-DVL2, PLK1, kinesin family member 2A (KIF2A), γ-tubulin and bardet-biedl syndrome 8 (BBS8) to regulate ciliogenesis in response to fluid shear stress (FSS)[108]. In particular, upon low FSS primary cilia assembly is promoted as VANGL2 recruits BBS8, which decreases the interaction of DVL2, PLK1 and KIF2A, resulting in the reduced phosphorylation

and activity of KIF2A, a kinesin that promotes cilia disassembly. In contrast, PLK1 and KIF2A are induced via DVL upon high FSS, leading to primary cilia disassembly[108,112].
Consequently, primary cilia are assembled and disassembled in a cell cycle- and Wnt-dependent manner[106,107,110]. Additionally, primary cilia-related proteins, such as BBS proteins, kinesin family member 3A (KIF3A) and intraflagellar transport 88 (IFT88), inhibit canonical Wnt signaling[113,114]. In agreement with this, the elimination of primary cilia or suppression of related genes increases canonical Wnt signaling[113-115].

1.1.3.3 Wnt signaling in neurogenesis

In line with ciliogenesis, cell polarization and cell fate determination, Wnt signaling also plays important roles in the development of the nervous system, mediating axon remodeling, cell polarity, neurite outgrowth as well as the proliferation and differentiation of neuronal progenitors[51,99-101,116-121]. At this, axonal and growth cone remodeling, which precedes synapse formation, as well as axon outgrowth are regulated by Wnt signaling via the inhibition of GSK3β[116,117,122]. The downregulation of GSK3β reduces the phosphorylation of MT-associated proteins, such as microtubule-associated protein 1B (MAP1B), microtubule-associated protein 2C (MAP2C), microtubule-associated protein tau (MAPT), kinesin light chains and APC, which leads to the stabilization of axonal microtubules (MTs)[117,118,122-125]. At this, GSK3β is inhibited on the one hand via DVL and AXIN[117] and likely by active non-canonical Wnt signaling, which induces the activation of CDC42 and the partitioning defective 3/6 (PAR3/6)/atypical protein kinase C (aPKC) complex[62,119,126]. On the other hand, nerve growth factor (NGF) has been shown to activate phosphatidylinositol-4,5-bisphosphate 3-kinase (PI3K), which downregulates GSK3β in axons[118]. Notably, the inhibitory actions also reduce the GSK3β-mediated phosphorylation of APC and thereby support its localization at the plus-ends of neuronal MTs, where APC promotes MT stability, cell polarity and neurite growth[118,119,126].
Complementing these actions, canonical Wnt signaling drives cortical development by balancing the self-renewal versus the differentiation of neuronal progenitor cells during neurogenesis[51,98-101,120,121].
In line with its functions in neuronal development, defects in Wnt signaling have been associated with cortical malformations and neurodegenerative diseases, including Alzheimer's and Parkinson's disease[99,127-130]. Neurodegeneration is likely caused by the hyperphosphorylation of tau (MAPT) by GSK3β upon Wnt inhibition, which is supported by high levels of beta-amyloid peptide and leads to apoptosis[128,130], however the exact causes of the neuronal defects observed upon disrupted Wnt signaling are still under investigation.

1.2 The eukaryotic cell cycle

1.2.1 Progression and regulation of the cell cycle

The eukaryotic cell cycle consists of alternating phases of interphase, comprising a G1 (gap 1), S (synthesis) and G2 (gap 2) phase, followed by mitosis (M phase) (Scheme 2, left). The progression of the cell cycle is tightly regulated by diverse proteins, including especially cyclins and their cyclin-dependent kinases (CDKs), which associate to drive or pause the cell cycle at specific stages[131,132]. Their activities are counteracted by CDK inhibitors (CKIs), which can be categorized into INK4 proteins and CIP/KIP proteins[133]. The latter family includes $p21^{CIP1/WAF1}$ (also known as cyclin-dependent kinase inhibitor 1A (CDKN1A)) and $p27^{KIP1}$ (also known as cyclin-dependent kinase inhibitor 1B (CDKN1B)), which can bind to CDK4/6 or CDK2 and thereby arrest the cell cycle in the G1 phase[133].

Cell cycle entry is induced by the interaction of cyclin D with CDK4/6, which leads to the phosphorylation and inhibition of the retinoblastoma (RB) complex and thereby release of the transcription factor E2F, activating cyclin E and its association with CDK2[134]. The cyclin E-CDK2 complex enhances the inhibitory RB phosphorylation and promotes cyclin A-CDK2 association and the progression from G1 to S phase, which induces DNA replication and centrosome duplication[134,135]. Additionally, the cyclinA-CDK2 complex activates the phosphatase cell division cycle 25 (CDC25), which eliminates two inhibitory phosphorylations of CDK1 at threonine 14 (T14) and tyrosine 15 (Y15), which are maintained by the wee1-like protein kinase (WEE1) and myelin transcription factor 1 (MYT1) to keep CDK1 inactive during interphase[136-140]. CDK1 complexes with cyclin A and cyclin B successively and its activation marks the entry into mitosis[132,141]. During mitosis the duplicated DNA is distributed to two newly forming daughter cells that divide during a process called cytokinesis before starting another round of the cell cycle[131,132] (Scheme 2).

To prevent the premature transitioning from one phase to another upon errors, the cell cycle is controlled by distinct checkpoints, which allows to halt the cell cycle for repair[142]. Briefly, the “DNA damage checkpoint” monitors proper DNA replication in S phase and is triggered upon replication stress or DNA damage, preventing the onset of mitosis by checkpoint kinase 1/2 (CHK1/2), which inhibits CDC25 activity and consequently CDK1 activation[143]. During mitosis, the so-called “spindle assembly checkpoint (SAC)” prevents the transition from metaphase to anaphase until all chromosomes are aligned at the spindle equator to ensure error-free chromosome segregation in anaphase. At this, the mitotic checkpoint complex (MCC), consisting of mitotic arrest deficient 2 (MAD2), BUB1 mitotic checkpoint serine/threonine kinase B (BUBR1 or BUB1B) and BUB3 mitotic checkpoint protein (BUB3), binds cell division cycle 20 (CDC20), thereby preventing the activation of the ubiquitin ligase complex anaphase-

promoting complex/cyclosome (APC/C), which induces anaphase (reviewed in [144] and described below). The dysregulation of checkpoint proteins involved in these surveillance mechanisms can cause uncontrolled proliferation, errors in DNA replication and chromosomal instability, which are hallmarks of cancer[142,144,145].

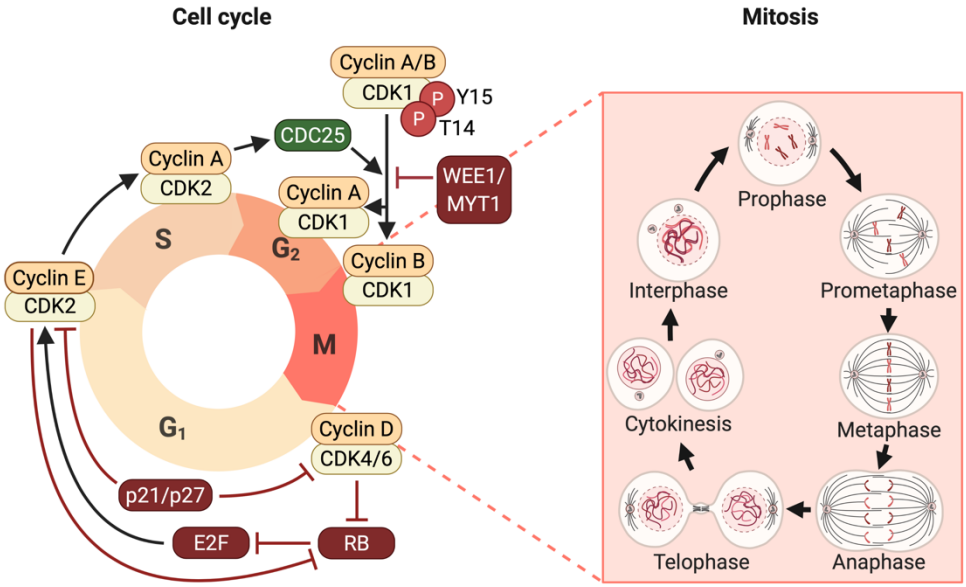

Scheme 2. Progression of the cell cycle (left) and mitosis (right). The different stages of the cell cycle are regulated by distinct cyclin-dependent kinases (CDKs) and their cyclins. Cell cycle initiation (G1 phase) is conferred by the assembly of CDK4 or CDK6 with cyclin D, which inhibits retinoblastoma (RB) and releases the transcription factor E2F. E2F facilitates CDK2-cyclin E complex formation and entry into S phase. The G1-to-S phase transition may be inhibited by the CDK inhibitors p21 or p27, which bind to both CDK4/6 and CDK2. During S phase, cyclin A associates with CDK2 and consecutively activates cell division cycle 25 (CDC25) in G2 phase. CDC25 removes the wee1-like protein kinase/myelin transcription factor 1 (WEE1/MYT1)-induced inhibitory phosphorylations at threonine 14 (T14) and tyrosine 15 (Y15) from CDK1, thereby activating the kinase. CDK1 complexes with cyclin A and cyclin B successively, which induces mitotic entry (M phase/mitosis is displayed on the right side of the scheme). During mitosis, DNA gets condensed into chromosomes (prophase). Microtubules emanate from the poles and navigate the chromosomes to the spindle equator (prometaphase), where they are aligned in one central metaphase plate (metaphase) and subsequently distributed to the opposing poles of the cell (anaphase). The DNA is enclosed into two new nuclei and decondenses, a cleavage furrow is built between the two prospective daughter cells (telophase) and the cells are separated (cytokinesis). Afterwards, the cells enter another round of the cell cycle, comprising G1, S, G2 phase, where they duplicate their DNA and centrosomes (interphase), followed by mitosis (M).

1.2.2 Progression and regulation of mitosis

Mitosis is an essential process in the development and regeneration of tissues. Accordingly, mitotic aberrations often result in malignancies, notably cancer[145]. The progression through mitosis is controlled by a complex network of proteins, whose correct and timely localization and activation is guided by post-translational modifications (PTMs), especially phosphorylations[146]. In particular, the kinases CDK1, CDK2, polo-like kinase 1 (PLK1), Aurora A (AURKA) and Aurora B (AURKB) emerged as drivers of mitosis, phosphorylating a variety of mitotic targets[147,148]. In fact, about 20% of proteins show an increase in phosphorylation site occupancy during mitosis, including 88% of the predicted substrates of CDK1/2, 72% of PLK1 substrates and 58% of AURKA/B substrates[148]. During exit from mitosis these phosphorylations are reversed by phosphatases, namely protein phosphatase 1 (PP1) and protein phosphatase 2A heterocomplex with B55 subunit (PP2A-B55)[149,150].

1.2.2.1 Structure and function of microtubules

Many processes in mitosis are driven by microtubules (MTs)[151,152]. MTs are hollow tubes, which consist of α- and β-tubulin heterodimers and are constantly build up and down by polymerization and depolymerization respectively, a feature termed dynamic instability[153,154]. The process is driven by the addition of tubulin dimers bound by GTP (polymerization) to the growing ends of MTs and hydrolyzation of tubulin-bound GTP to GDP+P_i (depolymerization)[153,154]. MT assembly can occur spontaneously or is induced from specialized nucleation sites, such as the γ-tubulin ring complex (γ-TuRC), which is activated when attached to a microtubule-organizing center (MTOC), mainly represented by the centrosome in animal cells[155]. A mitotic spindle displays three types of MTs, namely astral MTs (aMTs), interpolar MTs (ipMTs) and kinetochore MTs (kMTs), whose minus-ends are associated with the centrosomes and plus-ends grow away from the spindle poles[156]. The regulation of MT dynamics is essential for a variety of mitotic processes, including spindle formation, chromosome alignment, chromosome separation and cell cleavage, and is driven by MT motor proteins, especially kinesin and dynein[151,152].

1.2.2.2 The process of mitosis

Mitosis is subdivided into 5 phases, namely prophase, prometaphase, metaphase, anaphase and telophase, followed by cytokinesis[132] (Scheme 2, right). Once the DNA damage checkpoint is satisfied[143], **prophase** is initiated through CDC25, which eliminates the inhibitory phosphorylations of CDK1 at T14 and Y15, inducing the progression from G2 to M phase[136-138,140]. The activation of CDC25 is regulated by the S/G2 complex cyclin A-CDK2[139] and the

kinases Aurora A and PLK1, which get activated already in G2 and are subsequently recruited to the centrosomes, where they mediate centrosome maturation and separation[132,157,158]. In the following, the plus-end-directed MT motor kinesin family member 11 (KIF11, commonly referred to as EG5) gets enriched at the centrosomes, pushing the centrosomes away from each other to the opposite poles of the cell, which is promoted by PLK1 and CDK1 actions[157]. Additionally, CDK1 associates with cyclin B and phosphorylates a variety of downstream targets at the onset of mitosis, which enables the succeeding steps, including nuclear envelope breakdown, chromosome condensation, spindle assembly and chromosome alignment [132,141,159].

At **prometaphase**, the bipolar spindle is formed by MTs, which emanate from centrosomes and attach to the kinetochores (KTs) of chromosomes to align them in a central metaphase plate[151,152]. The congression of chromosomes is guided by the balanced action of polar ejection/pushing forces and KT pulling forces, which are induced by kinesins that regulate the polymerization of MTs at the centrosomes and KTs[160].

The alignment of all chromosomes at the spindle equator marks **metaphase**[151]. In the presence of aberrant MT-KT attachments or chromosome misalignments the SAC is triggered, inhibiting APC/C activation, which is supported by PLK1 and Aurora B actions[144]. When all chromosomes are properly aligned, the SAC is released, activating APC/C via CDC20, which presents the entry into **anaphase**[144]. APC/C is an ubiquitin ligase that ubiquitinates and degrades several proteins in anaphase, including cyclin B, upon whose removal CDK1 gets inactivated, and securin, whose degradation releases the protease separase (also known as separin), which cleaves the cohesin ring between sister kinetochores to induce chromatid separation[161-163]. Additionally, the phosphatases PP1 and PP2A-B55 are activated to rapidly dephosphorylate CDK1 targets[149,150]. Over the course of this, Aurora B levels at the centromeres drop and PP1 dephosphorylates Aurora B KT substrates, leading to the stabilization of MT-KT attachments[164]. Separated chromatids start to move to the spindle poles, which is supported by the depolymerization of kMTs at their plus-ends (so-called “Pac-Man” model) and minus-ends (“poleward flux” model), mediated by distinct members of the kinesin-13 family of MT depolymerases[165].

Once the two sets of chromosomes are located at the opposing poles, they are enclosed into new nuclei and the chromatin decondenses, a process called **telophase**. In parallel, a contractile ring forms between the two poles, whose constriction induces a cleavage furrow, narrowing to the so-called midbody before cells finally separate during **cytokinesis**[151]. The formation of the contractile ring and furrow ingression is guided by PLK1 and Aurora B, which are activated by RhoA[166].

1.2.2.3 Structure and function of kinesins

As introduced above, molecular motors, namely kinesins, are essential for the regulation of MT dynamics at various steps of mitosis[151,152]. Besides, kinesins participate in cilia formation and neuronal development[167]. In so doing, kinesins either control MT length via the polymerization or depolymerization of MT ends[152-154] or transport cargos along MT tracks[168].

Due to the consistent discovery of novel kinesins and obscure naming over the years, in 2004 a common nomenclature for kinesins was introduced, defining 14 kinesin families[169]. From these, all kinesins share a conserved "Motor" (or "head") domain, featuring the MT-binding site and ATPase activity, which is needed for ATP hydrolysis and the generation of energy, enabling the movement along MTs or modification of MT length[170]. The localization of the "Motor" domain determines the directionality of a kinesin and enables the definition of 3 groups: N-kinesins (or "Kin N") with their "Motor" domain in the NH_2-terminal region, M-kinesins (or "Kin I") possessing a middle or internal "Motor" domain, and C-kinesins (or "Kin C") displaying a COOH-terminal Motor domain[170].

1.2.2.3.1 KIF2A and its roles in mitosis and beyond

The motor protein KIF2A belongs to the kinesin-13 family of MT depolymerases and M-kinesins ("Kin I"), which comprises a central "Motor" domain and thereby can function at either the plus- or minus ends of MTs[171]. Structurally all kinesin-13 proteins, including KIF2A, consist of 4 domains, namely I) an NH_2-terminal "N" domain, which targets the kinesin to its site of action[172], II) a positively charged "Neck" domain, which cooperates with a "Motor" domain to support ATP turnover and MT depolymerization[173-175], III) the catalytic "Motor" domain, that comprises the ATP and MT binding sites to induce ATP hydrolysis and MT depolymerization[176], and IV) a COOH-terminal "Stalk" domain, being essential for protein dimerization[112] (Scheme 3, left).

KIF2A localizes to the minus-ends of MTs, being mainly concentrated at the centrosomes, where it modulates MT length and poleward flux during mitosis[177-181] (Scheme 3, right). Apart from mammalian KIF2A, orthologs of KIF2A with similar MT depolymerase activities have been reported in diverse species, including XKIF2 in *Xenopus*[182], KLP10A in *Drosophila*[165,183] and KLP-7 in *C. elegans*[184].

By controlling spindle MT dynamics and reorganization[178,180,185-188], KIF2A contributes to various processes in mitosis, including spindle scaling during development[189], centrosome separation and bipolar spindle formation[181,190], chromosome alignment[186,191], and chromosome segregation[185,186,192,193], as well as spindle assembly and chromosome alignment in oocyte meiosis[187,194] (Scheme 3, right). Of note, the requirement for KIF2A in bipolar spindle

formation, explored by Ganem and Compton[181], is under discussion as the findings may have originated from an siRNA off-target effect and couldn't be reproduced in studies with alternative KIF2A siRNAs[195].

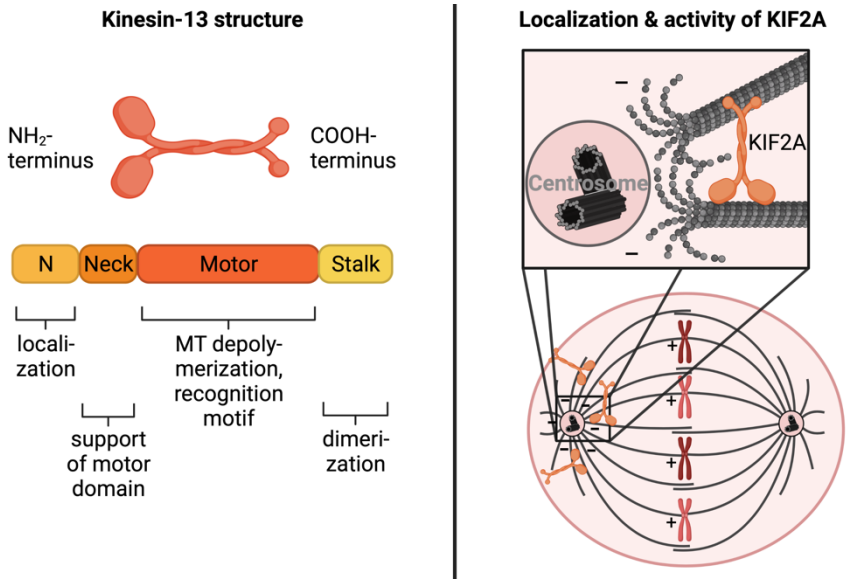

Scheme 3. Domain structure of the kinesin-13 family (left) and localization of KIF2A during metaphase (right). Kinesin-13 proteins consist of 4 domains, namely an NH_2-terminal "N" domain, a "Neck" domain, a catalytical "Motor" domain and one COOH-terminal "Stalk" domain, which fulfill distinct functions as indicated in the scheme (left). One exemplary kinesin-13 is the MT depolymerase KIF2A, which localizes predominantly to centrosomes, where it removes tubulin from the minus-ends of MTs to guide, for instance, the alignment of chromosomes during mitosis (right).

The localization and activity of KIF2A in mitosis is controlled by a variety of proteins and posttranslational modifications, especially phosphorylations, which are summarized in Scheme 4 and discussed in the following.

During nuclear envelope breakdown the motor proteins dynein/dynactin and nuclear mitotic apparatus (NuMA) recruit KIF2A to phase-separated droplets, localizing it to the spindle poles, where the kinesin is released to depolymerize MT ends, mediating spindle length and spindle assembly[180,196,197]. Additionally, the p53-transcriptional target proline and serine rich coiled-coil 1 (PSRC1 or DDA3)[198] promotes KIF2A recruitment to spindle MTs, which is followed by the precise localization of KIF2A to the spindle poles by the spindle and kinetochore associated complex subunit 1 (SKA1)[193,199]. In this process, the activity of KIF2A is counteracted by the MT stabilizer MAP7 domain containing 3 (MAP7D3 or MDP3), that can associate with DDA3 and KIF2A, thereby reducing KIF2A levels at the spindle[178]. Another unexpected regulator is presented by lysine methyltransferase 2A (KMT2A or MLL), which

normally builds a complex with WD repeat domain 5 (WDR5) and other proteins to methylate histone H3[186]. However, recently it was shown that the MLL/WDR5 complex also interacts with the N-terminal domain of KIF2A to recruit KIF2A to the spindle poles ensuring the proper chromosome alignment during mitosis[186].

Besides, the kinase PLK1 phosphorylates KIF2A and navigates its localization and activation at the minus ends of MTs[112,200,201]. The PLK1-KIF2A interaction and thereby activity of KIF2A is supported by the mMRN complex, comprising MRE11 double-strand break repair nuclease A (MRE11), RAD50 double-strand break repair protein (RAD50), nijmegen breakage syndrome 1 (NBS1) and WD repeat and coiled-coil-containing (WDCP or MMAP), in mitosis. At this, MRE11 and MMAP were revealed to be phosphorylated by PLK1 and interact with each other[185]. Conversely, phosphorylation of KIF2A by Aurora A inhibits its localization and activity during mitosis[200]. Similarly, phosphorylation of KIF2A by Aurora B, which distributes in a decreasing gradient from the spindle midzone to the poles, inhibits KIF2A activity at the spindle center and translocates it to the centrosomes[188,191,202]. The inactivation of KIF2A by Aurora B can be counteracted by inner centromere kin-I stimulator (ICIS)[202]. Another antagonist of KIF2A is represented by the casein kinase tau tubulin kinase 2 (TTBK2). By phosphorylating KIF2A, TTBK2 prevents its localization to the spindle MTs and depolymerase activity. Interestingly, a prerequisite for TTBK2 activity is the binding of the MT plus-end protein microtubule-associated protein RP/EB family member 3 (MAPRE3 or EB3) to TTBK2, indicating that the regulation of MT minus-ends is connected to plus-end MT dynamics[203].

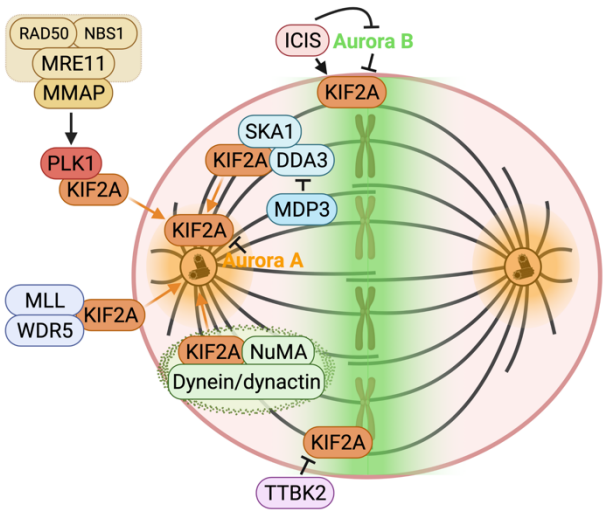

Scheme 4. Factors regulating KIF2A localization and activity at the mitotic spindle. The involved proteins regulate KIF2A either positively (⟞) by localizing it at the spindle poles and/or promoting its activity or negatively (⊣) by inhibiting its action. Aurora A is localized around the centrosomes, whereas Aurora B displays highest levels at the central metaphase plate and descends towards the poles. KIF2A

= kinesin family member 2A, RAD50 = RAD50 double-strand break repair protein, NBS1 = nijmegen breakage syndrome 1, MRE11 = MRE11 double-strand break repair nuclease A, MMAP = WDCP/WD repeat and coiled-coil-containing, PLK1 = polo-like kinase 1, MLL = lysine methyltransferase 2A, WDR5 = WD repeat domain 5, DDA3 = proline and serine rich coiled-coil 1, SKA1 = spindle and kinetochore associated complex subunit 1, MDP3 = MAP7 domain containing 3, ICIS = inner centromere kin-I stimulator, NuMA = nuclear mitotic apparatus, TTBK2 = tau tubulin kinase 2.

Apart from its functions in mitosis, KIF2A is involved in cilia disassembly as well as embryonic and adult neurogenesis[112,204,205]. At this, KIF2A regulates neurite outgrowth and brain wiring by restricting the branching of axons and dendrites[206-209]. Consistently, mutations in or depletion of KIF2A evoke excessive neurite growth, arborization and cortical malformations, including microcephaly and lissencephaly, hyperactivity or epilepsy[204-207,210,211]. In contrast, high levels of KIF2A have been associated with multiple types of cancer, correlating with increased rates of proliferation, migration, invasion and epithelial-to-mesenchymal transition (EMT), which was supposed to be relayed by the activation of PI3K-Akt, Wnt and Notch signaling[212-215].

1.3 Wnt signaling in cell cycle progression and mitosis

1.3.1 Functions of Wnt signaling in cell cycle regulation

In line with its roles in proliferation and self-renewal, canonical Wnt signaling also drives cell cycle progression (Scheme 5). By stabilizing β-catenin, active Wnt signaling induces the transcription of *MYC* (c-myc), *CCND1* (cyclin D1) and *CCNE1* (cyclin E1) in somatic cells, which promotes G1-to-S phase progression[38,39,216]. This effect is reinforced by the Wnt-mediated inhibition of GSK3, which, in the absence of a WNT ligand, phosphorylates and subsequently degrades c-myc, cyclin D and cyclin E(Diehl et al., 1998; Gregory et al., 2003; Welcker et al., 2003), and stabilizes the CDK inhibitor $p27^{KIP1}$ [217]. Furthermore, the increased levels of c-myc suppress the transcription of the cell cycle inhibitors *$p27^{KIP1}$* and *$p21^{CIP1/WAF1}$*, which supports the progression from G1 to S phase[82,218]. In contrast to its G1/S-promoting functions, Wnt signaling has been also suggested to reduce proliferation in some cells[219]. For instance, in murine embryonic stem cells (mESCs), Wnt activation reduces c-myc and induces the expression of distinct cell cycle repressors via TCF1, leading to impaired cell cycle progression[219]. Besides, active β-catenin/TCF transcription has been indicated to hinder the progression from G2 to M phase by maintaining the inhibitory phosphorylation of CDK1 at Y15 in mESCs[220]. Furthermore, β-catenin induces the expression of the separase inhibitor *securin*, which prevents cohesin cleavage and chromatid separation, a process that normally occurs

in anaphase, as shown in cancer cells[162,221]. Correlating with this, the transcription of β-catenin target genes was reported to be highly active in G1/S phase, but to drop at G2/M in response to increased levels of conductin/AXIN2[222], which matches the overall reduction of transcription during mitosis[223]. In late mitosis, transcriptional activities may be reactivated by the ubiquitination and proteasomal degradation of conductin/AXIN2 via the APC/C cofactor CDC20[222].

Nevertheless, Wnt signaling was indicated to take essential roles in mitosis. It was reported that cytosolic β-catenin peaks at G2/M phase and drops in G1 phase[29,49,224]. This is mediated on the one hand by the G2/M-induced phosphorylation of LRP6 by CDK14/cyclin Y, which primes the Wnt receptor to be phosphorylated by CK1γ[29], and on the other hand by the prevention of the clathrin-mediated endocytosis of Wnt components via CDK1-stabilized BCL9[56]. As a result, GSK3 targets, such as β-catenin as well as proteins that control cytoskeletal arrangements and cell cycle progression, are stabilized, presenting a transcription-independent action of Wnt signaling (referred to as WNT/STOP)[32,49,50,52].

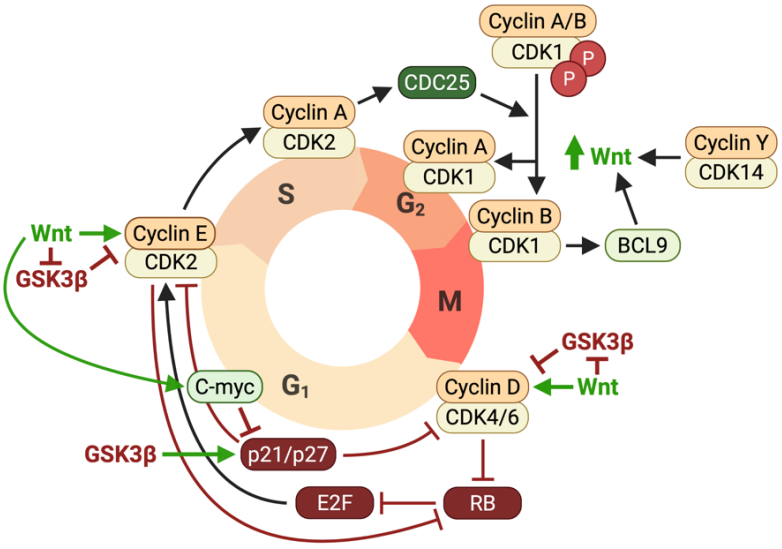

Scheme 5. The roles of Wnt signaling in cell cycle regulation. Wnt signaling promotes G1/S progression by the β-catenin-dependent transcription of the cell cycle activators cyclin D, cyclin E and c-myc. Additionally, cyclin D and cyclin E are stabilized and the G1 inhibitor p27 is destabilized by the inhibition of GSK3β upon active Wnt signaling. This effect is reinforced by c-myc, which inhibits the expression of the cell cycle inhibitors p21 and p27. The levels of canonical Wnt signaling peak at G2/M, which is supported by cyclin Y/CDK14 and the stabilization of BCL9 by CDK1. CDK = cyclin-dependent kinase, CDC25 = cell division cycle 25, BCL9 = B-cell CLL/lymphoma 9, RB = retinoblastoma, E2F = transcription factor.

Apart from canonical Wnt signaling, also non-canonical Wnt pathways take roles in the regulation of cell proliferation and cell division to shape tissues during development[68,225,226]. They contribute especially to the polarization and orientation of mitotic spindles, thereby directing asymmetric cell divisions[69,227-229]. However, as this work focused on the roles of canonical Wnt signaling during mitosis, I will concentrate on this pathway in the following and not discuss the functions of non-canonical Wnt/PCP and Wnt/Ca^{2+} signaling in detail here.

1.3.2 Functions of Wnt signaling in mitosis

As described in the preceded part, WNT/STOP signaling and β-catenin were shown to be under cell cycle control and peak at G2/M phase[29,49,56,224]. In response to the increased Wnt activity and related decrease in GSK3β a variety of mitotic proteins are stabilized, including CDC25A, CDC25B, PLK1, AURKB, cohesin and ubiquitin-conjugating enzyme E2C (UBE2C), which control mitotic entry, MT dynamics, spindle assembly, chromosome alignment, chromosome segregation and cell division[49,50,52,53,230]. However, even though multiple mitotic proteins were indicated to be regulated by active Wnt signaling, the exact mechanisms and functions of the interactions are rarely characterized.

In line with its high activity and diverse targets in mitosis, both attenuated as well as hyperactive canonical Wnt signaling was associated with mitotic defects across different cell types[50,52,79,231-236]. To name a few, knockdown of LRP6 and cyclin Y (WNT/STOP signaling) arrests early *Xenopus* embryos before the first or second cleavage during development, which is likely dependent on GSK3 inhibition, but independent of β-catenin[50]. Apart from *Xenopus*, impaired Wnt signaling also perturbs mitosis in mammalian cells. Loss of the Wnt secretion factor evenness interrupted (EVI) (also known as wntless (WLS)) causes a significant increase in anaphase lagging chromosomes and chromosomal instability (CIN) in human somatic cells and murine ESCs[53,79]. Similarly, inhibition of Wnt signaling by DKK1 or secreted frizzled-related protein (SFRP), and depletion of LRP or DVL induces chromosome missegregation and aneuploidy in human somatic cells[52,53]. Notably, CIN is a well-known characteristic and driver of cancer[145], a disease which is commonly associated with aberrant Wnt signaling[1]. Matching this, both *APC* truncation mutations and high levels of the Wnt target AXIN2, which are frequently observed in colon tumors, were correlated with chromosome missegregation and CIN[232-236]. Besides, β-catenin stabilization was shown to cause a higher prevalence of anaphase bridges in mouse ESCs[220]. Taken together, the data on hand suppose that a balanced regulation of mitotic Wnt signaling is necessary for the correct completion of mitosis and prevention of CIN, however the exact mechanisms that drive mitosis and their dependency on β-catenin remain to be clarified.

In addition to their signaling functions, several components of the canonical Wnt pathway directly associate with the cytoskeleton, especially MTs, to guide diverse mitotic processes, including spindle formation, spindle orientation, chromosome alignment and chromosome segregation[103,237], which will be discussed in the following. An overview of the localization and function of each component is given in Table 1.

Table 1. Localization and function of canonical Wnt signaling components during mitosis.

Wnt component	Main localization	Function	Phenotype upon depletion	References
DVL	Centrosomes & kinetochores (MT plus-ends)	- Centrosome separation - Spindle orientation - MT-KT attachment - Chromosome congression and alignment - Promotion of SAC	- Centrosome separation defects - Reduced astral MT growth - Spindle misorientation - Chromosome misalignment	52,231,238
AXIN1	Centrosomes (MT minus-ends)	- MT growth and stability - Centrosome duplication (AXIN phosphorylated at S157 by PLK1)	- Reduced MT growth - Supernumerary centrosomes (non-phosphorylated AXIN-S157)	239-241
AXIN2/ Conductin	Whole spindle, especially centrosomes (MT minus-ends)	- Centrosome cohesion - Attenuation of SAC	- Premature centrosome separation - Increased mitotic index - Chromosome missegregation - CIN	235,242
APC	Kinetochores, centromeres, centrosomes (MT plus-ends)	- MT stability - MT-KT attachment - Chromosome alignment and segregation - Contribution to SAC	- Chromosome misalignment - Chromosome missegregation - Mono- and multipolar spindles - Supernumerary centrosomes - CIN	220,232-236,243-251
GSK3β	Whole spindle, especially centrosomes & kinetochores	- Inhibition of MT growth - MT destabilization	- Increased astral MT growth - Increased mitotic index	117,252-257

		- Chromosome congression and alignment - Promotion of SAC	- Chromosome congression defects - Chromosome misalignment - Micronuclei - CIN	
β-catenin	Centrosomes (MT plus-ends)	- Centrosome cohesion - MT growth, stability, and organization (β-catenin phosphorylated by GSK3β)	- Premature centrosome separation - Reduced astral MT growth - Disorganized MTs (phospho-inactive β-catenin) - Monopolar spindles	[127,220,242,258-260]

1.3.2.1 Wnt signaling in centrosome cohesion and separation

The separation of duplicated centrosomes and their segregation to opposing poles at the onset of mitosis is an essential step to enable the outgrowth of MTs from the poles and formation of the mitotic spindle[151].

The Wnt scaffolding protein DVL positively regulates this process by interacting with and releasing the centrosomal linker proteins CDK5 regulatory subunit-associated protein 2 (CDK5RAP2) and centrosomal protein 250 (CEP250 or C-NAP1), which induces centrosome separation[238]. Conversely, centrosomal conductin/AXIN2 supports centrosome cohesion via GSK3β, which phosphorylates β-catenin at serine 33/37 and threonine 41. Interestingly, the phosphorylations lead to the stabilization and accumulation of β-catenin at the centrosomes rather than its proteasomal degradation[127,242,258-260]. In line with this, AXIN2 ablation, GSK3 inhibition or expression of a phospho-inactive mutant of β-catenin induces premature centrosome splitting[242]. Contrasting this, complete depletion or inhibition of β-catenin leads to a failure in centrosome separation and hence mono-astral MT formation[242,258,259].

1.3.2.2 Wnt signaling in centrosomal MT dynamics and spindle orientation

Apart from guiding centrosome separation, a great number of Wnt components, namely DVL, AXIN1, APC, GSKβ and β-catenin, has been indicated to localize at centrosomes to guide astral MT dynamics during mitosis.

In detail, APC localizes to the plus-ends of MTs close to the mother centrioles, where it interacts with the MT-associated protein RP/EB family member 1 (MAPRE1, also known as EB1), supporting MT stabilization and the attachment of astral MTs to the cell cortex[224,244,261,262]. The anchoring of MTs is positively regulated by the CDK2/cyclin A-mediated

phosphorylation of APC during late G2 phase[262], whereas APC association with MTs is restrained by the GSK3β-mediated phosphorylation of APC[244]. Similar to APC, DVL2 and AXIN1 localize to the centrosomes and promote astral MT nucleation during mitosis, supporting MT attachments[231,239]. AXIN localizes γ-tubulin and γ-tubulin complex protein 2 (GCP2) at the centrosomes, where they form the γ-TuRC[239]. This is regulated by PLK1, which reduces the association of AXIN1 with γ-tubulin by phosphorylating it at S157[241], and Aurora A, which presumably promotes AXIN localization at the centrosomes[240]. Conversely, AXIN1 controls PLK1 and GSK3β levels at the poles[240]. GSK3β reduces centrosomal MT growth rates by restricting the recruitment of γ-tubulin and GCP2 to the spindle poles by binding to γ-tubulin complex protein 5 (GCP5)[254]. Contrasting this, the phosphorylation of centrosomal β-catenin by GSK3β promotes radial MT growth and organization, likely by the recruitment of γ-tubulin to centrosomes[127,260]. Accordingly, the expression of non-phosphorylatable β-catenin impairs centrosomal MT nucleation, resulting in disorganized MTs and loss of cell polarity[127,260].

The correct regulation of astral MT plus-end dynamics and attachment to the cell cortex is essential for the anchoring and orientation of the mitotic spindle[263]. Consistently, Wnt signaling was implicated in the guidance of mitotic spindle orientation in various species. Namely, FZD, DVL, GSK3β, CKIα (KIN-19 in *C. elegans*), β-catenin (WRM-1) and APC (APR-1) were proposed to direct the orientation and division of 4-cell and 8-cell stage blastomere spindles in *C. elegans*[264,265]. Similarly, FZD, DVL and APC orient asymmetric cell divisions in *Drosophila*[266,267], and DVL, FZD and LRP6 define the plane of mitotic spindles in human cells[231]. In line with this, Wnt inhibition and depletion of LRP or DVL accelerate MT plus-end polymerization rates and cause defects in spindle orientation[52,231]. However, both DKK1 and WNT3A treatment were reported to evoke aberrant spindle angles, indicating that the balanced regulation of Wnt signaling is needed to orient the mitotic spindle correctly[56].

Of note, spindle orientation is also decisive for the determination of symmetric versus asymmetric cell divisions in metazoans[263], a process in which Wnt signaling has been well-known to participate in diverse species[83,127,264-268] and which correlates with the decision on self-renewal versus differentiation in stem cells[19]. Matching this, both in *Drosophila* and *C. elegans* canonical Wnt components, especially APC, were shown to localize asymmetrically within the cell to guide asymmetric cell divisions and differentiation[265-268]. In this process, elevated levels of APC (APR-1 in *C. elegans*) stimulate the outgrowth of astral MTs at one side, while the opposing side is enriched for β-catenin (WRM-1), which leads to the polarization and asymmetric division of the cell, creating two daughter cells with differential fates[265,268]. This mechanism is likely conserved in mammals as the presentation of a local Wnt

source to mouse ESCs induces similar asymmetric divisions and differential daughter cell fates[83]. The link between cytoskeletal dynamics, spindle symmetry and cell fate was strengthened by a study from the Niehrs laboratory, which found that depletion of WNT/STOP increases astral MTs and thereby alters spindle orientation and favors symmetric cell divisions in NPCs[51]. The researchers suggest that WNT/STOP signaling promotes asymmetric cell divisions and differentiation, whereas WNT/β-catenin signaling induces symmetric divisions and proliferation/self-renewal, which matches and provides an explanation for previous studies[99,127,264].

1.3.2.3 Wnt signaling in kinetochore MT dynamics and MT-KT attachments

In addition to the regulation of MT growth at the spindle poles, distinct proteins of the Wnt pathway also modulate MT dynamics at the KTs of chromosomes.

APC localizes and interacts with EB1 also at the plus-ends of kMTs, supporting MT stabilization and MT-KT attachments[234,236,244,245,247,248,269-271]. The interaction of APC with EB1 is reduced by the phosphorylation of APC via CDK1 and possibly protein kinase A (PKA) and hence is prevented at the beginning of mitosis, while restored when CDK1 activity drops during anaphase[247,272]. Additionally, APC interacts with the plus-end MT depolymerase KIF2C (also known as MCAK), which weakens MT-KT attachments to enable the correction of erroneous linkage[273,274]. In line with this, upon *APC* gene truncations MT-KT attachments and error correction are impaired, leading to chromosome segregation defects and CIN[232-236].

Apart from APC, DVL also localizes to KTs upon disruption of MTs, where it may interact with APC to cooperatively regulate MT plus-end dynamics and stabilize MT-KT attachments during mitosis, which is supported by the phosphorylation of DVL-T206 by PLK1[231]. Consistently, inhibition of canonical Wnt signaling, e.g. by DKK1, SFRP, EVI knockout or depletion of LRP or DVL, increases mitotic MT plus-end assembly rates, which can lead to MT-KT malattachments, lagging chromosomes and aneuploidy[52,53,231]. Notably, these defects are likely driven by WNT/STOP signaling, as the depletion of β-catenin or TCF does not increase MT plus-end polymerization rates[52].

1.3.2.4 Wnt signaling and its contribution to the spindle assembly checkpoint (SAC)

Another origin of aneuploidy are defects in the mitotic SAC, which can cause the premature onset of anaphase, causing chromosome missegregation and CIN, which is a common characteristic of tumors[142,144,145].

DVL was shown to contribute to a functional SAC by activating the SAC component monopolar spindle 1 (MPS1) and supporting the recruitment of the checkpoint proteins BUB1 and BUBR1

to the KTs[231]. Similarly, GSK3β has been proposed to localize MAD2, BUB1 and BUBR1 to the KTs, thereby triggering the SAC[253,257]. APC phosphorylation by GSK3β promotes its stabilizing activity, MT-KT attachments and additional APC phosphorylations by BUB1/BUBR1 and BUB3[232,250]. In line with this, the levels of BUB1 and BUBR1 bound to chromosomal KTs are reduced upon APC knockdown or GSK3 inhibition[236,246,253] and both loss of *APC* and *GSK3* leads to misaligned chromosomes and CIN, e.g. in colon cancer[220,232,233,236,245,246,250,252,253]. However, there is conflicting evidence on the requirement of APC in the checkpoint[246,250,251,275,276]. The data currently available propose that APC is not a component of the SAC per se, but compromises the checkpoint indirectly, e.g. via GSK3 or other proteins[275,276].

1.3.2.5 Synopsis of the roles of Wnt signaling in mitosis

Overall, the current state of research suggests that Wnt signaling and its components are substantially involved in centrosome separation, mitotic spindle orientation, MT-KT attachments, SAC control, and thereby the error-free alignment and segregation of chromosomes. Consequently, the correct spatial and temporal regulation of both the activity and components of mitotic Wnt signaling is crucial for the orderly completion of mitosis, while disruption of the pathway can induce severe mitotic aberrations, such as centrosome separation defects, spindle misorientation, chromosome misalignment, chromosome missegregation and ultimately CIN[52,53,79,220,232-236,246,253].

However, although the Wnt signaling pathway takes a prominent role in the regulation of mitosis and its disruption causes distinct mitotic defects, which may notably result in CIN and tumorigenesis, the exact molecular mechanisms and mitotic proteins, that are involved in these processes, are still poorly understood.

2. Aims of the thesis

Throughout the last years it was shown that the levels of canonical WNT/LRP6 signaling fluctuate throughout the cell cycle, reaching their highest activity at mitosis[29,49,56,224]. This is conveyed by the cell cycle-dependent kinase CDK14 in association with CCNY/CCNYL1, which primes LRP6 to be phosphorylated, and the recruitment of BCL9 by CDK1, which stabilizes LRP6 signalosomes[29,49,56,224]. In line with this, various mitotic defects, such as arrest, chromosome misalignments and chromosome segregation errors, have been reported upon impaired Wnt signaling in somatic cells, stem cells and whole embryos[50,52,53,79,232,233,235,253]. However, even though these aberrations can lead to CIN, which is tightly associated with cancer[145,277], the exact functions and targets of Wnt signaling in mitosis remain largely uncharacterized.

As described previously, Wnt signaling can regulate proteins by different modes of action, including β-catenin-dependent transcriptional regulation, protein stabilization in response to GSK3β inhibition (WNT/STOP), or the direct interaction of proteins with components of the LRP6 signalosome[278].

Therefore, the aim of this thesis was to characterize the exact molecular roles and modes of action that Wnt signaling takes in the regulation of mitosis, focusing on the following sub-aims:

1. Identification of Wnt-regulated proteins that participate in mitosis.
2. Characterization of Wnt-mediated functions and modes of action during mitosis, including the mitotic targets identified.
3. Validation of the conservation and transferability of the roles of Wnt signaling in mitosis using stem cells and organotypic models.

3. Results

3.1 Phosphoproteomic screen reveals targets of Wnt signaling in mitosis

Wnt signaling peaks in G2/M phase[29,49,56,224] and was found to be relevant for the completion of faithful mitosis[50,52,79], however the Wnt-regulated proteins that are involved in this process are yet unknown. To get an insight into the targets involved, I employed a mass spectrometry screen in combination with stable isotope labeling by amino acids in cell culture (SILAC-MS) upon Wnt activation or inhibition in mitosis, which was done in collaboration with Prof. Dr. Holger Bastians (Georg-August-University Göttingen) and Prof. Dr. Petra Beli (Institute of Molecular Biology (IMB) Mainz). As mitosis is driven mainly by post-translational modifications, especially phosphorylations[148], we specifically analyzed the proteins for changes in phosphorylation site occupancy. The details of the screen and obtained results will be outlined in the following.

3.1.1 Wnt signaling can be modulated by home-made WNT3A and DKK1 media

Before running the MS screen, I initially established the production of WNT3A and DKK1 conditioned media (CM), the purification of recombinant DKK1 and determined the best treatment times for the experiments.

In so doing, I firstly produced Control and WNT3A CM from L-cells stably transfected with *WNT3A* (ATCC CRL-2647) or wildtype L-cells (ATCC CRL-2648) respectively using full DMEM medium as describes in the methods (section 6.2.2.1). To optimize the culture time, I collected fractions of CM one, two, three or four days after transfection and tested the potency of the fractions using TOPflash reporter assays in HEK293T cells. I detected the highest activation of Wnt signaling upon treatment with WNT3A CM fractions harvested on day 3 and 4 after transfection (fraction #3 and #4) using a 1:5 dilution in full DMEM medium (Figure 1A). Conclusively, to produce the Control and WNT3A SILAC CM and all other CM used in this work, I harvested the media 3 days after seeding and applied them in a 1:5 dilution to cells in all experiments displayed in this work.

A similar optimization strategy was used to evaluate the potency of DKK1 CM and purified DKK1. To produce DKK1 CM, I transiently transfected HEK293T cells with a *DKK1-FLAG* plasmid and harvested the medium 2 days later. For application in the SILAC-MS approach, DKK1 was purified to maximize its potency and evade off-target effects due to the medium and factors secreted by HEK293T cells (for the exact procedures consult the methods section 6.2.2.2). The purification of DKK1 from the CM worked successfully as the flow through of the column did not inhibit Wnt activity as effectively as the original DKK1 CM in TOPflash assays

(Figure 1B). Supporting this observation, purified DKK1 reduced active Wnt signaling almost to the basal level when added 1:50 to the medium. DKK1 CM showed a similar efficiency when used 1:5 (Figure 1B). Based on these results, we applied purified DKK1, diluted 1:50 in heavy SILAC medium, for the MS experiment. For all other assays displayed in this work, I used DKK1 CM, diluted 1:5 in the respective full medium of the surveyed cell line.

Analysis of β-catenin levels by Western blotting confirmed the potency of both WNT3A CM and purified DKK1 in regulating Wnt signaling (Figure 1C). As expected, the canonical Wnt pathway was activated by WNT3A and inhibited by DKK1. The increase in Wnt signaling upon treatment with the GSK3 inhibitor BIO could not be reduced by DKK1 as BIO activates the pathway downstream of LRP5/6 (Figure 1C).

Consequently, I produced SILAC CM, including either WNT3A ligands (labelled with light isotope-containing amino acids), no ligands (labelled with medium isotopes; also referred to as “Control”) or DKK1 proteins (labelled with heavy isotopes), according to the described methods (see above and 6.2.2). The produced SILAC CM efficiently activated or inhibited Wnt signaling respectively in RPE1 cells, as verified by TOPflash assays (Figure 1D). The reduction of Wnt signaling below the activity of control cells upon DKK1 treatment indicated that RPE1 cells display endogenous Wnt signaling activity (Figure 1D).

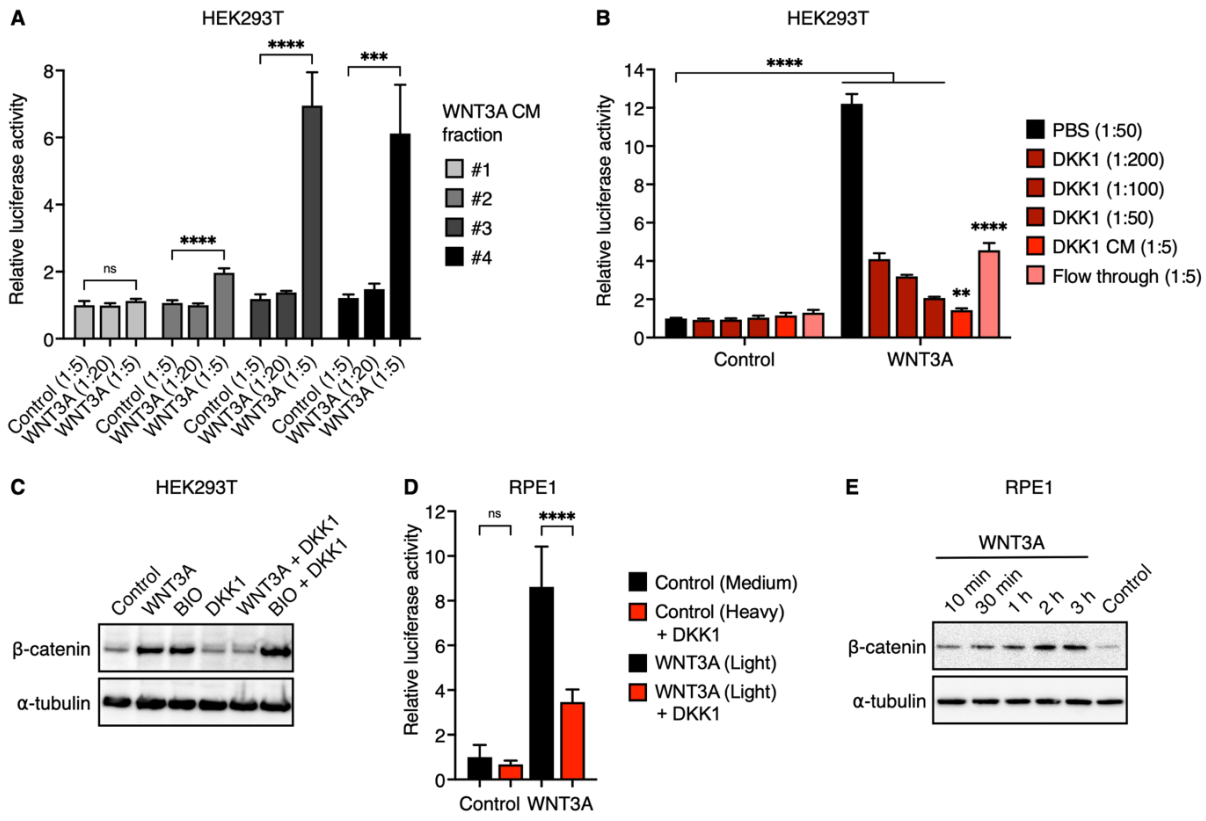

Figure 1. Home-made WNT3A conditioned medium (CM) and purified DKK1 are potently modulating Wnt signaling activity. (A),(B) TOPflash reporter assays in HEK293T cells treated with home-made

Control and WNT3A CM alone or in combination with PBS (control), DKK1 CM and purified DKK1 as indicated. Used dilutions are given in brackets. Means with SD of 3 biological replicates are shown. (C) Representative Western blot of cytoplasmic lysates from HEK293T cells that were treated with the produced CM, purified DKK1 and/or the GSK3 inhibitor BIO. (D) TOPflash reporter assays in RPE1 cells treated with control or WNT3A SILAC CM with or without DKK1. Means with SD of 6 biological replicates are shown. (E) Representative Western blot of cytoplasmic lysates from RPE1 cells that were treated for 10 min-3 h with WNT3A CM or for 3 h with control CM.

As mitosis is driven by dynamic changes in the phosphorylation pattern of distinct cell cycle proteins[147,148], we aimed to record post-translational dynamics rather than transcriptional activities with the performed MS screen. To determine the minimum treatment time needed to evoke post-translational changes, without inducing transcriptional activation, upon WNT3A and DKK1 incubation, I used the accumulation of β-catenin, whose degradation is based on its phosphorylation by GSK3, as a readout. Thus, I treated RPE1 cells for 10 min or up to 3 h with WNT3A CM and quantified cytoplasmic β-catenin levels in Western blots and found that β-catenin peaks 2 h after Wnt induction (Figure 1E). Based on these data, we decided to employ 1.5 h treatments in the following experiments to catch post-translational changes upon Wnt modulation in their dynamic phase.

3.1.2 Mitotic Wnt signaling regulates various mitotic proteins post-translationally

To assess what targets are regulated by Wnt signaling in mitosis, we performed a phosphorylation-targeted mass spectrometry (MS) screen using stable isotope labeling by amino acids in cell culture (SILAC) probes to label the medium[148,279,280]. We synchronized RPE1 cells by thymidine in G1/S and subsequently released them into dimethylenastron (DME) to arrest them in mitosis. In parallel to the treatment with DME, cells were treated for 1.5 h with Control, WNT3A or DKK1 SILAC CM (Figure 1D,E). Cells were harvested, lysed in full lysis buffer and prepared for MS analysis. To enrich for phosphopeptides a TiO_2 column to bind phospho(STY)-sites was employed. Notably, in parallel to their phosphorylation sites, the samples were also analyzed for changes in their ubiquitination site occupancy, however as most mitotic processes are primarily driven by phosphorylations[147,148] and there was no clear overlap between the phosphorylation and ubiquitination MS dataset, we focused on the phosphorylation changes in this work.

The experiment was performed in duplicates and showed high reproducibility both for the DKK1 and WNT3A condition compared to the Control (Figure 2A,B). We obtained 12,193 hits that came up in both experiments for Control, WNT3A and DKK1 treatments (Figure 2C). From

these phosphopeptides, 176 sites were significantly regulated upon DKK1 (30 downregulated, 146 upregulated) and 104 sites significantly modified upon Wnt activation (60 downregulated, 44 upregulated). In the further analysis of the data, I considered all values that were 2-fold up- or downregulated in comparison to the basal "Control" condition ($n < 0.5$ or > 2) as significantly regulated. 4 proteins showed an antagonal regulation by DKK1 and WNT3A in at least one phospho-site, indicating that they may represent traditional Wnt targets. These were: coiled-coil domain-containing protein 175 (CCDC175), glutamate receptor ionotropic kainate 2 (GRIK2), band 4.1-like protein 1 (EPB41L1) and cell division cycle-associated protein 3 (CDCA3) (Figure 2C). However, there was in general little overlap between the mode of regulation of the phosphopeptides that came up upon WNT3A versus DKK1 (Figure 2C), which is why we decided to focus in the proceeding analysis on the DKK1 treated cells, comparing them to the control condition.

Upon DKK1 I identified 12,208 phosphopeptides that were present in both experiments. Functional annotation of the significantly up- and downregulated proteins using the gene ontology (GO) analysis tool *GOrilla* enriching for the GO terms of biological processes[281,282] revealed that especially proteins of I) actin filament-based processes, including actin filament severing ($P = 2.54 \times 10^{-6}$) and actin filament-based movements ($P = 3.80 \times 10^{-4}$), II) cellular component disassembly, e.g. protein-DNA complex disassembly ($P = 5.38 \times 10^{-4}$) and the regulation of protein complex disassembly ($P = 5.6 \times 10^{-4}$), III) cytoskeleton organization ($P = 1.34 \times 10^{-4}$), and IV) the regulation of supramolecular fiber organization ($P = 7.46 \times 10^{-4}$), including the regulation of protein depolymerization ($P = 4.80 \times 10^{-5}$), were modified upon Wnt inhibition by DKK1 (Figure 2D). As these processes contribute to the faithful progression through mitosis, these findings indicate a notable role of Wnt signaling in mitotic regulation.

To identify the best Wnt-regulated candidates, I compared the top hits that came up in our screen with the Mitocheck database, which comprises an extensive dataset of phenotypic aberrations occurring in cell division upon knockdown of diverse cell cycle proteins[283]. In this, I found kinesin family member 2A (KIF2A), cyclin-dependent kinase 1 (CDK1), spermatogenesis associated 2 like (SPATA2L), microtubule associated serine/threonine kinase like (MASTL) and lysine acetyltransferase 6A (KAT6A) to show distinct phenotypes upon knockdown in mitosis (Figure 2E). In CDK1 and KIF2A depleted cells most mitotic defects were detected (Figure 2E), which is in line with their known roles in mitosis[141,181,284] (for more details please refer to the section 1.2.2).

For the most dominantly regulated targets that we identified in our screen and that were confirmed to have roles in mitosis based on the Mitocheck database, I analyzed their protein levels upon Wnt activation (WNT3A) or inhibition (DKK1) by Western blotting to test whether

they may resemble WNT/STOP targets (Figure 2F,G). CDK1 seemed to be positively regulated, whereas RAN binding protein 2 (RANBP2) seemed to be negatively regulated by Wnt signaling. For KIF2A no changes on the protein level were detectable. Of note, I observed huge variations between the replicate experiments for CDK1 and especially RANBP2 (Figure 2F,G). Therefore, we put these findings on hold, however it may be interesting to investigate the interactions between Wnt signaling and CDK1 or RANBP2 in more detail in the future.

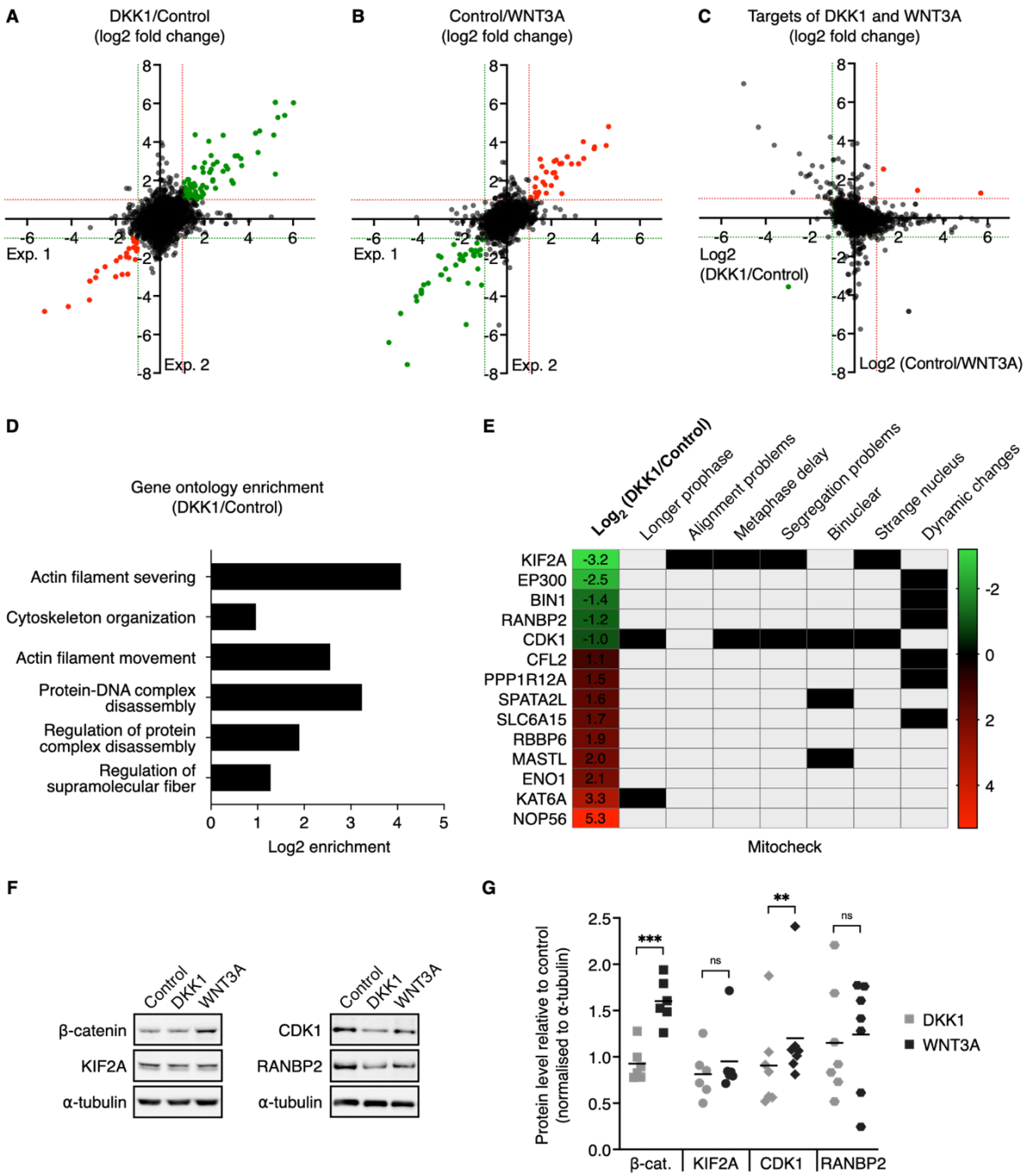

Figure 2. Phosphoproteomic analysis reveals Wnt targets in mitosis. (A),(B) Comparison of the log2 fold changes in phosphopeptide counts of two independent phospho-SILAC-MS experiments in RPE1

cells, displaying DKK1 versus Control treatment (A) or Control versus WNT3A treatment (B). Upregulated phospho-sites are colored green and downregulated sites red. (C) Comparison of the log2 fold changes in phosphopeptide counts in DKK1/Control conditions (x-axis) mapped against Control/WNT3A conditions (y-axis). Targets that were positively regulated by Wnt, namely upregulated upon WNT3A and downregulated upon DKK1 in their phosphorylation site, are marked green. Targets that were negatively regulated by Wnt signaling are marked in red. (D) Top hits of gene ontology enrichment analysis (GO term biological processes) of all detected phosphopeptides varying more than 2-fold upon DKK1 compared to control treatment (DKK1/Control < 0.5 or > 2). (E) Log2 fold changes of the most dominantly regulated phosphopeptides in DKK1/Control conditions (left column) and mitotic phenotypes upon knockdown of the target proteins, derived from the Mitocheck database. Note: The data for panels A-E (MS screen) were produced jointly with the Bastians laboratory (H. Bastians, Georg-August-University Göttingen) and Beli laboratory (P. Beli, Institute of Molecular Biology (IMB) Mainz). The displayed analyses were performed by me. (F) Representative Western blots of cytoplasmic lysates from RPE1 cells that were treated for 1.5 h with Control, DKK1 or WNT3A CM. (G) Quantification of β-catenin, KIF2A, CDK1 and RANBP2 protein levels upon DKK1 or WNT3A relative to Control treatments and normalized to α-tubulin from n ≥ 6 Western blots.

For other proteins that were tested, including lamin A/C (LMNA), histone acetyltransferase p300 (EP300), LIM domain only protein 7 (LMO7), talin 1 (TLN1), antigen KI67 (MKI67) and MASTL no clear changes were detected upon Wnt regulation in Western blots (data not shown).

3.2 The kinesin KIF2A is positively regulated by Wnt signaling in mitosis

Even though no changes in KIF2A protein levels were detected upon Wnt inhibition or activation, we continued analyzing KIF2A in immunofluorescence (IF) experiments, since the KIF2A site S100 was one of the most dominantly regulated phospho-sites detected in the phosphoproteomic screen. Besides, it is known that KIF2A is an important player in mitosis and that a misregulation of KIF2A in mitosis can lead to aberrant chromosome alignment in metaphase as well as chromosome missegregation in anaphase[185,186,188,192,283].

3.2.1 Wnt signaling and S100 phosphorylation promote KIF2A localization at the mitotic spindle

Using IF analysis, we could validate the positive regulation of KIF2A by Wnt signaling. Namely, Wnt inhibition by DKK1 reduced the localization of KIF2A at the spindle poles in mitosis, whereas activation of Wnt signaling increased KIF2A levels at the poles (Figure 3A-C).

It is known that Wnt signaling can act through different regulatory mechanisms, such as β-catenin induced transcriptional activation, Wnt-dependent stabilization of proteins (WNT/STOP) or direct interaction of Wnt signaling pathway components[278]. Interestingly, the changes in KIF2A at the spindle were independent of transcriptional changes[285] (data not shown) or changes on the protein level (Figure 2F,G), suggesting a post-translational mode of regulation.

In the performed MS screen, we detected 4 phospho-sites, which were all located in the N-terminal domain of KIF2A, namely T78, T97, S100 and S140. Upon those, serine 100 was one of the most prominently modified sites in the whole screen being more than 9-fold downregulated in its phosphorylation site occupancy upon DKK1 in both independent experiments. Apart from this, the known KIF2A site threonine 97, that is phosphorylated by Aurora B to exclude KIF2A from the center of the spindle in anaphase [188] was more than 2-fold upregulated. Threonine 78 and serine 140 were not significantly modified by Wnt inhibition. Based on this, we decided to focus specifically on the function of the non-characterized phospho-site S100 of KIF2A (Figure 3D). To elucidate its role in mitosis, we created a phospho-inactive mutant by substitution of the serine at position 100 by an alanine (referred to as S100A in the following). Both the KIF2A mutant and wildtype KIF2A were equally expressed (Figure 3E), however localization of KIF2A-S100A at the mitotic spindle was greatly impaired in comparison to wildtype KIF2A (Figure 3F,G), phenocopying KIF2A mislocalization upon Wnt inhibition (Figure 3A,B).

Wnt signaling activity is controlled by feedback loops, e.g. via AXIN or brachyury [40,65,66]. Therefore, I tested whether KIF2A also regulates Wnt signaling. In epistasis experiments using TOPflash assays and knockdown of LRP6 as a positive control for Wnt regulation I did not detect changes in Wnt activity on any level of the signaling cascade upon KIF2A depletion (Figure 3H), excluding a feedback mechanism of KIF2A.

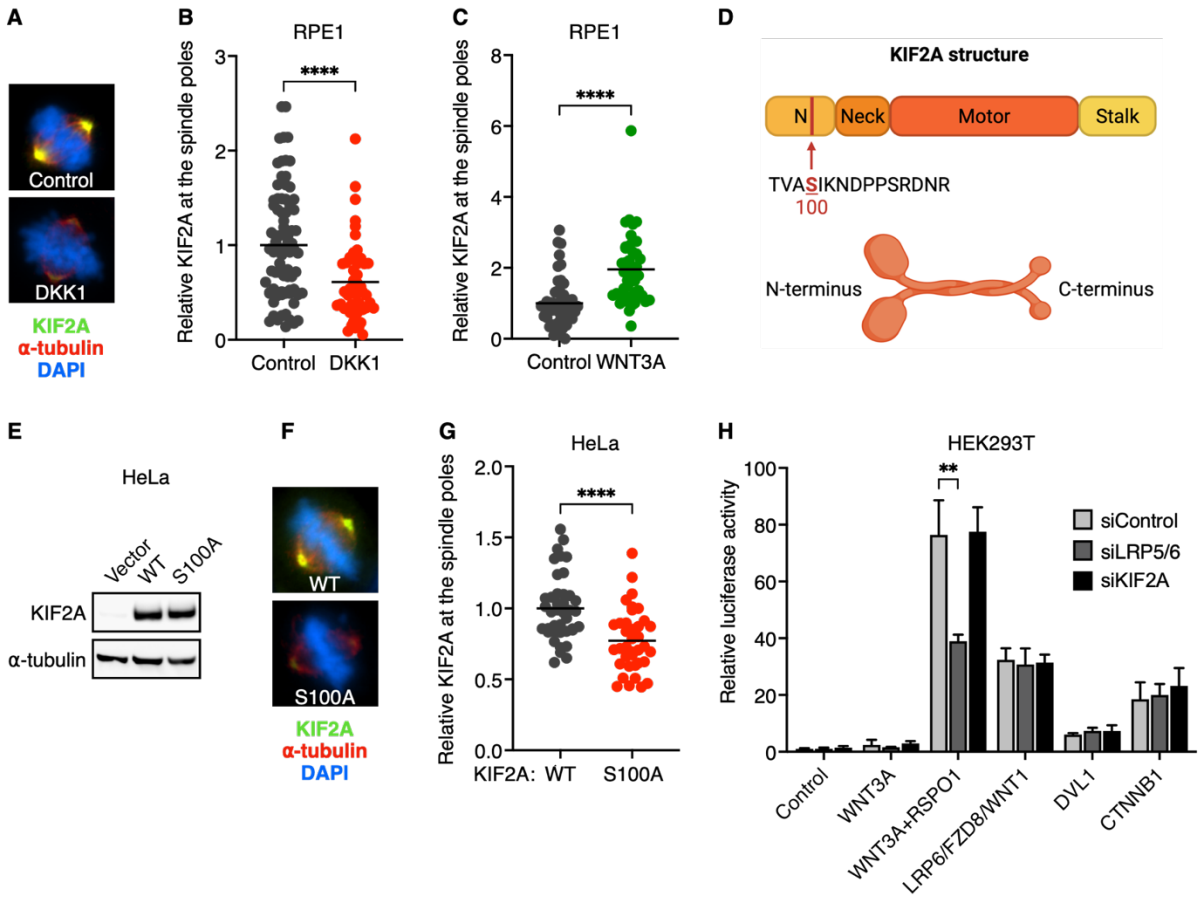

Figure 3. Wnt signaling and the phosphorylation of serine 100 are crucial for the localization of KIF2A. (A) Representative immunofluorescence images of mitotic RPE1 cells treated for 1.5 h with Control or DKK1 CM and stained for KIF2A (green), α-tubulin (red) and DNA (blue). (B),(C) Quantification of endogenous KIF2A levels at the spindle poles of mitotic RPE1 cells upon 1.5 h Control, DKK1 (B) and WNT3A (C) CM treatments. Means of n > 43 cells per condition of one out of three independent experiments (B) and n > 44 cells from n = 2 pooled experiments are shown. The imaging and analysis were done by Ana Garcia del Arco. (D) Scheme of KIF2A domains including the peptide sequence encompassing the phospho-site S100 (top) and sketch of a typical kinesin structure with its N- and C-terminal ends (bottom). (E) Representative Western blots of full lysates from HeLa cells transfected with empty vector, *EGFP-KIF2A WT* or *EGFP-KIF2A S100A*. (F) Representative immunofluorescence images of mitotic HeLa cells transfected with *EGFP-KIF2A WT* or *S100A* (green), stained for α-tubulin (red) and DNA (blue). (G) Quantification of overexpressed *EGFP-KIF2A WT* or *S100A* levels at the spindle poles. Means of n > 61 cells per condition of one experiment from n = 3 independent experiments are shown. (H) TOPflash reporter assays of HEK293T cells transfected with control, LRP5/6 or KIF2A siRNA and treated with Control, WNT3A and RSPO1 or transfected with *LRP6*, *FZD8*, *WNT1*, *DVL1* and *CTNNB1* as indicated. Means with SD of ≥ 3 biological replicates are shown.

3.2.2 KIF2A is recruited via DVL, which is supported by LRP6 signalosome formation

In a next step I aimed to understand at which level of the Wnt signaling cascade KIF2A is regulated. For this purpose, I employed proximity ligation assays (PLA) in HeLa cells. In brief, I overexpressed *EGFP-KIF2A* and one *FLAG*-tagged component of the Wnt pathway and used primary antibodies against EGFP and FLAG for the detection in all overexpression experiments to exclude differences based on the binding affinity or quality of the antibodies. Upon addition of specific oligonucleotide-coupled secondary antibodies (PLA probes), if the two proteins were in close proximity, connector oligos ligated and created circular DNA that was amplified, inducing complementary oligos labelled with fluorophores to hybridize with the amplified DNA[286]. The red PLA signals thus corresponded to in situ complexes of the two targeted proteins and reflected the localization of interaction. At this, as expected, KIF2A was in close proximity to WDR5, a protein that was shown to recruit KIF2A and hence served as a positive control for the PLA experiment[186] (Figure 4A,B). However, the highest number of KIF2A-PLA complexes I observed with DVL2 and AXIN1 (Figure 4A,B). The red signals emanating from the KIF2A-DVL2 interaction were localized in the cytoplasm, whereas KIF2A-AXIN1 complexes were concentrated at the spindle poles (Figure 4A). The interaction of DVL2 with KIF2A was positively regulated by Wnt signaling, showing an increase upon WNT3A treatment and decrease in PLA signals upon DKK1 exposure (Figure 4C). For the AXIN1-KIF2A interaction I was not able to show such a relation (data not shown). Upon expression of *KIF2A* with *GSK3β*, *CK1ε*, *β-TrCP* and *β-catenin* (*CTNNB1*) there was no increase in PLA signals compared to the control condition (Figure 4A,B).

DVL and AXIN, which were shown to interact with KIF2A in PLAs, are components of the LRP6 signalosome, which consists of WNT3A, LRP6, FZD8, AXIN1 and DVL2 and is internalized upon Wnt ligand binding, supporting Wnt pathway activation[31]. Overexpression of the complete LRP6 signalosome not only boosted Wnt signaling activation in TOPflash assays (Figure 4D), but also the interaction of DVL with KIF2A in PLAs (Figure 4E,F). I could additionally support the Wnt-promoted interaction of DVL with KIF2A by endogenous PLAs showing that the DVL-KIF2A interaction was detectable in non-overexpressing conditions and diminished upon knockdown of KIF2A or DVL1-3 as well as Wnt inhibition by DKK1 (Figure 4G,H).

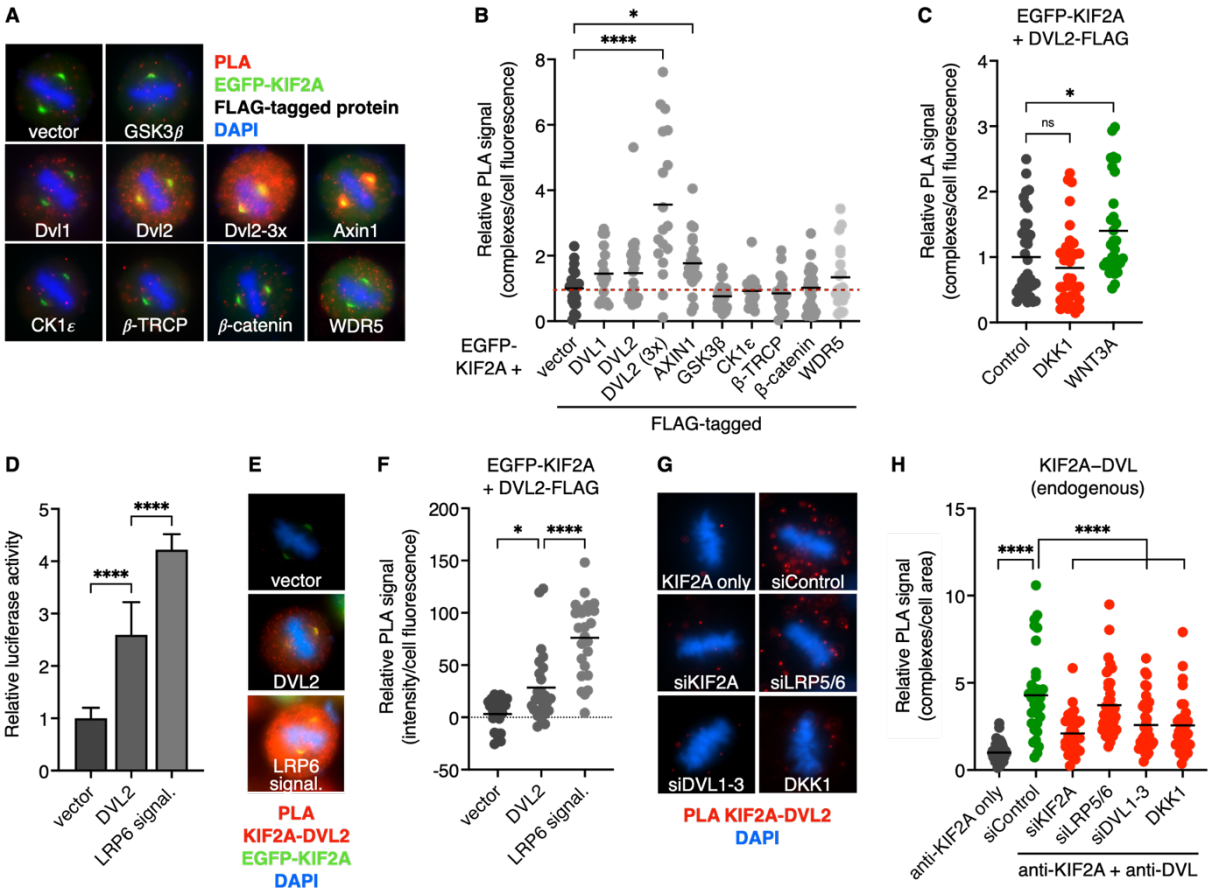

Figure 4. DVL interacts with KIF2A, which is supported by active Wnt signaling. (A) Representative immunofluorescence images of proximity ligation assays (PLAs) in mitotic HeLa cells transfected with *EGFP-KIF2A* (green) and a *FLAG*-tagged Wnt protein as indicated (3x = 3xFLAG). Primary antibodies against EGFP and FLAG were employed for the PLA (red) and DNA was stained with DAPI (blue). (B) Quantification of PLA signal from *A* normalized to empty vector. Means of n ≥ 16 mitotic cells per condition are shown. (C) Quantification of PLA signal of HeLa cells transfected with *EGFP-KIF2A* and *DVL2-FLAG* and treated for 1.5 h with Control, DKK1 or WNT3A CM. Primary antibodies against EGFP and FLAG were employed for the PLA and values were normalized to the control. Means of n > 31 mitotic cells per condition are shown. (D) TOPflash reporter assays of HeLa cells transfected with empty vector, *DVL2* or all LRP6 signalosome components (*LRP6*, *FZD8*, *AXIN1, DVL2* and treated with WNT3A CM). Means with SD of 6 biological replicates are shown. (E) Representative immunofluorescence images of PLAs in mitotic HeLa cells transfected with *EGFP-KIF2A* (green) and either empty vector, *DVL2-FLAG* or the whole LRP6 signalosome (*LRP6*, *FZD8*, *AXIN1, DVL2-FLAG*, treatment with WNT3A CM). Primary antibodies against EGFP and FLAG were employed for the PLA (red) and DNA was stained with DAPI (blue). (F) Quantification of PLA signal from *E* normalized to empty vector. Means of n ≥ 23 mitotic cells per condition are shown. (G) Representative immunofluorescence images of endogenous PLAs in mitotic HeLa cells transfected with control siRNA, siKIF2A, siLRP5/6 or siDVL1-3, or treated with DKK1 for 1.5 h. Primary antibodies against KIF2A and DVL2 were employed for the PLA (red) and DNA was stained with DAPI (blue). As a control, KIF2A

antibody was used alone. (H) Quantification of PLA signal from *G* normalized to the control condition, in which only one antibody was added. Means of n ≥ 27 mitotic cells per condition are shown from one out of two independent experiments.

In addition to the PLA assays, I analyzed the localization of overexpressed KIF2A and DVL in immunofluorescence experiments. Under normal conditions, KIF2A was mainly localized in the nucleus in interphase. However, upon *DVL2* overexpression KIF2A was recruited to cytoplasmic puncta, which are specific protein assemblies that were shown previously to form upon *DVL* overexpression and have similarity to LRP6 signalosomes[31,287] (Figure 5D and [285]). As these interphase puncta seemed to be hubs of co-localization, we employed them to investigate which domains of KIF2A were interacting with DVL. For this, I created truncation mutants of *EGFP-KIF2A* (Figure 5A) and verified the constructs by PCR (data not shown) as well as Western blotting (Figure 5B). Once the constructs were proven correct, they were overexpressed together with *DVL2-FLAG* in HeLa cells and KIF2A-DVL co-localization was analyzed by Sergio P. Acebrón (Figure 5C,D). In summary, in the absence of the C-terminal Stalk domain (KIF2A ΔSTALK) and Neck domain (KIF2A ΔNECK) KIF2A was still recruited to DVL puncta (Figure 5C,D). Contrasting this, upon deletion of the N-terminal domain (KIF2A ΔN), Motor domain (KIF2A ΔMOTOR and KIF2A N only) or expression of the phospho-inactive *KIF2A-S100A* mutant, the localization of KIF2A in cytoplasmic puncta was eliminated and KIF2A concentrated mainly in the nucleus (Figure 5C,D; detailed results are available in [285]). These findings suggest that both the Motor domain as well as the KIF2A-S100 site located in the N-terminal domain are necessary for the interaction between DVL and KIF2A.

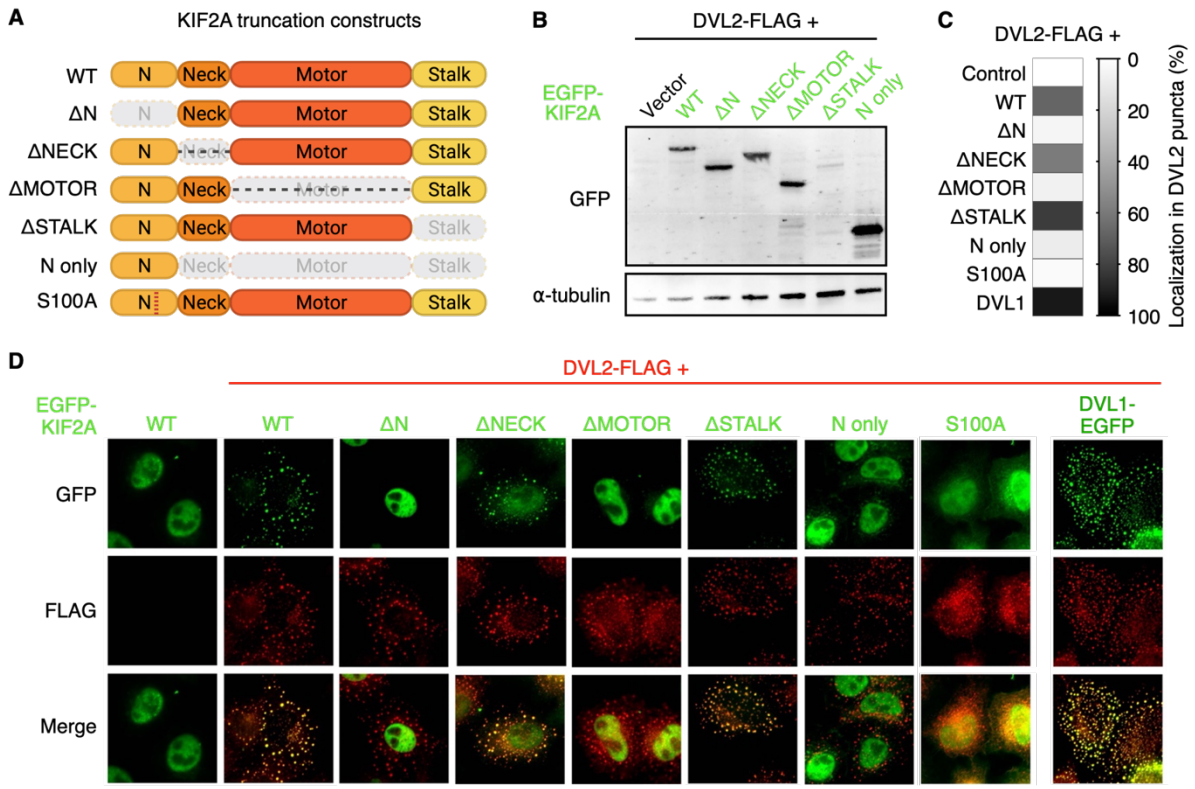

Figure 5. DVL recruits KIF2A via its Motor domain and the S100 site of its N-terminal domain. (A) Scheme of KIF2A truncation mutants that were created for the following experiments. The deleted domains a marked in grey. (B) Representative Western blots of full lysates from HeLa cells transfected with *DVL2-FLAG* and empty vector, *EGFP-KIF2A WT* or one of the truncation mutants displayed in *A*. (C) Graphical summary of immunofluorescence experiments in interphase HeLa cells transfected with *DVL2-FLAG* and either *EGFP-KIF2A WT,* the truncation mutants displayed in *A*, or *DVL1-EGFP*. In the control, only *EGFP-KIF2A WT* was expressed omitting *DVL2-FLAG* co-expression. KIF2A or DVL1 co-localization in DVL2 puncta was quantified and is displayed as the mean of 3 independent experiments with n ≥ 20 cells per condition. Data was adapted from Bufe et al., 2021[285]. (D) Representative immunofluorescence images of HeLa cells transfected with *DVL2-FLAG* (red) and either *EGFP-KIF2A WT,* the truncation mutants from *A* or *DVL1-EGFP* (green). The analyses and imaging of the co-localization (*C* and *D*) were performed by Sergio P. Acebrón and can be found in Bufe et al., 2021[285].

3.2.3 Wnt signaling and signalosome formation support the KIF2A-PLK1 interaction

As outlined previously, the detected S100 site of KIF2A was modified in its phosphorylation both in our screen upon Wnt inhibition (Figure 2A,E) as well as upon PLK1 inhibition in a screen performed by the Nigg laboratory[201]. Besides, PLK1 is known to regulate KIF2A via the phosphorylation of multiple sites to guide its localization and activity at microtubules[112,185,200] and associates with DVL in mitosis[231]. Based on this, I investigated whether the interaction of PLK1 with KIF2A is affected by Wnt signaling. Using endogenous PLAs, I observed that the signal evoked by KIF2A in proximity with PLK1 was reduced upon knockdown of *KIF2A*,

LRP5/6 or *DVL1-3*, inhibition of Wnt signaling by DKK1, and PLK1 inhibition by BI-2536[288] (Figure 6A,B). The data was further supported by coimmunoprecipitation experiments in mitosis, in which I pulled down endogenous PLK1 in association with KIF2A (Figure 6C). Both upon PLK1 and Wnt inhibition as well as depletion of *LRP5/6* or *DVL1-3*, the amount of coprecipitated KIF2A and thereby KIF2A interaction with PLK1 was greatly impaired (Figure 6C). Additionally, in immunofluorescence analysis under overexpressing conditions, PLK1 was recruited, together with KIF2A, to DVL puncta in interphase. At this, the number of puncta containing PLK1 and KIF2A was significantly increased upon overexpression of the whole LRP6 signalosome (Figure 6D,E). The depicted results suggest that PLK1 is involved in the DVL-dependent regulation of KIF2A and possibly phosphorylation of serine 100 in mitosis, however the detected site does not fully match a typical PLK1 consensus motif[289] (Figure 6F). Therefore, another kinase or multiple kinases, that function downstream of PLK1 to regulate the phosphorylation of serine 100, may be involved, which remains to be identified.

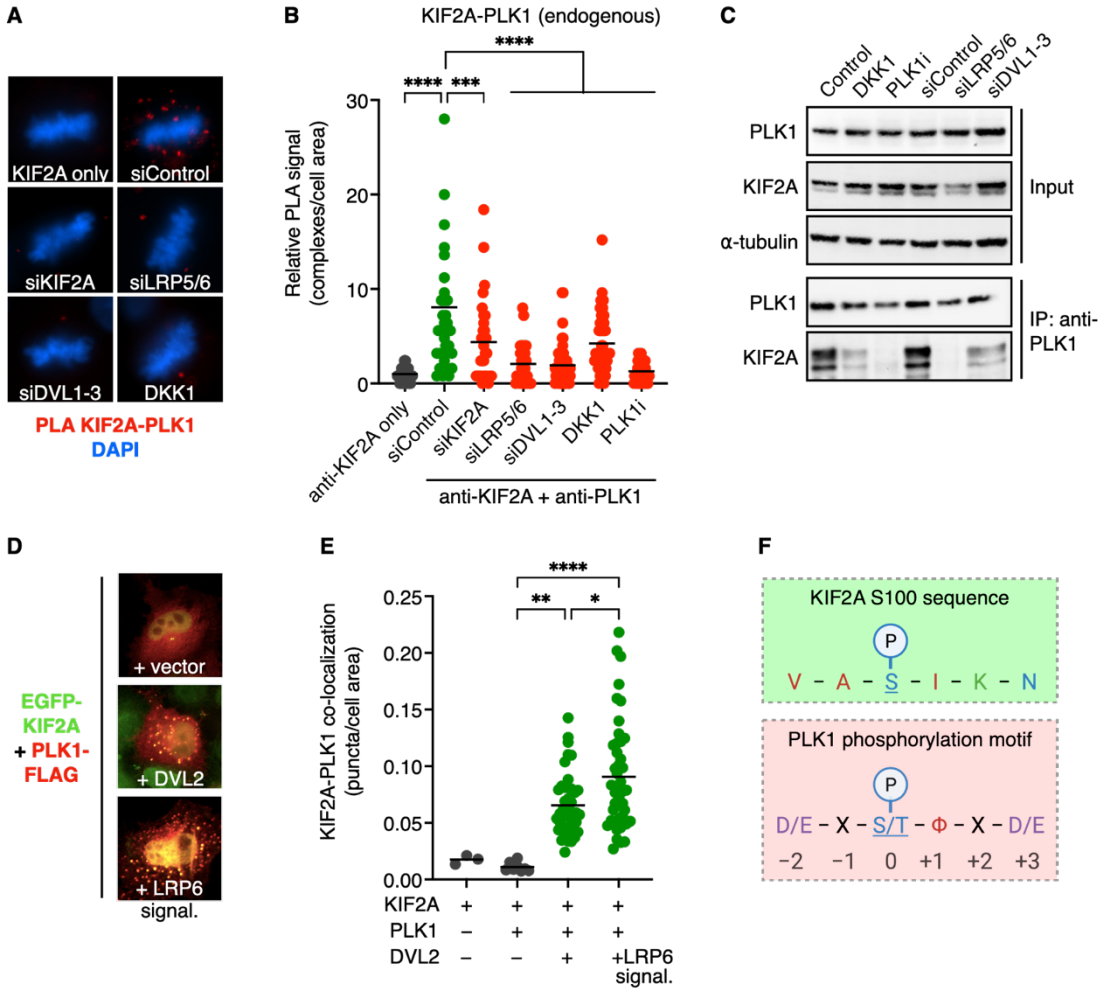

Figure 6. Active Wnt signaling supports KIF2A-PLK1 interaction and its recruitment to DVL puncta. (A) Representative immunofluorescence images of endogenous PLAs in mitotic HeLa cells transfected with

control siRNA, siKIF2A, siLRP5/6 or siDVL1-3, or treated with DKK1 for 1.5 h. Primary antibodies against KIF2A and PLK1 were employed for the PLA (red) and DNA was stained with DAPI (blue). As a control, KIF2A antibody was applied alone (KIF2A only). (B) Quantification of PLA signals upon transfections and treatments from *A* as well as upon PLK1 inhibitor BI-2536 (PLK1i) treatment, normalized to the control condition. Means of n ≥ 29 mitotic cells per condition are shown from n = 2 experiments. (C) Representative Western blots of endogenous coimmunoprecipitation of PLK1 from HeLa cells synchronized in mitosis and treated for 1.5 h with Control CM, DKK1 CM or PLK1 inhibitor, or transfected with control siRNA, siLRP5/6 or DVL1-3. N = 3 independent experiments. (D) Representative immunofluorescence images of HeLa cells in interphase transfected with *EGFP-KIF2A* (green) and *PLK1-FLAG* (red) in parallel with empty vector, *DVL2* or the whole LRP6 signalosome (*LRP6*, *FZD8*, *AXIN1, DVL2-FLAG*, treatment with WNT3A CM). (E) Quantification of colocalization of KIF2A with PLK1 in interphase puncta. Means of n = 60 cells per condition of one out of n = 2 independent experiments are shown. (F) KIF2A sequence including serine 100 (top) and PLK1 consensus motif needed for the phosphorylation of a serine or threonine at position 0 (bottom). Amino acids are color-coded: hydrophobic amino acids (red), polar (blue), acidic (purple), basic (green). For optimal phosphorylation by PLK1, a hydrophobic amino acid at position +1 and acidic amino acids at positions –2 and +3 are required.

3.2.4 Wnt signaling and KIF2A control chromosome alignment and genome stability

As demonstrated above, Wnt signaling supports KIF2A localization at the spindle and interaction with PLK1 in mitosis (Figure 3A-C, Figure 6A-C). The Wnt transducer DVL is most likely a key component of this regulation (Figure 4). As shown in previous studies, misregulation of KIF2A and PLK1 causes aberrant mitotic phenotypes, such as chromosome alignment and segregation defects[178,185,186,200,290,291]. Hence, I aimed to test whether depletion of Wnt signaling and KIF2A induce similar aberrations.

As certain siRNAs can have specific or non-specific off-target effects[195,292], I tested three independent siRNAs for KIF2A (please consult Table 4 in the methods section for more details on the siRNAs). For siLRP5/6 and siDVL1-3 I used siRNAs that were validated before. When I surveyed the siRNA-induced knockdown, I could validate that all of the used siRNAs depleted their target protein efficiently, as tested by Western blots (Figure 7A), and siKIF2A #1 and #2 as well as siLRP5/6 and siDVL1-3 reduced KIF2A levels at the mitotic spindle in IF (Figure 7B; quantification available in [285]). Knockdown of a microtubule (MT) depolymerase is expected to increase spindle length [180,188], which was observed upon depletion of DVL1-3 and two of the tested siRNAs against KIF2A (KIF2A #1 and #2), but not upon the third siRNA (siKIF2A #3[181]) and siLRP5/6 (Figure 7B; detailed analysis in [285]). On the contrary, all tested siRNAs induced chromosome alignment defects (DAPI channel in Figure 7B and

quantification in [285]), which was also observed upon PLK1 inhibition (Figure 7C,D). To understand the mechanism behind the observed problems in chromosome alignment, I analyzed possible defects in centrosome numbers and spindle multipolarity, as both can lead to chromosome alignment problems and lagging chromosomes[293,294], and as Ganem & Compton reported that KIF2A is important for bipolar spindle assembly[181,284]. Therefore, I knocked down KIF2A, LRP5/6 or DVL1-3 in HeLa cells, synchronized cells in metaphase and inhibited EG5 (KIF11), which induces monopolar spindles in metaphase only if a component of spindle maintenance is impaired (protocol modified from Tanenbaum et al., 2009[195]). As a positive control I depleted cells of kinesin family member 2C (KIF2C), which is known to be important for spindle bipolarity[195]. Upon transfection with siLRP, siDVL and two of the siKIF2As (#1 and #2), we did not observe an increase in monopolar spindles, but with the siRNA reported by the Compton laboratory (siKIF2A #3[181]) or siKIF2C the number of cells failing to assemble a bipolar spindle increased (Figure 7E). Notably, the KIF2A siRNA from Ganem & Compton also resulted in a higher rate of cell death during the experiment (data not shown). In contrast, none of the tested siRNAs induced centrosome multiplication (Figure 7F). The increased number of dead cells, induction of monopolar spindles and invariable spindle length upon siKIF2A #3 [181] suggests that this siRNA may regulate other components of spindle formation and dynamics apart from KIF2A and hence causes off-target effects, as indicated by Tanenbaum et al.[195]. In the further course of our work, we therefore used one of the two specific siRNAs, namely siKIF2A #1, which depleted KIF2A efficiently and induced both an increase in spindle length and chromosome misalignment.

In summary, upon knockdown of KIF2A with two independent siRNAs and knockdown of the Wnt signalosome component DVL, I observed reduced KIF2A levels, problems in the alignment of chromosomes at the metaphase plate and an increase in pole-to-pole distance in mitosis (Figure 7B and further analyses by Sergio P. Acebrón, which are provided in Bufe et al., 2021[285]). Chromosome alignment defects were phenocopied by inhibition of the kinase PLK1, which is known to localize KIF2A at the mitotic spindle (Figure 7C,D). The results are in line with the previously reported roles of KIF2A and PLK1[178,185,186,188,200].

Chromosome alignment defects in mitosis can lead to lagging chromosomes, which are a common cause for chromosomal instability (CIN)[160,295]. Such chromosome segregation problems were also observed upon Wnt depletion or inhibition, leading to aneuploidy both in somatic and stem cells[52,53,79]. However, in recent work by Fonseca et al. it was revealed that chromosome misalignment does not predefine CIN, as knockdown of the kinesin KIF18A induced severe chromosome alignment defects in mitosis but resulted in normal euploid cells[296]. Though, when I analyzed, in collaboration with the Bastians group, the karyotype of

RPE1 cells that were depleted of KIF2A or LRP5/6 over 30 days, I detected a clear increase in chromosome copy numbers varying from a normal karyotype of 46 chromosomes. About 70% of KIF2A and LRP depleted cells displayed an aneuploid karyotype in contrast to 25% in the control condition (Figure 7G,H). These data indicate that the defects that we detected upon knockdown of KIF2A, LRP and DVL in mitosis may lead to successive problems during cell cycle progression and eventually genomic instability.

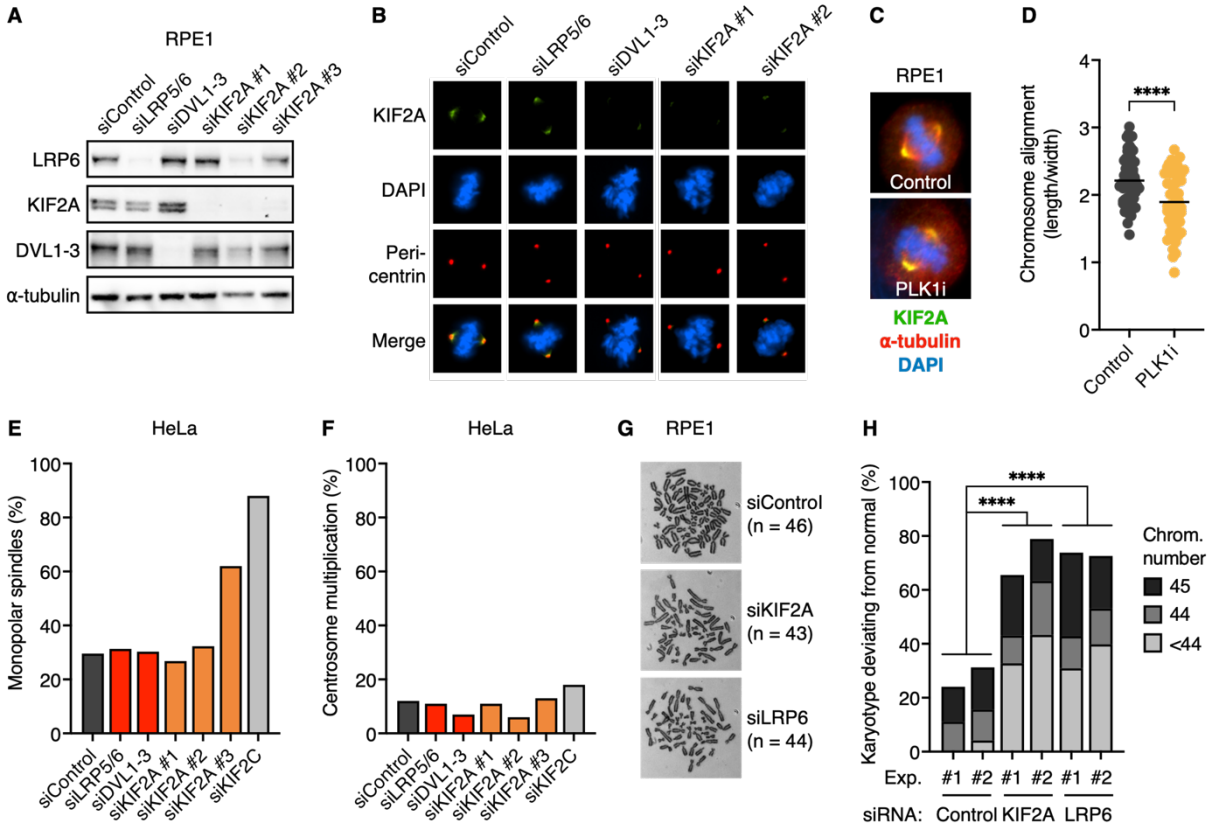

Figure 7. KIF2A and Wnt signaling ensure correct chromosome alignment in mitosis. (A) Representative Western blots of full lysates from RPE1 cells transfected with control siRNA, siLRP5/6, siDVL1-3 and three different siRNAs against KIF2A. N = 2 independent experiments. (B) Representative immunofluorescence images of mitotic RPE1 cells transfected with siControl, siLRP5/6, siDVL1-3, siKIF2A #1 or siKIF2A #2, and stained for KIF2A (green), DNA (blue) and pericentrin (red). Images are adopted from Bufe et al., 2021 and quantifications of KIF2A levels, spindle length and chromosome alignment were done by Sergio P. Acebrón and can be found in the named publication[285]. (C) Representative immunofluorescence images of mitotic RPE1 cells treated with PLK1 inhibitor (BI-2536, 10 nM) for 1.5 h and stained for KIF2A (green), α-tubulin (red) and DNA (blue). (D) Quantification of chromosome alignment, measured as length of the forming metaphase plate versus its width towards the poles, from *C*. Means of n ≥ 52 cells per condition are shown. (E,F) Quantification of the occurrence of monopolar spindles (E) and supernumerary centrosomes (F) in HeLa cells transfected with the indicated siRNAs, synchronized in metaphase by MG132 and treated with the EG5 inhibitor DME.

Means of n = 100 cells per condition from n = 2 independent experiments are shown. (G) Representative microscopy images of metaphase spreads from RPE1 cells transfected every 5 days over 30 days with control siRNA, siKIF2A #1 or siLRP6. The regular karyotype of RPE1 cells is composed of 46 chromosomes. (H) Quantification of aneuploid karyotypes displaying < 46 chromosomes after 30 days depletion of control, KIF2A or LRP6. Percentage of cells with aberrant karyotypes from 50 metaphase spreads per condition and 2 experiments (Exp. #1 and #2) are shown. The experiment and analysis were performed in collaboration with the Bastians laboratory.

3.2.5 Wnt signaling and KIF2A ensure the timing and correct progression of mitosis

To validate the defects in chromosome alignment that I saw in fixed mitotic cells and their consequences in the further progression of mitosis, I performed live cell imaging experiments in HeLa-Kyoto cells stably transfected with *EGFP-α-tubulin* and *H2B-mCherry*. In this, I observed an increase in mitotic timing from chromosome condensation until cytokinesis upon Wnt inhibition, which especially arose from a prominent delay in metaphase (Figure 8A). I noticed that the detected delays often emerged from a lag or even failure in aligning the chromosomes at the metaphase plate as well as from the formation of multipolar spindles (Figure 8B,C). Both the delays and phenotypes in mitosis were decreased upon WNT3A treatments in comparison to the control situation, indicating that Wnt signaling supports the correct completion of mitosis (Figure 8C).

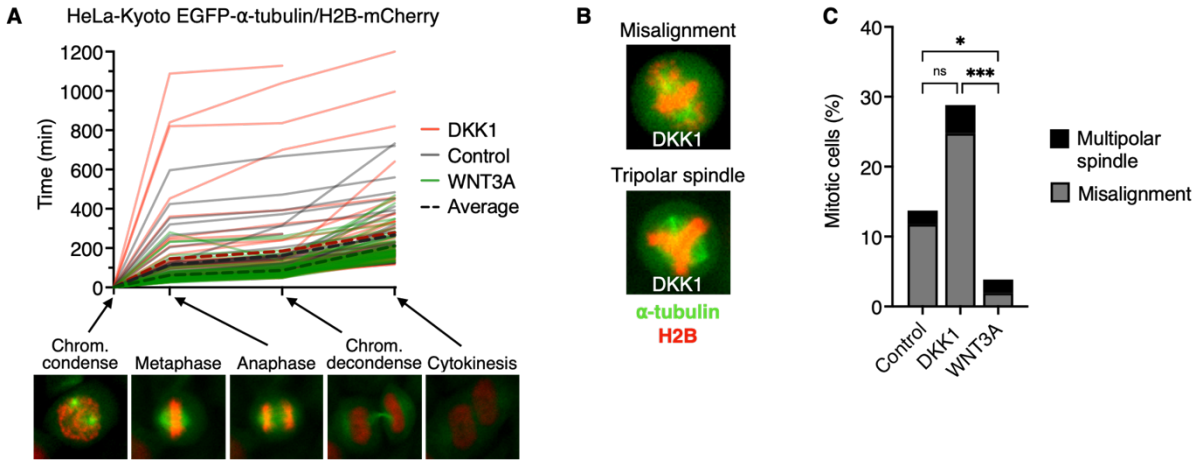

Figure 8. Basal Wnt signaling guides the timely and correct completion of mitosis by regulating metaphase. (A) Tracking of mitotic progression from chromosome condensation (nuclear envelope breakdown (NEB)) until cytokinesis of n ≥ 41 HeLa-Kyoto EGFP-α-tubulin/H2B-mCherry cells per condition, that were treated with Control, DKK1 or WNT3A CM just before imaging. All single cells as well as the average timing of the different stages are displayed. Representative immunofluorescence images of the mitotic phases, at which the time points were taken, are depicted below. (B)

Representative images of the chromosome misalignment and multipolar spindle phenotype in HeLa-Kyoto EGFP-α-tubulin (green)/H2B-mCherry (red) cells treated with DKK1 CM. (C) Quantification of the occurrence of chromosome misalignments and multipolar spindles upon Control, DKK1 or WNT3A treatments in ≥ 49 mitotic HeLa-Kyoto EGFP-α-tubulin/H2B-mCherry cells per condition.

To resolve which aberrant phenotypes are responsible for the delay in mitosis and track how cells, which face mitotic errors upon Wnt or KIF2A depletion, end up, I repeated the live cell imaging analysis, recording more details, namely the time spent in mitosis (nuclear envelope breakdown (NEB) until anaphase), metaphase defects (mild or severe misalignments and multipolar spindles), anaphase defects (lagging chromosomes, chromosome bridges) and the fate of the diving cells (division into more than 2 daughter cells, binuclear daughter cells, occurrence of micronuclei or cell death/apoptosis). Upon knockdown of KIF2A, LRP5/6 and DVL1-3, cells showed an increase in mitotic timing (Figure 9A,B), which was accompanied, similar as upon Wnt inhibition (Figure 8), by the appearance of aberrant phenotypes, including multipolar spindles and chromosome alignment problems (Figure 9A). The misalignment of chromosomes was categorized into two groups, reaching from I) mild alignment problems with the chromosomes being slightly wider spread at the forming metaphase plate, but still in contact with each other and II) severe alignment problems, showing single or multiple chromosomes being clearly detached from the centrally forming metaphase plate before anaphase (Figure 9C). Both types were increased upon knockdown of KIF2A, LRP5/6 and DVL1-3 (Figure 9D). Besides, I detected a slight increase in multipolar spindles upon KIF2A and Wnt knockdown (Figure 9D), however as these effects were not consistent throughout all experiments that I performed, I focused on the chromosome alignment problems in the further course of this work.

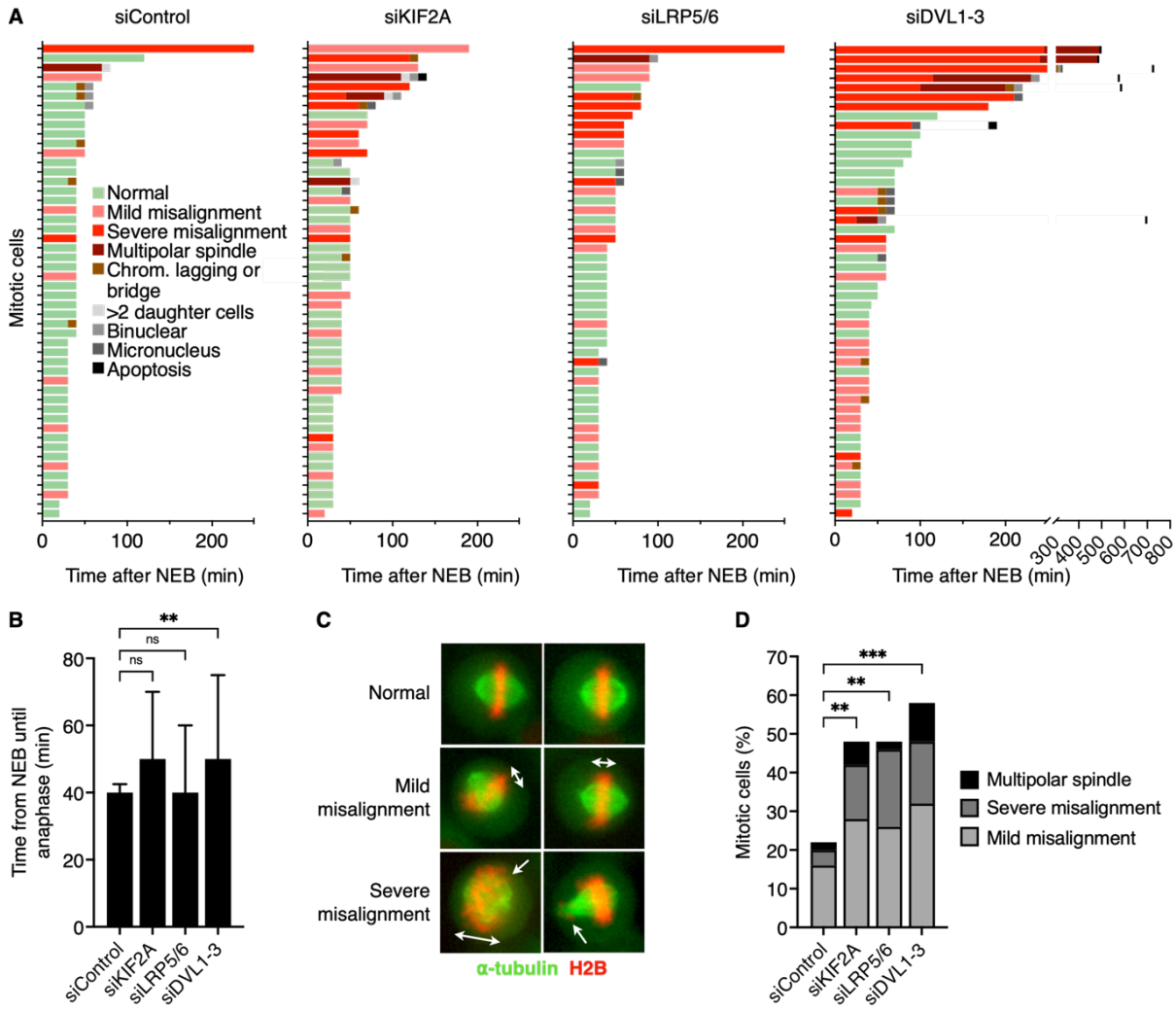

Figure 9. Depletion of mitotic Wnt signaling or KIF2A leads to mitotic delays, which are driven by chromosome alignment defects and can result in consequential errors. (A) Tracking of mitotic progression from nuclear envelope breakdown (NEB) and chromosome condensation until anaphase in line with metaphase phenotypes and their consequences in n = 50 single HeLa-Kyoto EGFP-α-tubulin/H2B-mCherry cells transfected with siControl, siKIF2A, siLRP5/6 or siDVL1-3. (B) Quantification of mitotic timing (NEB until anaphase) of HeLa-Kyoto cells from *A*. Medians with interquartile range of n = 50 cells per condition are shown. (C) Representative immunofluorescence images of mitotic HeLa-Kyoto EGFP-α-tubulin (green)/H2B-mCherry (red) cells from *A* showing aligned chromosomes (normal), mild misalignment or severe misalignment in metaphase. (D) Quantification of the most common aberrant phenotypes (illustrated in *C* and *Figure 8B*) upon siKIF2A, siLRP5/6 and siDVL1-3 from *A*. Proportions of n = 50 mitotic HeLa-Kyoto cells per condition are shown.

To rule out misinterpretations of the alignment of chromosomes due to differently oriented cells and further validate my results, I repeated the live imaging with HeLa-Kyoto EB3-EGFP cells. EB3 (or MAPRE3) is located at the plus-ends of MTs and thereby enables the visualization of the poles of the mitotic spindle to ensure that only non-tilted cells are

considered. To visualize chromosomes, I labelled the cells with the live cell DNA probe SiR-DNA one hour before imaging (Figure 10A). HeLa-Kyoto EB3-EGFP cells showed a similar increase in chromosome misalignment and metaphase delay upon Wnt inhibition by DKK1 treatment and knockdown of KIF2A, LRP5/6 or DVL1-3 as the HeLa-Kyoto EGFP-α-tubulin/H2B-mCherry cell line (Figure 10A-E). In about 20% of cells, in which Wnt signaling was inhibited, and 4-12% of cells depleted of KIF2A, LRP and DVL, the observed problems in chromosome alignment even led to an arrest in mitosis (Figure 10A-E).

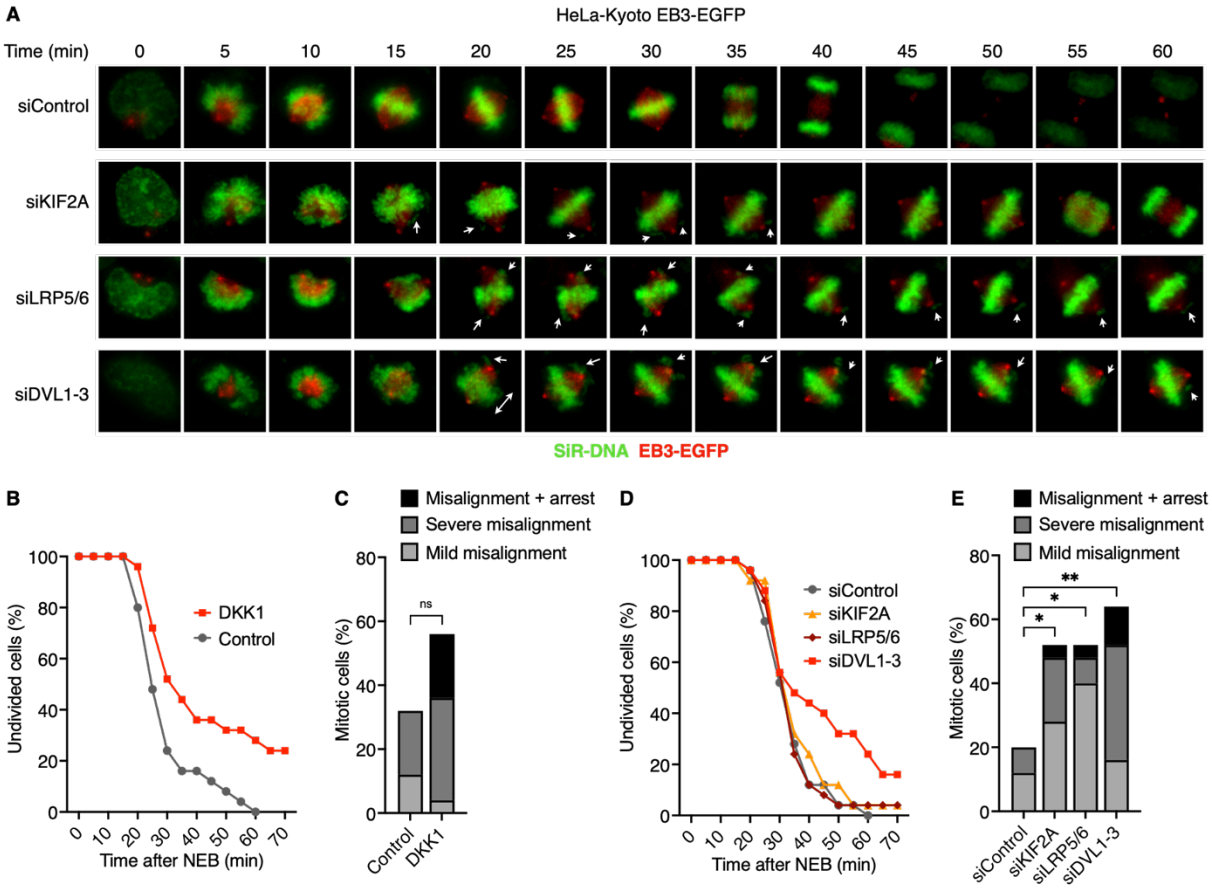

Figure 10. Wnt signaling and KIF2A support the proper alignment of chromosomes and timely progression through mitosis. (A) Representative fluorescence time lapse images of mitotic HeLa-Kyoto EB3-EGFP cells, transfected with siRNA against control, KIF2A, LRP5/6 or DVL1-3. Chromosomes were stained with SiR-DNA (displayed in green) before imaging. Expressed EB3-EGFP is presented in red. (B,D) Quantification of mitotic progression from nuclear envelope breakdown (NEB) until anaphase upon Wnt inhibition (*B*) or depletion of KIF2A, LRP or DVL (*D*) of 25 cells per condition. (C,E) Quantification of chromosome alignment defects in HeLa-Kyoto EB3-EGFP cells, treated with DKK1 or transfected with siControl, siKIF2A, siLRP5/6 or siDVL1-3, before the onset of anaphase. N = 25 cells per condition are shown.

3.2.6 Wnt signaling ensures timely chromosome alignment during mitosis via KIF2A

Proceeding from the chromosome alignment defects I obtained by live cell imaging upon the depletion of Wnt signaling or KIF2A in HeLa cells (Figure 8-10), I next aimed to validate my results in fixed cells and rescue the aberrations using IF analysis. For this purpose, I employed the length versus width ratio of the chromosomes in the centrally forming metaphase plate as a readout to assess the efficiency of chromosome alignment. In so doing, I detected that the length versus width ratio of the metaphase plate was significantly reduced upon depletion of KIF2A and LRP5/6 or inhibition of Wnt signaling by DKK1, indicating an increase in chromosome misalignment (Figure 11B-G). To test the dependency of the observed phenotype on KIF2A and assure that no off-target effects were caused by the used siRNA, siKIF2A resistant constructs of *KIF2A WT* and *S100A* were created by me and Anja Ciprianidis (Figure 11A and methods section 6.2.4.1). The ectopic expression of siRNA-resistant *EGFP-KIF2A*^{R} rescued the siKIF2A-induced defects in mitotic chromosome alignment, confirming the specificity of the used siRNA (Figure 11B,C). In contrast, *EGFP-KIF2A S100A*^{R} expression did not compensate the chromosome misalignments (Figure 11B,C). Similarly, wildtype *EGFP-KIF2A* rescued the elevated ratios of chromosome misalignment upon siLRP5/6 and Wnt inhibition in mitosis, whereas the phospho-inactive mutant *KIF2A S100A* failed to do so (Figure 11D-G).

These results confirmed that the mitotic aberrations that I observed were mediated by Wnt signaling via KIF2A and that the phosphorylation of serine 100 in KIF2A is relevant for the correct alignment of chromosomes during metaphase.

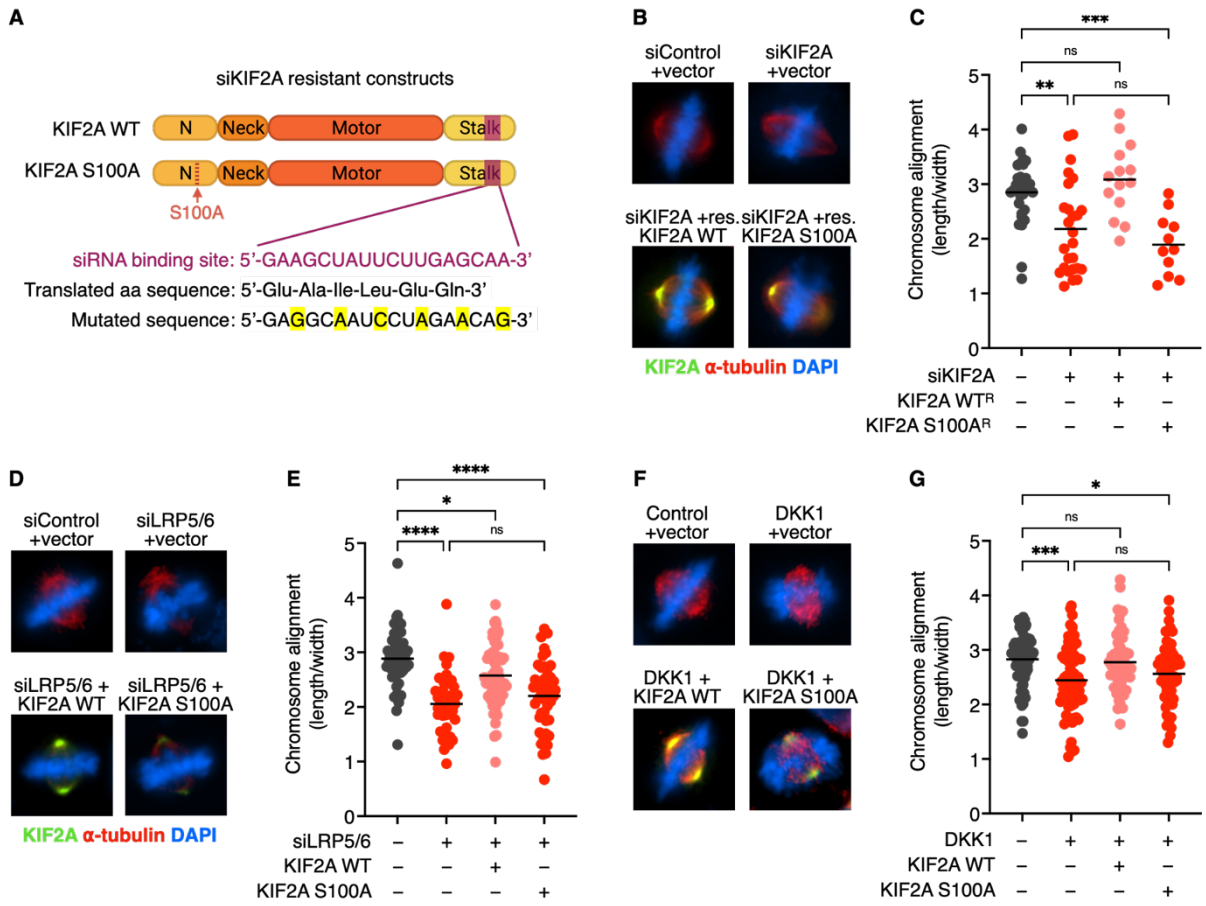

Figure 11. Mitotic Wnt signaling regulates chromosome alignment through KIF2A. (A) Scheme of siKIF2A resistant mutants that were created for *B,C*. The third base of each triplet included in the siRNA bound sequence was modified without changing the encoded amino acid. (B,D,F) Representative immunofluorescence images of mitotic HeLa cells transfected as indicated with siControl, siKIF2A or siLRP5/6, treated for 1.5 h with Control or DKK1 CM, and transfected with empty vector, siKIF2A-resistant *EGFP-KIF2A WT/S100A*^{R} or non-modified *EGFP-KIF2A WT/S100A*. Cells show overexpressed *EGFP-KIF2A* (green) and were stained for α-tubulin (red) and DNA (blue). (C,E,G) Quantification of chromosome alignment from *B*, *D* and *F*, measured by the length of the forming metaphase plate versus its width towards the spindle poles. Means of n ≥ 11 cells (*C*), n ≥ 49 cells (*E*) and n ≥ 55 cells (*G*) per condition of one out of n ≥ 2 independent experiments are shown.

3.2.7 Wnt signaling ensures chromosome alignment via KIF2A, also in stem cells

As Wnt signaling is important for stem cell self-renewal, maintenance, and differentiation [19,297], I next tested whether the revealed regulation of chromosome alignment by mitotic Wnt signaling via KIF2A also holds true for stem cells.

As expected, human induced pluripotent stem cells (hiPSCs) responded to Wnt pathway activation by WNT3A and RSPO3 treatments as well as Wnt inhibition by DKK1 (Figure 12B). Using live cell imaging, I observed that the number of hiPSCs showing misaligned

chromosomes and a delay in mitosis increased upon inhibition of endogenous Wnt signaling by DKK1 (Figure 12A,C,D). The chromosome alignment defects upon Wnt inhibition were confirmed by IF experiments, enabling us to analyze a higher number of cells, which was done by Anchel de Jaime Soguero and discussed in Bufe et al., 2021[285]. The defects as well as the delay in mitosis could be rescued by ectopic expression of *EGFP-KIF2A*, both in live and fixed cells (Figure 12A,C,D; IF results are available in Bufe et al., 2021[285]). This indicates that, also in stem cells, Wnt signaling modulates KIF2A to enable the correct alignment of chromosomes and progression through mitosis.

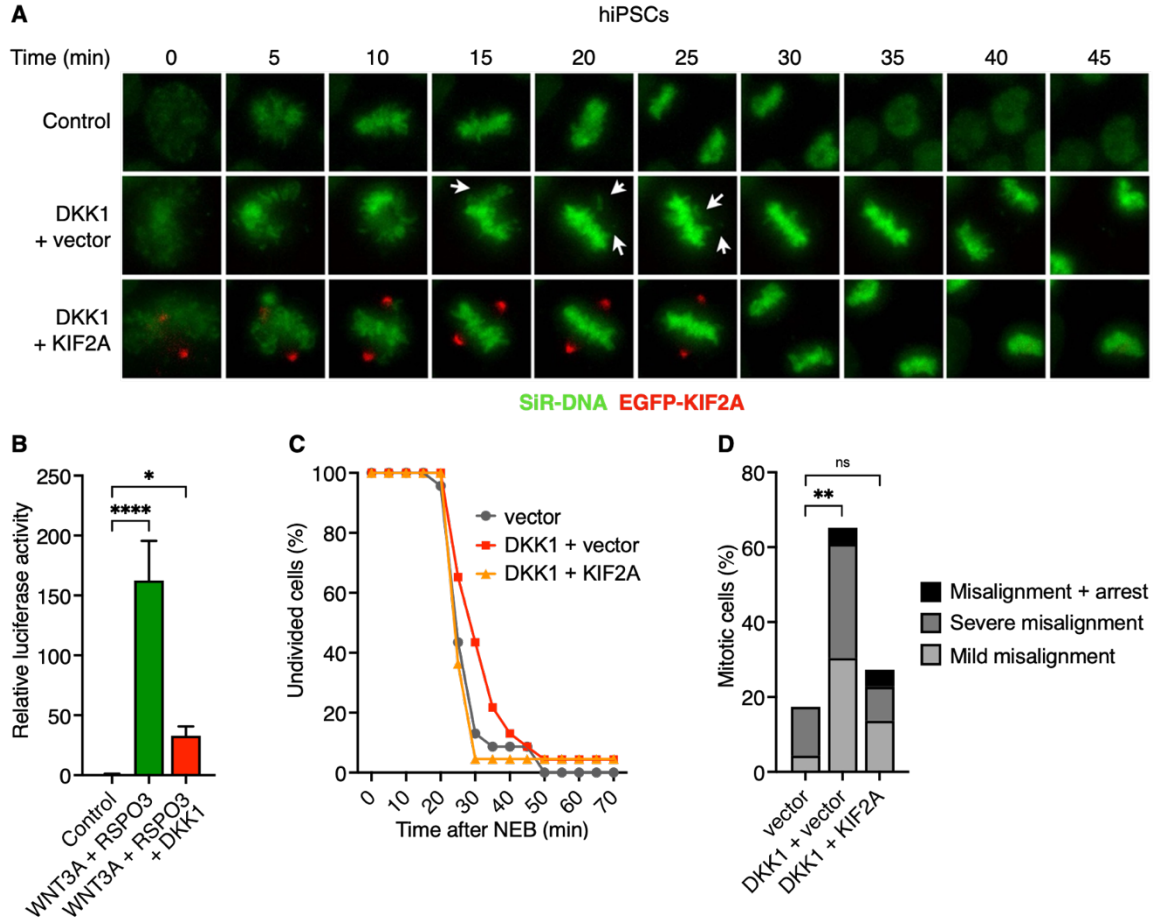

Figure 12. Wnt signaling promotes chromosome alignment through KIF2A in pluripotent stem cells. (A) Representative fluorescence time lapse images of mitotic human induced pluripotent stem cells (hiPSCs) transfected with empty vector or *EGFP-KIF2A* (red), treated with Control or DKK1 CM overnight and stained with SiR-DNA (green) just before imaging. (B) TOPflash Wnt reporter assays of hiPSCs treated with Control, WNT3A + RSPO3 and DKK1 CM as indicated. Means with SD of 5 biological replicates are shown. (C) Quantification of mitotic progression and completion of cell division of 22-23 hiPSCs per condition from *A*. (D) Quantification of chromosome alignment defects of 22-23 mitotic hiPSCs per condition from *A*.

Finally, my work provides a link explaining how a misregulation of Wnt signaling can lead to mitotic aberrations. I propose that the Wnt scaffolding protein DVL localizes the mitotic kinesin KIF2A to the spindle poles in mitosis, which is supported by LRP6 signalosome formation and phosphorylation on serine 100 of KIF2A. Additionally, Wnt signaling positively regulates the interaction of KIF2A with PLK1, which ensures its localization and activity at the mitotic spindle. These regulatory mechanisms combine to assure the proper function of the MT depolymerase in mitosis and alignment of chromosomes at a central metaphase plate before chromosome segregation and cell division (Figure 13A). When this cascade is interrupted, leading to a mislocalization of KIF2A, cells face mitotic delays and may fail to align their chromosomes in metaphase, which can result in chromosome missegregation and chromosome instability (CIN) (Figure 13B).

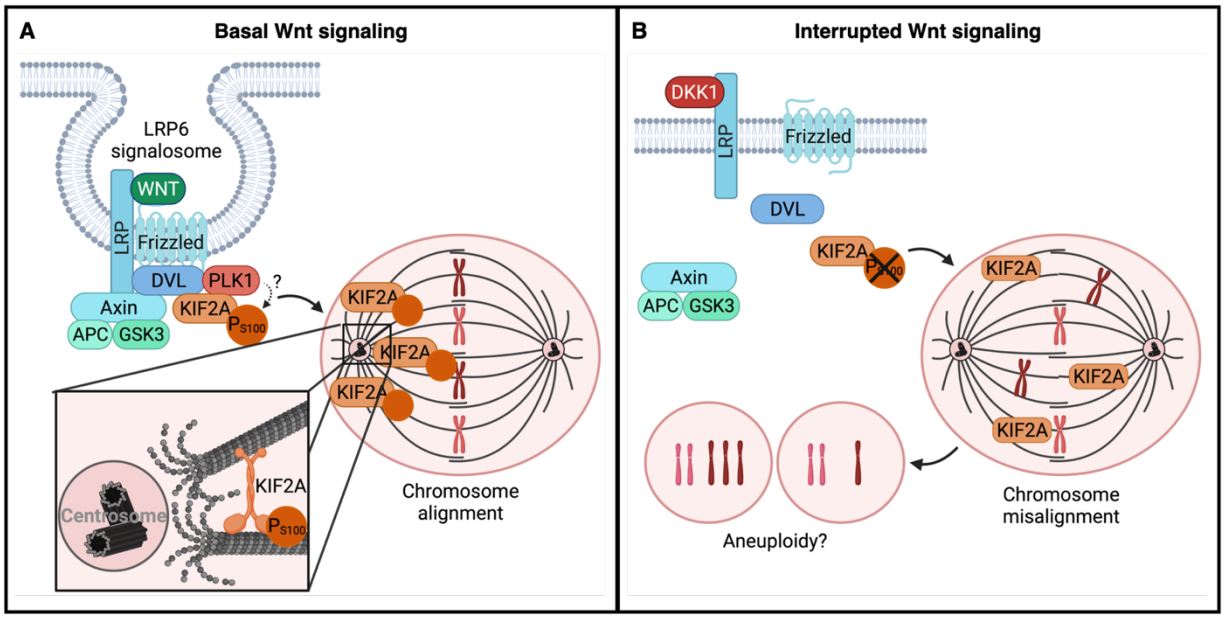

Figure 13. Active Wnt signaling assures the correct localization of KIF2A, which guides chromosome alignment in mitosis. (A) Upon binding of a canonical Wnt ligand to its receptors frizzled and LRP, DVL is recruited and LRP6 signalosomes are formed. Apart from binding to the destruction complex components AXIN, APC and GSK3, DVL binds directly to KIF2A and PLK1, supporting their interaction and the phosphorylation of KIF2A at serine 100 (P_{S100}), which directs the localization of KIF2A to the mitotic spindle poles. At the spindle poles, KIF2A depolymerizes microtubules at their minus-ends to guide faithful chromosome alignment, ensuring the correct segregation of chromosomes. (B) When Wnt signaling is interrupted, the recruitment of KIF2A to the signalosome as well as its phosphorylation at serine 100 is impaired, which disrupts its localization, thereby leading to errors in chromosome alignment and possibly aneuploidy.

3.3 Wnt signaling maintains genome stability across different cellular systems and cell cycle phases

As outlined in the previous chapter, Wnt signaling guides the progression of mitosis through the regulation of the mitotic kinesin KIF2A, which mediates the alignment of chromosomes in metaphase. Notably, the disturbance of chromosome alignment can lead to chromosome segregation defects and thereby chromosomal instability[145,253]. However, I did not observe a clear increase in chromosome segregation errors, e.g. in the form of lagging chromosomes, upon KIF2A depletion. This matches a report, where it has been indicated that KIF2A cannot reduce the rate of chromosome missegregation in chromosomally unstable cells[298]. Consistent with that, a study from Fonseca and his colleagues suggested that chromosome alignment is not a prerequisite for euploidy[296]. However, the attenuation of Wnt signaling has been shown to cause increased numbers of lagging chromosomes and aneuploidy in somatic cells as well as pluripotent stem cells[52,53,79]. Hence, other mechanisms, in addition to KIF2A modulation, may contribute to the regulation of mitosis. Therefore, in the further course of my work, I focused on validating and characterizing mitotic defects induced by Wnt inhibition and revealing what mechanisms are underlying the aberrations, especially in stem cells. In so doing, I surveyed pluripotent stem cells (hiPSCs) as well as 3D organotypic models containing adult stem cells (mouse intestinal organoids), which are highly responsive to Wnt signals[82,85-88]. Using the 3D multicellular organoids, I not only wanted to elucidate, whether the Wnt-induced effects are conserved in different cell types, but also whether cells in a physiological context might be protected from chromosome instability due to the architecture of their tissues, as suggested in the literature before[299].

3.3.1 S phase and direct mitotic effects concur to ensure genome stability in stem cells

Wnt signaling is known to drive the proliferation, self-renewal and differentiation of stem cells [2,19] and its misregulation is associated with chromosome instability (CIN)[79]. To understand which roles Wnt signaling takes in mitosis and how such aberrations arise, I analyzed mitotic hiPSCs in live cell imaging. As I observed previously, inhibition of mitotic Wnt signaling led to chromosome alignment problems through a misregulation of KIF2A, not only in somatic, but also in stem cells (Figure 12, Figure 14A, Figure 14B column 1 and 3). Besides, overnight treatments with the Wnt inhibitor DKK1 evoked chromosome segregation defects, such as chromosome bridges and lagging chromosomes in anaphase (Figure 14A,B). These results support that basal Wnt signaling facilitates the correct execution of mitosis, and are in accordance with previous studies from the Boutros laboratory in murine ESCs[79] and the

importance of Wnt signaling in stem cell self-renewal and maintenance[2,19]. However, especially the high rates of chromosome missegregation could not be explained by direct effects of Wnt signaling in mitosis, such as the modulation of KIF2A.

In recent work by the Bastians laboratory and other groups, it became evident that also defects in S phase can impact mitosis, notably by slowing down replication fork speed and increasing mitotic microtubule (MT) dynamics, leading to chromosome segregation errors and genome instability[300-302]. Based on this, I tested whether the increased levels of chromosome missegregation upon DKK1 treatment (Figure 14A,B) are caused by I) replication stress and thus can be rescued by supplementation of nucleosides[300,301,303,304] and II) an increase in MT polymerization rates and thereby can be counteracted by stabilizing MTs with the drug taxol[52,305]. In doing so, I was able to partially reverse the effects of DKK1 treatment, namely the number of cells showing lagging chromosomes, both with nucleosides and taxol treatment (Figure 14B).

To validate that the lagging chromosomes arise from increased MT polymerization rates upon Wnt inhibition, I measured MT plus-end assembly rates by tracking transiently transfected *EGFP-EB3* in mitotic hiPSCs in live cell imaging(Figure 14C). For the experiments, cells were mitotically arrested with the EG5 inhibitor dimethylenastron (DME) to assure comparable conditions for the measurements[305](Figure 14C). As hypothesized, I observed that the defects in chromosome segregation (Figure 14A,B) correlated with increased MT polymerization rates in stem cells (Figure 14D), as reported before for somatic and cancer cells[52,305]. Notably, also the accelerated MT dynamics were reversable by supplying the cells with nucleosides, indicating that the increased polymerization rates arise from defects in DNA replication[300,303,304]. In summary, the results support a mechanism in which Wnt modulates DNA replication in S phase by a yet unknown mode of action, which safeguards proper MT polymerization rates in mitosis and thereby the faithful segregation of chromosomes (Figure 14E).

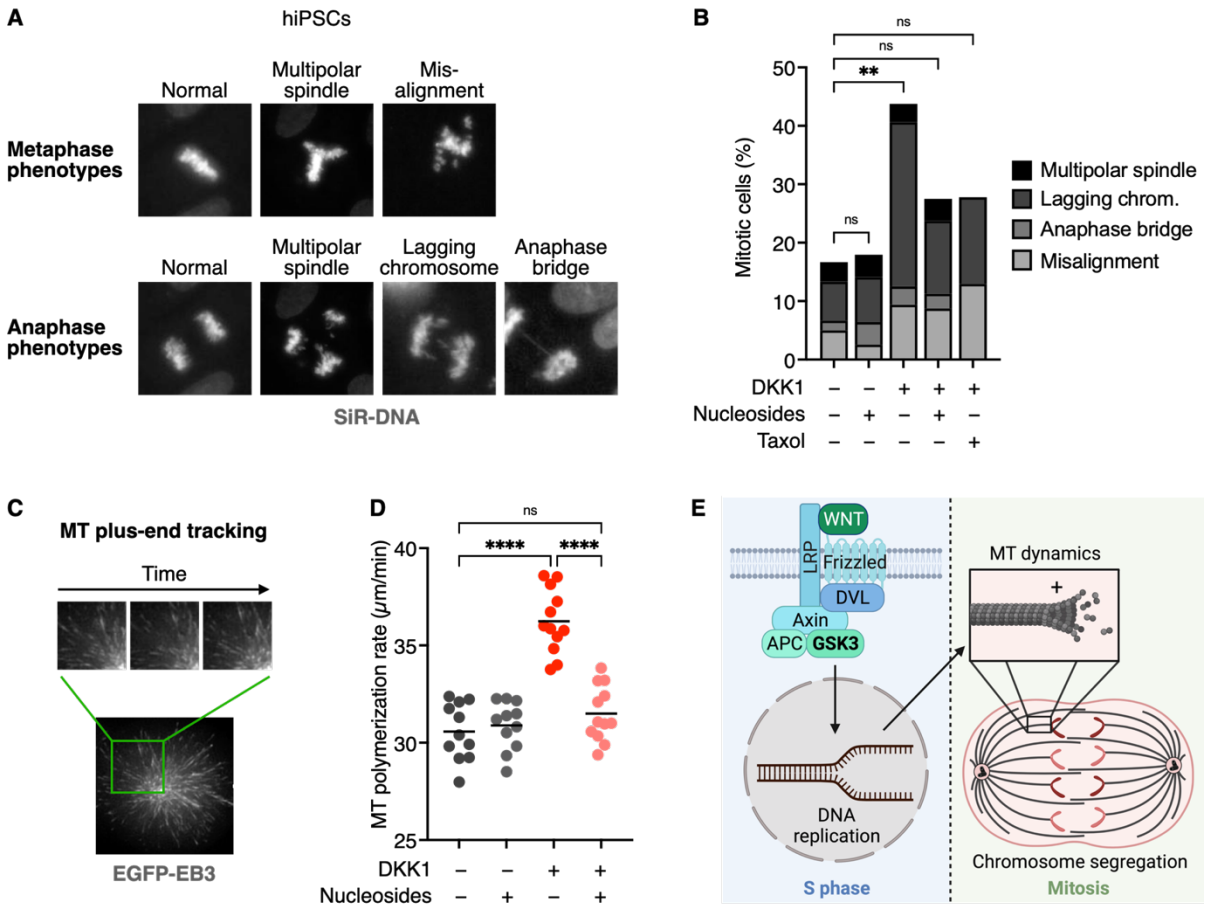

Figure 14. Chromosome instability is driven by replication stress and accelerated MT dynamics in stem cells. (A) Representative fluorescence images of mitotic phenotypes observed in live cell imaging experiments of human induced pluripotent stem cells (hiPSCs) treated with Control or DKK1 CM overnight and stained with SiR-DNA. (B) Quantification of proportion of cells showing the mitotic phenotypes displayed in *A* upon Control or DKK1 treatment with or without nucleosides or taxol supplementation in ≥ 54 mitotic hiPSCs per condition. (C) Representative fluorescence image of one hiPS cell transfected with *EGFP-EB3* and arrested with the EG5 inhibitor dimethylenastron (DME) in mitosis (bottom) and close-ups of one section of the image over time, showing the growth of MT plus-end tips, which are tracked by EGFP-EB3 (top). (D) Quantification of mitotic MT plus-end assembly rates upon Control or DKK1 CM supplemented with or without nucleosides in hiPSCs. Means of ≥ 11 spindles per condition, comprising measurements of ≥ 30 MTs per spindle, are shown. (E) Scheme of S phase-dependent regulation of mitosis by Wnt signaling. Active Wnt signaling ensures error-free DNA replication in S phase, which mediates MT dynamics in mitosis, which are essential for the correct segregation of chromosomes during anaphase.

3.3.2 Inhibition of Wnt signaling leads to aberrant mitotic phenotypes in 3D organoids

To explore the conservation of the observed roles of Wnt signaling in mitosis and its relevance for multicellular systems, mouse intestinal organoids stably expressing *H2B-EGFP* were

analyzed using live cell imaging. Intestinal organoids are highly Wnt-dependent and build typical crypt-villi structures *ex vivo* with the crypts harboring LGR5-positive stem cells and high levels of Wnt signaling[85,86,88]. The pluripotent crypt cells give rise to differentiated cell types, which migrate, in correlation with a decreasing Wnt gradient, towards the villi (Figure 15A)[82,85,86,88,89]. Under homeostatic conditions, the imaging of intestinal organoids is challenging due to their extensive branching by building crypts and villi, and the interpretation of results can be demanding as the organoids are composed of different cell types[85,89]. For this reason, I cultured the 3D cultures under high Wnt conditions, which causes the formation of cystic shapes and the enrichment of stem cells (Figure 15B, left). The home-made high WNT medium comprised the growth factors WNT3A, EGF, NOGGIN and RSPO1 (in the following referred to as "WENR medium"). To elucidate the effects of Wnt signaling during mitosis, I depleted the medium of WNT and RSPO or replaced the Wnt activators by the Wnt inhibitor DKK1 to inhibit basal Wnt signaling. The removal of Wnt ligands from the medium raised the presence of cells with chromosome segregation defects only slightly (Figure 15B,C). However, the additional blockage of endogenous Wnt signaling by DKK1 increased the occurrence of aberrant phenotypes in the organoids significantly (Figure 15B,C). These results endorse the dependency of intestinal organoids on Wnt signaling and suggest, together with the previously presented data, that Wnt inhibition induces similar mitotic defects in various systems, including somatic cells, stem cells and 3D organotypic cultures. Therefore, the roles of Wnt signaling in mitosis may be conserved across different systems and may be worth being explored in more depth in the future.

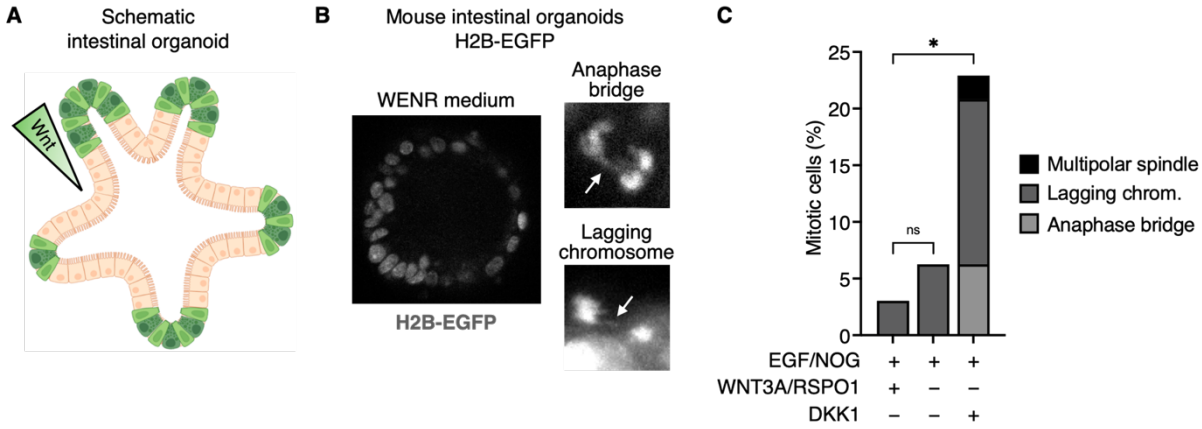

Figure 15. Wnt signaling ensures chromosome stability in 3D organoids. (A) Scheme of a typical intestinal organoid. Stem cells (light green), paneth cells (dark green) and the Wnt gradient, emerging from the crypts to the villi, are highlighted. (B) Representative fluorescence image of live cell imaging of one mouse intestinal organoid stably expressing *H2B-EGFP* and cultured in WENR (WNT3A, EGF, NOGGIN, RSPO1) medium (left) and representative fluorescence images of a single mitotic organoid

cell exhibiting an anaphase bridge or lagging chromosome upon culture in EN+DKK1 (EGF, NOGGIN, DKK1) conditions (right). (C) Quantification of the proportion of aberrant mitotic phenotypes in mouse intestinal organoids expressing H2B-EGFP upon removal or inhibition of Wnt signaling in ≥ 33 mitotic cells per condition.

4. Discussion

4.1 Mitotic Wnt signaling regulates KIF2A and possibly other targets to ensure the correct progression through mitosis

During the last years Wnt signaling has emerged as a key player in the execution of mitosis[103]. In line with this, many components of the Wnt pathway have been shown to associate with the mitotic spindle to regulate spindle orientation, chromosome alignment and chromosome segregation[50,52,79,127,145,220,231-233,235,245,250,252]. Despite that the misregulation of these processes can generate severe mitotic defects and chromosome instability, which is associated with cancer[50,52,53,79,145,233,235,236,246,253,306], little is known about the exact molecular framework of proteins underlying these mechanisms.

Over the course of my work, I was able to reveal a set of novel mitotic Wnt targets, that are associated with cellular processes promoting mitosis, such as cytoskeleton organization, actin filament regulation and protein complex formation (Figure 2). From these, I have investigated KIF2A in more detail to understand its involvement in mitosis and relation to the Wnt signaling pathway (Figure 3-12). Finally, I provide evidence that Wnt signaling monitors KIF2A activity at the spindle during mitosis to ensure timely chromosome alignment and mitotic progression[285]. In this process KIF2A is translocated by DVL and PLK1 to the spindle. The interaction of KIF2A with PLK1 as well as its phosphorylation at serine 100 are supported by Wnt activation (Figure 13A). A misregulation of this mechanism can lead to chromosome misalignment and possibly genome instability in somatic and stem cells (Figure 13B).

Thus, my work supports a role of Wnt signaling in mitosis and provides new insights into the underlying molecular mechanism, which yields a basis for further research in the mitotic field, but also the areas of stem cell research and neurogenesis, which will be discussed below.

4.1.1 The identified novel Wnt targets provide insights into the regulation of mitosis

Mitosis is a highly complex process, that is linked to Wnt signaling. In fact, the disruption of Wnt signaling has been reported to cause mitotic aberrations, such as chromosome misalignments, chromosome missegregation and consequently aneuploidy[52,53,79,253,306]. Thus, Wnt signaling may regulate a variety of proteins that govern mitosis at different levels.

Matching this, the phospho-specific mass spectrometry (MS) screen performed within this work yielded a comprehensive set of mitotic targets that were post-translationally modified upon Wnt inhibition. As KIF2A-S100 was one of the most distinctively regulated phosphopeptides, this kinesin was further analyzed and identified as an important regulator of chromosome alignment that relies on Wnt signaling[285]. Importantly, the MS displayed

additional DKK1 targets with critical functions in mitosis, whose investigation could deepen our understanding of the mechanisms and protein network controlled by mitotic Wnt signaling. Proteins that were explored in this study and require further investigation in the context of Wnt signaling include the following: I) The serine-threonine kinase CDK1, a master regulator and checkpoint protein of mitosis, that regulates mitotic entry and many other proteins that are essential for mitotic progression[132,141,146], II) the E3 SUMO-protein ligase RANBP2, a member of the nuclear pore complex, which mediates chromatid separation in mitosis by localizing topoisomerase IIα (TOP2A) to the centromeres of chromosomes[307,308], and III) the serine-threonine kinase MASTL, which inactivates the phosphatase PP2A indirectly during M phase, maintaining the phosphorylation of mitotic substrates and thereby supporting mitosis[309,310]. Notably, MASTL knockdown has been shown to induce chromosome segregation defects and polyploidy[309], which are phenotypes that also arise upon Wnt depletion[52,53,79,306], and has been proposed recently as a positive regulator of Wnt signaling[311].
Our results suggest that Wnt signaling modulates the phosphorylation status and thereby possibly the activity and function of the named proteins during mitosis.

4.1.2 Wnt signaling mediates KIF2A phosphorylation at S100 via a yet unknown kinase

As described in this work, Wnt signaling positively regulates KIF2A phosphorylation at serine 100 (S100), which is essential for its localization and function at the mitotic spindle poles (Figure 2E, Figure 3D-G). However, the question remains, which kinase is inducing the phosphorylation at KIF2A serine 100. Although PLK1 inhibition has been shown to reduce the phosphorylation of S100 in a previous screen[201], the phospho-site does not reflect a PLK1 motif[289] (Figure 6F). Kinases that would match the phosphorylation site motif around S100 include protein kinase C (PKC), calcium/calmodulin-dependent protein kinase 2 (CAMK2), GSK3, CK1 or a yet unknown kinase, based on predictions by the NetPhos-3.1 server (https://services.healthtech.dtu.dk)[312,313]. Additionally, the “kinase predictor” from PhosphoNET (www.phosphonet.ca) revealed several potential candidates that could phosphorylate KIF2A-S100, such as protein kinase B (PKB), serine/threonine protein kinase PIM1/2/3, protein kinase Y-linked or X-linked (PRKY/X) or protein kinase CAMP-activated catalytic subunit alpha/beta (PRKACA/B, also known as PKACα/β)[314].
To answer this question, using Phos-tag and 2D gels with subsequent Western blots, I tested common kinases known to phosphorylate KIF2A, namely Aurora A, Aurora B and PLK1[112,188,200,202], the Wnt kinases GSK3β and CK1α[22,27], as well as the predicted kinases PKA, PKB and PKC, for their capability to phosphorylate the KIF2A-S100 site. However, the disruption or overexpression of none of the kinases led to changes in the phosphorylation

status of KIF2A-S100 (data not shown), which was possibly due to issues with the techniques, including difficulties to see clear band separations (in Phos-tag gels) and unspecific dots (in 2D gels). To circumvent the mentioned issues, the methods need to be further optimized and the phosphorylation patterns of KIF2A may be validated with alternative techniques, such as phospho-mass spectrometry, to unambiguously identify the relevant kinase.

4.1.3 The coordinated actions of DVL, PLK1 and other factors mediate KIF2A localization and activity at the mitotic spindle

We have demonstrated that the N and Motor domains of KIF2A are needed for its interaction with DVL, which mediates its localization and function at the spindle poles (Figure 5 and [285]). These results are in accordance with the previously characterized roles of these domains, as the N domain conveys the localization of KIF2A at the spindle poles[172,186,188] and the Motor domain facilitates ATP hydrolysis and MT binding[175], which are both needed for the depolymerizing activity of KIF2A and the proper alignment of chromosomes[186,188]. Notably, the Neck and Stalk domain of kinesin-13 (Kin I) were shown to be dispensable for its ATPase and MT depolymerization activity[315], similarly as for the interaction with DVL (Figure 5C,D).

So far, DVL has mainly been implicated in the regulation of plus-end MT growth at the centrosomes during mitosis[52,231]. Here, I provide evidence that DVL also modulates MT dynamics at the minus-ends via the depolymerase KIF2A. Notably, DVL was shown to interact with distinct kinases, particularly KIF5B[316], KIF26B[317] and *C. elegans* KLP7[318], to regulate MT dynamics and thereby directed MT growth, cell polarization and cell migration in the context of non-canonical PCP signaling. Consequently, to my knowledge, I provide the first evidence of canonical Wnt signaling positively regulating a minus-end kinesin to ensure correct MT dynamics and the alignment of chromosomes in mitosis (Scheme 6).

Interestingly, the activity of DVL at the plus tips of astral MTs as well as the functions of KIF2A in spindle assembly, chromosome alignment and chromosome segregation are controlled by PLK1-mediated phosphorylations[185,200,231]. My work suggests that PLK1 is also involved in the DVL-mediated regulation of KIF2A, as DVL recruited both PLK1 and KIF2A to signalosome-like puncta (Figure 6D,E), their interaction was impaired upon reduced Wnt signaling in mitosis (Figure 6A-C), and depletion of DVL, KIF2A and PLK1 evoked similar mitotic phenotypes (Figure 7B-D). However, how Wnt signaling supports PLK1-KIF2A association exactly and how the regulation of DVL at the plus- and minus-ends of MTs is balanced remains to be characterized.

Moreover, apart from DVL and PLK1, additional Wnt components or kinases may be involved in the regulation of KIF2A. It has been shown previously that AXIN1 also localizes at the

centrosomes and interacts with PLK1[239-241]. As AXIN is known to additionally interact with DVL[319], co-localize in LRP6 signalosomes ([31,319] and our data) and yielded a strong, localized PLA signal with KIF2A at the spindle poles (Figure 4A,B), it is likely that AXIN represents another component of the DVL-PLK1-KIF2A axis. However, it remains to be investigated whether this protein interacts with KIF2A and is important for its activity. Besides, other components of the LRP6 signalosome as well as known KIF2A interactors may be investigated to refine the exact mode of action of the DVL-KIF2A axis. Therefore, it would be of interest to test whether Wnt signaling cooperates with other KIF2A regulators that localize and activate KIF2A at the spindle, including components of the mMRN complex[185], MLL/WDR5[186], DDA3[193], SKA1[199], or NuMa and dynein[180,196] (Scheme 6).

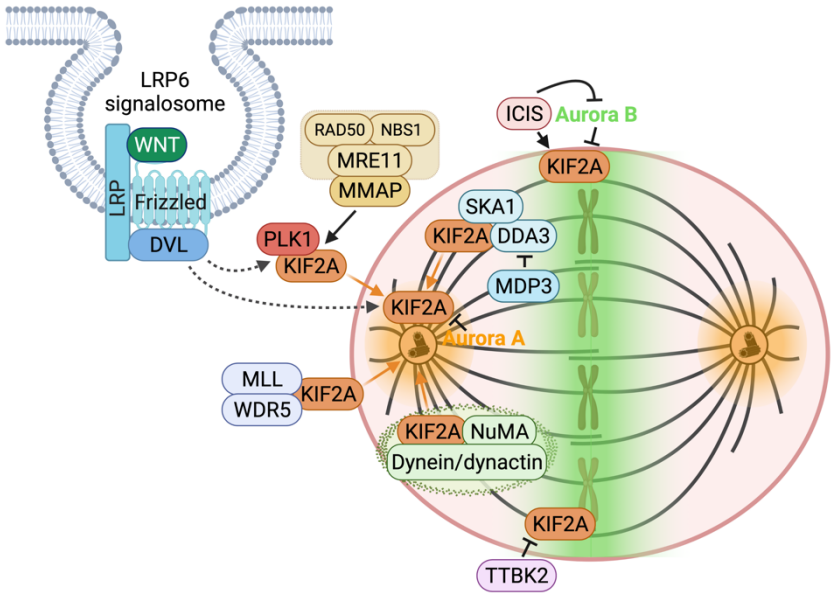

Scheme 6. Various factors, including the Wnt signalosome, regulate the localization and activity of KIF2A at the mitotic spindle. Positive regulation = ⟶, Negative regulation/inhibition = ⊣. LRP = low-density lipoprotein receptor-related protein, DVL = dishevelled, KIF2A = kinesin family member 2A, RAD50 = RAD50 double-strand break repair protein, NBS1 = nijmegen breakage syndrome 1, MRE11 = MRE11 double-strand break repair nuclease A, MMAP = WDCP/WD repeat and coiled-coil-containing, PLK1 = polo-like kinase 1, MLL = lysine methyltransferase 2A, WDR5 = WD repeat domain 5, DDA3 = proline and serine rich coiled-coil 1, SKA1 = spindle and kinetochore associated complex subunit 1, MDP3 = MAP7 domain containing 3, ICIS = inner centromere kin-I stimulator, NuMA = nuclear mitotic apparatus, TTBK2 = tau tubulin kinase 2.

4.1.4 Wnt signaling directs MT dynamics and chromosome alignment via KIF2A, which may ensure genome integrity, also in stem cells

Over the course of my work, I revealed that the alignment of chromosomes in metaphase is driven by the newly defined WNT-KIF2A axis (Figure 7B, Figure 10-12). Notably, both Wnt signaling and KIF2A were indicated in the regulation of chromosome alignment and segregation in several species[52,53,178,186,187,191,192,233,235,283]. Hence, my work provides a mechanism connecting the reported mitotic functions of Wnt signaling and KIF2A, which may be conserved across species. At this, I present evidence for a role of the Wnt signalosome component DVL at the minus-ends of MTs regulating the depolymerase KIF2A in metaphase to ensure chromosome congression and alignment. This observation supplements previous work demonstrating that WNT/STOP signaling regulates MT plus-end dynamics in anaphase to guide chromosome segregation and maintain euploidy[52,53].

Accordingly, both plus-end and minus-end MT dynamics are controlled by Wnt signaling and need to be balanced to ensure the correct alignment and segregation of chromosomes in mitosis, securing chromosome stability. Furthermore, a recent study proposes that Wnt signaling activities are also modulated reciprocally by varying MT dynamics[320]. Kumari et al. (2021) reported that microtubule-targeting agents (MTAs) impair canonical Wnt signaling in oral squamous cell carcinoma, which was reflected by increased levels of AXIN and APC and decreased levels of DVL and β-catenin[320].

Besides, Wnt signaling and KIF2A both contribute to the regulation of stem cell proliferation and self-renewal versus differentiation during development, especially in cortical neurogenesis[51,98-101,120,121,204,206,208,321]. Consequently, as I could validate the association of DVL with KIF2A in pluripotent stem cells, the established connection may benefit the fields of developmental biology and regenerative medicine. Both during development and in regenerative approaches, deciphering the exact mechanisms of mitotic Wnt signaling is essential to understand the downstream effects evoked by a manipulation of the pathway, and enable the safe generation of tissues, without causing deleterious off-target effects, such as excessive growth or genomic aberrations. Interestingly, it was reported recently that genome integrity is coupled tightly to the self-renewing properties of ESCs and fate determination[322], a trait that is also known to be controlled by canonical Wnt signaling[78,80-82,297]. Accordingly, both the known transcriptional functions of Wnt signaling and posttranslational roles of Wnt signaling in mitosis may converge to balance cell fate and genome stability in stem cells.

Moreover, Wnt signaling and KIF2A have been implicated to drive tumorigenesis, likely by supporting proliferation, migration, invasion and epithelial-mesenchymal transition (EMT)[1,82,212-215,323-325]. In line with this, the abrogation of KIF2A or Wnt signaling leads to an

increased sensitivity to respond to chemotherapeutic agents, such as paclitaxel (taxol)[215,326]. Hence, the interconnection of Wnt signaling and KIF2A revealed in this work and further characterization of the modes of action may provide novel therapeutic strategies to intervene with the emergence and progression of cancer.

4.1.5 The explored WNT-KIF2A interaction may have implications for cellular processes beyond mitosis

Besides its function in chromosome alignment and segregation, other roles of KIF2A in cellular processes may be modulated by Wnt signaling[178,185,186,188,192,193,285]. Given that KIF2A not only co-localized with DVL2 and PLK1 in mitosis (Figure 4, Figure 6A-C), but also in interphase (Figure 6D,E), it is likely that the proteins associate and fulfill functions beyond mitosis. Namely, it remains to be uncovered whether Wnt activation also regulates spindle scaling during development via KIF2A[189] and how the known roles of Wnt signaling and KIF2A in ciliogenesis and neurogenesis are interconnected in detail[51,99,106,107,112-115,120,121,127,204-208,327,328]. Both the canonical and non-canonical Wnt pathway have been implicated in ciliogenesis, supporting primary cilia assembly[106] and cilia disassembly[107] respectively. Interestingly, primary cilia proteins, such as BBS, KIF3A and IFT88, inhibit canonical Wnt/β-catenin signaling, representing a negative feedback loop[113-115]. These findings and the cell cycle-dependency of ciliogenesis, with primary cilia being assembled during G0/G1 phase and disassembled before entering mitosis[110], fit well with the observed peak in canonical Wnt signaling at the G2/M transition[29,49,224]. DVL may represent a switch between the canonical (cilia assembly) and non-canonical (cilia disassembly) Wnt pathway, which is likely transferred by inversin, BBS1/4/6 and KIF3A, which restrain DVL levels and activity in the cytoplasm, favoring the Wnt/PCP pathway[113,114,329].

Notably, KIF2A is also well known to induce cilia disassembly by depolymerizing MTs[112,204]. Matching this, the non-canonical Wnt component VANGL2 was shown to interact with phosphorylated DVL2 and PLK1, which phosphorylates KIF2A to promote cilia disassembly[107,108,112]. Conversely, recruitment of BBS8 by VANGL2 releases the DVL2-KIF2A-PLK1 interaction, resulting in reduced KIF2A-induced MT depolymerization and favoring cilia assembly[108]. These findings support that DVL2, PLK1 and KIF2A interact both during mitosis and interphase, where they take distinct roles, namely guiding I) the alignment and segregation of chromosomes in mitosis, which is driven by canonical Wnt signaling[285], and II) Wnt/PCP-induced cilia disassembly throughout G2/S phase[107,108,112]. Hence, the DVL-PLK1-KIF2A axis represents a connection between the canonical and non-canonical Wnt pathway and may couple primary cilia assembly and disassembly with the cell cycle[106,107]. Which

pathway is induced is decided possibly based on the cell cycle phase, cellular context (presence of ligands, receptors and effectors) and DVL localization (membrane-localized DVL versus cytoplasmic DVL)[10,15,63], however further research is needed to clarify the exact molecular mechanisms involved. In fact, since misregulation or mutations in KIF2A can lead to severe cilia-associated diseases, including neurodevelopmental disorders and brain malformations[112,204-207,210,211], insights into the modes of action of ciliogenesis and KIF2A regulation would be valuable for the development of future therapies.

Noteworthy, it was shown in *C. elegans* that Wnt/PCP signaling positively regulates the KIF2A homolog KLP7 in the posterior process of posterior lateral microtubule (PLM) neurons to guide oriented MT growth and establish neuronal polarity[318]. However, despite that these findings provide evidence that the DVL-KIF2A interaction plays a role in axon growth and polarity via non-canonical Wnt signaling, it remains to be clarified to what extend these observations can be transferred to mammalian cells and how canonical Wnt pathways contribute to the functions of KIF2A during neurogenesis.

Notably, both KIF2A and canonical Wnt signaling are involved in neuronal migration, neuronal differentiation and cortical development[51,99,120,121,127,205-207,321,327,328]. Consistently, KIF2A has been shown to support the proliferation or self-renewal of murine neural stem cells, whereas its depletion induces neuronal differentiation[321]. In addition, the silencing of KIF2A leads to an increase in GSK3β activity and decrease in β-catenin levels in these cells[321], which strongly suggests that KIF2A and the canonical Wnt pathway are interwoven to guide proper neocortical neurogenesis in mammals.

4.2 Wnt signaling maintains genome stability across different cellular systems via S and M phase-dependent mechanisms

In the first part of my work, I could show that Wnt signaling ensures proper mitotic progression via DVL and PLK1, which support the localization and activity of KIF2A at the spindle to guide the correct alignment of chromosomes during metaphase (Figure 3-13). To further explore the actions and physiological relevance of Wnt signaling during mitosis, I expanded my studies to pluripotent stem cells (hiPSCs) as well as mouse intestinal organoids. I was able to reproduce an increased rate of chromosome misalignment as well as number of lagging chromosomes in mitotic cells in response to Wnt inhibition. Digging deeper on the causes of the detected chromosome missegregations, I was able to identify that, beyond the mitotic roles of Wnt signaling through KIF2A, Wnt signaling may control other cell cycle regulators in S phase to modulate mitotic MT dynamics and maintain genome stability, which was revealed in close collaboration with the laboratory of H. Bastians (Georg-August-University of Göttingen).

4.2.1 Wnt signaling ensures chromosome alignment and segregation in stem cells

Over the course of my studies, I found that Wnt inhibition induces a mild mitotic delay coupled with chromosome misalignments and missegregation in hiPSCs(Figure 12A-D and Figure 14A,B), which confirms previous observations and supports the importance of Wnt signaling in the maintenance of genome stability in pluripotent stem cells[79]. Remarkably, defects in chromosome segregation often result in numerical and structural chromosomal aberrations[277], which are phenotypes that were also reported upon Wnt inhibition or depletion of distinct Wnt components[52,79] (Figure 7G,H). Conversely, a considerable number of studies indicate that hyperactive Wnt signaling supports chromosomal instability (CIN)[220,232-236,253,306], a hallmark of cancer[145]. In detail, β-catenin stabilization due to APC truncation or β-catenin phospho-inactive mutants was reported to cause anaphase bridges, lagging chromosomes and multipolar spindles, resulting in increased CIN and aneuploidy in mouse ES cells and colon tumors[220,232-236,253,306]. Mechanistically it was proposed that active Wnt signaling decreases CDK1 activity and thereby bypasses the G2/M checkpoint, which is normally activated when the cells face problems. Consequently, cells progress through mitosis, even if there are errors, which results in CIN. In this scenario, the increase in chromosome missegregation can be rescued by inhibiting β-catenin/TCF-mediated transcriptional activities in ES cells, suggesting that active Wnt signaling contributes to CIN via the transcription of target genes[220]. Of note, in studies from the Bastians group WNT3A treatment or GSK3 inhibition did not impair chromosome stability, but rather rescued the Wnt depletion phenotypes[52,53]. Besides, the observed aberrations arose likely independent of β-catenin, as β-catenin depletion did not evoke increased MT dynamics[52].

In short, the current state of knowledge and my data suggest that both the overstimulation and restriction of Wnt signaling can cause CIN. Consequently, the activation of Wnt signaling, involving both β-catenin-dependent and -independent branches, needs to be precisely balanced to ensure genome integrity.

Importantly, it should be kept in mind, that distinct Wnt components also fulfill direct functions in cytoskeletal regulation, especially APC, which localizes both to centrosomes and kinetochores to modulate MT dynamics, MT-KT attachments and possibly SAC activation in mitosis[232-234,236,244,250,261,273]. Hence, CIN may not only arise due to aberrant Wnt signaling activities, but also due to defects in cytoskeletal regulation and checkpoint maintenance caused by the actions of specific proteins of the pathway.

Additionally, as both active and diminished Wnt signaling have the potential to induce CIN, it is likely that the effects of active Wnt signaling are also defined based on the downstream

effectors that are induced. At this, as described above, the transcriptional activation of Wnt/β-catenin target genes has been reported to induce CIN[220], whereas the Wnt-dependent stabilization of proteins (WNT/STOP) as well as direct interactions of Wnt signalosome components with target proteins, acting upstream of β-catenin, favor the correct progression through mitosis and genome stability[52,53,285].

The regulatory roles and effects of Wnt signaling may be also dependent on the cellular context, namely the developmental stage, characteristics, and microenvironment of the cell[97,98,330]. Commonly, canonical Wnt signaling is active in pluripotent stem cells to maintain their self-renewing potential and its modulation stimulates differentiation[78,80,297]. However, throughout the development and differentiation of distinct tissues, Wnt signaling was shown to harbor differential effects, for instance during cardiogenesis, where Wnt signaling levels fluctuate to drive the differentiation of progenitors in a highly time-dependent manner[96,97]. In neurogenesis, Wnt signaling also guides both the self-renewal and differentiation of neuronal progenitors[51,98-101,120,121], which has been proposed to derive from the presence of distinct cell populations[99] or different downstream cascades[51]. Supporting the latter hypothesis, Da Silva et al. (2021) suggested recently that the self-renewal of progenitors is driven by WNT/β-catenin signaling, whereas their differentiation is driven by WNT/STOP signaling[51].

Overall, the fine-tuned regulation of Wnt signaling seems to be essential to ensure correct mitotic progression and genome stability by the interplay of I) Wnt signaling activities including their outputs and II) designated Wnt components harboring additional cytoskeleton- and SAC-associated roles. Yet, further studies should be employed to elucidate the mechanisms underlying this regulation and to test, whether stem cells at variable developmental and differentiated stages respond differently to Wnt misregulation with regards to chromosomal stability. This may broaden the understanding of mitotic defects that arise upon aberrant Wnt signaling during embryonic development or adulthood, especially considering diseases that are characterized by chromosomal instability, such as cancer[1,145].

4.2.2 Chromosome segregation defects derive from replication stress and accelerated MT dynamics

As I detected increased levels of chromosome missegregation upon Wnt inhibition in somatic cells and hiPSCs, which were not that dominant upon KIF2A depletion (data not shown), I searched for alternative mechanisms to explain these aberrations.

As reported in human cancer cells and pluripotent stem cells, S phase-dependent defects in DNA replication can result in chromosome missegregations during mitosis and consequently CIN[300,302]. Based on this, together with the group of H. Bastians, we tested whether these

effects may contribute to the aberrant mitotic phenotypes we observed in somatic and stem cells upon Wnt inhibition. Over the course of this, the Bastians laboratory was able to show that replication stress leads to increased MT dynamics, chromosome segregation defects and eventually aneuploidy in somatic cells[301], which are phenotypes that were previously observed upon Wnt depletion[52,53]. In my work, I could affirm that this mode of action applies to hiPSCs and is driven by Wnt inhibition (Figure 14B-E). Consequently, we propose a mechanism in which misregulated Wnt signaling induces replication defects in S phase, which leads to elevated MT polymerization rates during mitosis, lagging chromosomes in anaphase and finally aneuploidy(Figure 14E). To validate the proposed mode of action and complement my data on MT dynamics and chromosome missegregation, it would be recommendable to substantiate the occurrence of replication stress by measuring the rates of origin firing and replication fork progression upon Wnt inhibition in stem cells[301,331]. Additionally, rescue experiments with agents that act on different levels of the suggested signaling cascade, namely activators targeting Wnt signaling, the replication machinery, DNA damage repair and MT dynamics, would further support the proposed mechanism. As the accelerated MT dynamics, induced by Wnt depletion, occur independently of β-catenin, the defects may be caused by a yet unknown target of GSK3 via WNT/STOP signaling, which would be interesting to characterize[52].

Noteworthy, hiPSCs have been reported to possess high basal levels of replication stress and DNA damage due to increased events of double-strand breaks, which likely derives from their high proliferative capacity and fast replication rate due to a short G1 and long S phase [332-334]. Matching this, I observed high basal levels of MT polymerization rates in hiPSCs compared to somatic cells[52] (Figure 14D). Consistently, human pluripotent stem cells were described to possess, in comparison to their non-pluripotent parent cells or somatic cells, increased levels of genomic instability, including deletions of tumor suppressor genes and oncogenic gene duplications, which likely arise during reprogramming or continuous culture[335-337]. The aberrant activation of oncogenes, such as *MYC*, *CCNE* and *CDC25A*, has been indicated to evoke DNA damage and replication stress, supporting CIN and tumorigenesis[145,300,338,339]. Interestingly, the oncogenes *MYC*, *CCNE* and *CDC25A* were all shown to be positively regulated by active canonical Wnt signaling, both transcriptionally[38,39,216] and post-translationally[54,230,340,341]. As the self-renewing capacities of many stem cells are dependent on Wnt signaling[76-82], these observations match with the higher rates of CIN.

Of note, human iPSCs yield a high potential for therapeutic use in regenerative medicine, due to their properties to be differentiated in various cell types. However, to ensure their safe application and prevent oncogenesis or the emergence of other deleterious diseases

associated with CIN, it is essential to characterize the exact mechanisms of mitosis and genome stability in these cells first, before using them for therapy.

Based on my data, Wnt signaling appears to be critical for both DNA replication in S phase and the correct progression through mitosis, which are two steps that contribute to the maintenance of genome stability in pluripotent stem cells. As shown previously, the reduction of replication stress by nucleoside supplementation decreases genomic aberrations in hiPSCs[300,303,304], which is also supported by my work (Figure 14A,B). Additionally, I provide a mechanism explaining the observed mitotic defects upon Wnt inhibition in more detail, proposing that S phase-related replication stress modifies mitotic MT dynamics and thereby disrupts proper chromosome segregation during anaphase, resulting in CIN (Figure 14E). Taken together, these findings, combined with my previous data and results from the Bastians group (unpublished data), provide evidence that both Wnt-mediated effects in S phase and direct effects of Wnt signaling in mitosis concur to guide the correct execution of mitosis, equal chromosome segregation and genome stability.

4.2.3 Wnt signaling ensures faithful mitosis in organotypic adult stem cell cultures

Over the course of my work, I was able to corroborate the importance of canonical Wnt signaling during mitosis also in 3D organoid cultures, which comprise adult stem cells and reflect more physiological conditions. Using mouse intestinal organoids, I observed that the inhibition of Wnt signaling evokes, similarly as in 2D stem cell cultures (Figure 12A-D, Figure 14A,B), chromosome segregation defects (Figure 15C,D). These results affirm that Wnt signaling reflects a crucial pathway in pluripotent as well as adult stem cells in the guidance of accurate mitosis, and that cells organized in 3D tissue structures are not protected from genome instability arising from Wnt depletion.

Based on my results in somatic and pluripotent stem cells, which showed similar defects in chromosome segregation upon Wnt inhibition, I propose two different mechanisms ensuring the error-free completion of mitosis, namely I) the direct Wnt-mediated regulation of mitosis via KIF2A and II) the indirect regulation of mitosis by interfering with DNA replication in S phase, which secures proper MT dynamics in mitosis. In the 3D organotypic model, it remains to be uncovered whether the observed aberrant phenotypes are based on one or both of the aforementioned mechanisms. To clarify this, rescue experiments need to be performed, using either KIF2A overexpression (mechanism I) or treatments with nucleosides and the MT stabilizing drug taxol (mechanism II). However, limitations may arise in the 3D system concerning the monitoring of MT dynamics by plus-end tracking as described in the somatic and stem cells[301,305](Figure 14C,D). Firstly, achieving steady expression levels in organoids is

not trivial and transfection with traditional methods, such as lipofection, yields low efficiency[342]. Secondly, arresting the cells with an EG5 inhibitor might induce differentiation and affect the characteristics of the organoids. Lastly, organoids assemble in multi-cellular 3D clusters, which is essential for their growth and survival and therefore prohibits the extraction and culture of single organoid cells, making it difficult to monitor single cell MT dynamics. Hence, the fine-tuning of this approach or alternative methods may be necessary to examine the proposed mechanisms in multicellular 3D organotypic models in more detail and validate their conservation.

The confirmation of the revealed mechanisms in organoids would raise the significance of the Wnt actions in the context of mitosis and endorse their applicability for adult stem cells and potentially native tissues and the whole organism.

However, it should be considered that Wnt signaling may have variable roles and modes of action in different cell types and cellular fates, depending on their cell cycle, susceptibility to replication stress and requirement of Wnt activity. Of note, most stem cells are highly dependent and susceptible to Wnt signaling, which maintains their pluripotency and proliferative capacity[76-82]. This may be correlated with the higher rates of replication stress observed in pluripotent stem cells compared to somatic cells[304,333,343]. The increased errors in DNA replication foster high levels of DNA damage and chromosomal copy number variations over the course of prolonged culture in human iPSCs[304,333-337]. However, in murine ESCs no increases in mitotic defects, genomic instability or mutation rates were reported in comparison with somatic cells[343,344], indicating interspecies differences, variations based on the culture conditions and/or different participating pathways. In line with this, Blakemore et al. (2021) suggested that ESCs respond differently to replication stress than somatic cells, showing higher levels of the cell cycle regulator MYB proto-oncogene like 2 (MYBL2), which activates the serine/threonine protein kinase ATM and thereby the response to replication stress and double-strand breaks[345]. However, more research is needed to decipher the exact origins of the differences observed between cell types and expand our knowledge on the underlying actions.

Notwithstanding, my work provides a basis for the understanding of the mitotic defects, that arise upon Wnt depletion, by introducing a molecular mechanism explaining how the correct distribution of chromosomes and maintenance of genome integrity is guided by Wnt signaling, by way of example in human pluripotent stem cells.

5. Conclusion

My work supports a key role of canonical Wnt signaling in mitosis. Besides validating the emergence of chromosome alignment and segregation defects in response to Wnt depletion, I provide evidence for two distinct Wnt-associated mechanisms that act independently of β-catenin to secure faithful mitosis.

First, I unveiled the interaction between the Wnt scaffolding protein DVL and the MT depolymerase KIF2A. At this, I found that DVL supports KIF2A localization and activity at the mitotic spindle poles to ensure the proper alignment of chromosomes during mitosis. This process is promoted by LRP6 signalosome formation, phosphorylation of KIF2A at serine 100 and the association of KIF2A with PLK1. Second, I found, in close collaboration with the Bastians laboratory, that Wnt signaling may safeguard DNA replication in S phase to ensure proper MT dynamics and thereby chromosome segregation in mitosis.

Accordingly, I provide evidence that Wnt signaling takes different actions in particular cell cycle phases, which combine to ensure the correct progression through mitosis.

As I verified the validity of both mechanisms in stem cells, the submitted work may have implications for the further understanding of stem cell self-renewal and differentiation, the mechanisms of genome stability, as well as diseases arising from a misregulation of these processes, such as cancer. The observed mechanisms can likely be transferred to more physiological, multicellular systems, such as organoids, which remains to be verified.

The identified association of KIF2A with DVL may additionally provide a pitch for the field of ciliogenesis and neurogenesis, as it connects the known roles of KIF2A and Wnt signaling in neuronal development, but also neuronal diseases and brain malformations. Besides, a possible interconnection with non-canonical Wnt signaling and mutual function of the explored DVL-KIF2A-axis may be considered and tested in further experiments.

Ultimately, my work outlines similar mitotic defects arising from compromised Wnt signaling in somatic cells, pluripotent stem cells and organotypic adult stem cell systems, indicating the conservation and importance of Wnt signaling in mitosis. In addition, I introduce two modes of action, explaining how Wnt signaling can ensure accurate mitosis by either acting directly in M phase or via S phase.

Further research may be conducted to characterize to what extend the proposed mechanisms can be transferred to 3D cultures, complex tissues and the whole organism to get deeper insights into the roles of Wnt signaling during mitosis and enable the application of these findings in a clinical setting.

6. Materials and Methods

6.1 Materials

6.1.1 Cell lines

Table 2. Cells used within this work.

Cell line	Source
RPE1-hTERT	ATCC, CRL-4000
HEK293T	ATCC, CRL-3216
HeLa	ATCC, CCL-2
L cells wildtype	ATCC, CRL-2648
L cells WNT3A	ATCC, CRL-2647
HeLa-Kyoto EB3-EGFP	CLS, 330668 (depositor: Jan Ellenberg, EMBL Heidelberg)
HeLa-Kyoto EGFP-α-tubulin/H2B-mCherry	Gift from Jan Ellenberg, EMBL Heidelberg
hiPSCs	Gift from Kyung-Min Noh, EMBL Heidelberg
Mouse intestinal organoids H2B-EGFP	Extracted in collaboration with Rocio Sotillo, DKFZ Heidelberg, and Nicole Giebel, University Heidelberg

6.1.2 Buffers

6.1.2.1 Notes on the preparation of stocks and buffers

For all stock solutions and buffers, the respective components were dissolved in 4/5 of the final volume. The pH was adjusted, where necessary, using a pH meter (Sartorius Basic Meter PB-11) and titration with 10 M or 1 M HCl or NaOH solutions, and the solutions were filled up to their final volume with the respective solvent.

6.1.2.2 Common stocks and buffers

4% Paraformaldehyde (PFA) solution: 10 g PFA, 25 ml 10X PBS, 225 ml H_2O

➔Heat up solution to 65 °C to dissolve PFA. Optionally, add 1 M NaOH drop-wise to facilitate the dissolution. Let cool down, aliquot in 2 ml aliquots and store at –20 °C.

1 M Dithiothreitol (DTT): 1.54 g DTT, 10 ml H_2O

➔Aliquot in 1 ml aliquots and store at –20 °C in the dark.

10% Ammonium persulphate solution (APS): 2.5 g APS, 25 ml H_2O

➔Aliquot in 1 ml aliquots and store at –20 °C.

10 mM Dimethylenastron (DME): 3.024 mg DME, 1 ml DMSO

➔Aliquot in 1 ml aliquots and store at –20 °C.

2 M Calcium chloride ($CaCl_2$): 29.4 g CaCl2, 100 ml H2O

➔Sterile filter (0.2 μm filter), aliquot in 1 ml aliquots and store at –20 °C.

2X HEPES buffered saline (HBS): 50 mM HEPES, 10 mM KCl, 280 mM NaCl, 10 mM Na_2HPO_4, 0.1% D-glucose, in H_2O

➔Adjust pH to 7.05 with NaOH, sterile filter (0.2 μM filter), aliquot in 2 ml aliquots and store at –20°C.

20X Tris buffered saline (TBS): 400 mM Tris, 3000 mM NaCl, in H_2O

➔Adjust pH to 7.6 with HCl, fill up to final volume with H_2O and store at RT.

➔1X TBS: 50 ml TBS (20X) + 950 ml H_2O

➔1X TBST (TBS + 0.1% Tween-20): 50 ml TBS (20X) + 1 ml Tween-20 + 949 ml H_2O

5 mM Nucleoside stock: 5 mM 2'-Deoxyadenosine 5'-monophosphate monohydrate, 5 mM Thymidine, 5 mM 2'-Deoxyguanosine monohydrate, 5 mM 2'-Deoxycytidine hydrochloride (all from Santa Cruz)

➔Firstly dissolve every nucleoside individually, preparing a 20 mM stock for each:

- 2'-Deoxyadenosine 5'-monophosphate monohydrate: in 0.1 M NaOH
- Thymidine: in H_2O
- 2'-Deoxyguanosine monohydrate: in 1 M NH_4OH
- 2'-Deoxycytidine hydrochloride: in 1 M NaOH

➔Mix individual nucleoside stocks of deoxyadenine, thymidine, deoxyguanosine and deoxycytidine (each 20 mM) in a ratio of 1:1:1:1 (= 5 mM nucleoside stock), aliquot in 10 μl aliquots and store at –20 °C. Use 1:250 in experiments (20 μM final conc. per nucleoside).

6.1.2.3 Solutions and buffers for TOPflash assay

P/Rluc-A (pH 8, including firefly luciferase substrate): 200 mM Tris-HCl, 15 mM $MgSO_4$, 0.1 mM EDTA pH 8, 25 mM DTT, 0.2 mM coenzyme A (optional), 200 μM D-Luciferin, in H_2O

➔Mix Tris-HCl, $MgSO_4$ and EDTA, adjust pH to 8.0 and store at RT.

➔DTT, ATP and D-Luciferin should be added fresh before use.

P/Rluc-B (pH 5, including renilla luciferase substrate): 25 mM $Na_4P_2O_7$, 10 mM NaAc, 15 mM EDTA pH 8, 500 mM Na_2SO_4, 500 mM NaCl, 50 μM phenyl-benzothiazole, 4 μM coelenterazine h, in H_2O

➔Mix $Na_4P_2O_7$, NaAc, EDTA, Na_2SO_4 and NaCl, adjust pH to 5.0 and store at RT.

➔Phenyl-benzothiazole and coelenterazine h should be added fresh before use.

5X Passive lysis buffer: 125 mM tris-phosphate (pH 7.8), 10 mM DTT, 10 mM EDTA, 50% glycerol, 5% Triton X-100, in H_2O

➔1X Passive lysis buffer: 10 ml Passive lysis buffer (5X) + 40 ml H_2O

6.1.2.4 Lysis buffers for Western blot and Immunoprecipitation

Note: Lysis buffers were prepared without proteinase and phosphatase inhibitors (PPI), aliquoted in 1 ml aliquots and stored at –20 °C. 1X of 100X Proteinase-phosphatase-inhibitor-mix (Thermo Fisher Scientific) was added fresh to the lysis buffer before use.

Full lysis buffer: 20 mM Tris-HCl pH 7.5, 150 mM NaCl, 1% NP-40 or Triton X-100, 1 mM β-mercaptoethanol, 0.05% SDS, 2 mM EDTA (optional), 1X Proteinase-phosphatase-inhibitor-mix (Thermo Fisher Scientific), in H_2O

Cytoplasmic lysis buffer: 0.05% saponin, 2 mM EDTA, 10 mM β-mercaptoethanol, 1X Proteinase-phosphatase-inhibitor-mix (Thermo Fisher Scientific), in DPBS

IP lysis and wash buffer: 25 mM Tris-HCl pH 7.5, 150 mM NaCl, 1% NP-40, 1 mM EDTA, 5% glycerol, 1X Proteinase-phosphatase-inhibitor-mix (Thermo Fisher Scientific), 0.1% benzonase nuclease or DNAse, in H_2O

➔Add 1X PPI-Mix and nuclease/DNAse fresh before use.

➔IP blocking buffer: IP lysis buffer + 5% BSA (filtered)

➔IP wash buffer after antibody-beads: IP lysis buffer + 10 μM MG132 (added fresh)

6.1.2.5 NuPAGE buffers for Gel electrophoresis and Western blot

NuPAGE loading/sample buffer: 4X NuPAGE loading buffer with 50 mM DTT

20X NuPAGE MOPS SDS running buffer: 50 mM MOPS, 50 mM Tris, 0.1% SDS, 1 mM EDTA, in H_2O

➔The pH should be 7.7. Do not use acid or base to adjust the pH and store at 4°C.

➔1X NuPAGE MOPS SDS running buffer: 50 ml running buffer (20X) + 950 ml H_2O + 1 ml $NaHSO_3$ (optional)

20X NuPAGE transfer buffer: 25 mM Bicine, 25 mM Bis-Tris, 1 mM EDTA, in H_2O

➔The pH should be 7.2. Do not use acid or base to adjust the pH and store at 4°C.

➔2X NuPAGE transfer buffer + 10% methanol (for semi-dry blot): 100 ml transfer buffer (20X) + 800 ml H_2O + 100 ml methanol. Note: For small proteins up to 20% methanol may be added, whereas for big proteins methanol may be neglected.

Gel buffer: 1.25 M Bis-Tris-HCl, in H_2O

➔Adjust pH to 6.8 with HCl and store at 4 °C.

BSA blocking buffer: 5% BSA, 2 mM EDTA (optional), in TBST

Milk blocking buffer: 5% milk powder, 0.02% sodium azide (optional), in TBST

➔Note: EDTA or sodium azide can be added for longer storage to prevent contamination. Sodium azide is toxic! Always use gloves and remove any spilled powder immediately with a wet tissue! No sodium azide should be used with secondary antibodies.

ECL solution #1: 50 mM Tris-HCl pH 8.5, 0.5% cumaric acid, 1% luminol, in H_2O

ECL solution #2: 50 mM Tris-HCl pH 8.5, 0.02% H_2O_2, in H_2O

6.2 Methods

6.2.1 Cell culture

6.2.1.1 Culture, passaging, freezing and thawing of cells

RPE1 cells were cultured in DMEM-F12 medium (Gibco) supplemented with 10% FBS (Gibco), 1% penicillin-streptomycin (Gibco) and 4% sodium bicarbonate (7.5%) (Gibco). HEK293T, HeLa, HeLa-Kyoto and L cells were cultured in DMEM medium (Gibco) supplemented with 10% FBS (Gibco), 1% penicillin-streptomycin (Gibco). Human induced pluripotent stem cells (hiPSCs) were cultured in Essential 8 Basal Medium (Gibco) supplemented with 1% penicillin-streptomycin (Gibco). For the first day after splitting, 1X RevitaCell supplement (Gibco) was added to the hiPSC medium and afterwards normal Essential 8 medium was used and changed every day. Only hiPSCs below passage 13 were used for the described experiments. All cell lines were grown at 37 °C with 5% CO_2.

For passaging, cells were washed with prewarmed DPBS (Gibco), incubated with prewarmed 0.05% Trypsin-EDTA (Gibco) for 10-40 seconds and detached using prewarmed full medium of the respective cell line. Cells were split every 2-3 days. For hiPSCs, Versene solution (Gibco) instead of trypsin was used for 3 min at 37 °C to detach cells and cells were split every 4-5 days into plates that were previously coated with DPBS including 1% vitronectin (rhVTN-N) (Gibco) for 1 h.

For long-term storage, cells were detached as described above, collected in full medium and pelleted by centrifugation (3 min, 1200 rpm). The pellet was taken up in FBS containing 10% DMSO and cell resuspension frozen at –150 °C. When needed, cells were thawn quickly in a water bath at 37 °C, taken up in prewarmed medium, spun down, taken up in full medium again and plated in a flask.

6.2.1.2 Culture and passaging of mouse intestinal organoids

Intestinal organoids were extracted by Nicole Giebel from the Acebrón laboratory (University Heidelberg) from an 8-week-old female mouse, stably expressing *H2B-EGFP*. The mouse was provided by R. Sotillo (DKFZ Heidelberg).

After extraction, mouse intestinal organoids with *H2B-EGFP* were cultured in IntestiCult OGM Mouse Basal Medium (Stemcell Technologies) supplemented with 1% penicillin-streptomycin (Gibco) and grown at 37 °C with 5% CO_2. For live cell imaging experiments, organoids were cultured in WENR medium after plating, which contained 1X B27 supplement (Gibco), 1X N2 supplement (Gibco), 1.25 mM n-Acetyl-L-cysteine (Thermo Fisher Scientific), 0.05 µg/ml recombinant mouse EGF (Thermo Fisher Scientific), 0.1 µg/ml recombinant mouse Noggin (Stemcell Technologies), 1:4 home-made WNT3A CM and 1:10 home-made RSPO1 CM in advanced DMEM-F12 (Gibco). The organoids were cultured in 48-well plates for suspension cells (Sarstedt).

For passaging, Matrigel matrix (Corning Matrigel Basement Membrane Matrix, growth factor reduced and phenol red-free) was thawn on ice for 45-60 min. The organoids were detached and dissociated with Gentle Cell Dissociation Reagent (Stemcell Technologies) for 5 min, transferred to a falcon tube, mixed with DPBS and spun down (3 min, 1200 rpm). The pellet was resuspended in DMEM-F12, spun down and taken up in a small volume of fresh medium. Resuspended cells were mixed 1:1 with the Matrigel matrix and plated immediately as small Matrigel domes in a prewarmed plate (e.g. 15 µl cells resuspended in medium + 15 µl Matrigel = 30 µl cell-Matrigel-mix per well of a prewarmed 48-well plate). The organoids were split every 7-9 days.

For long-term storage, mouse intestinal organoids were frozen in the same manner as described above (see 6.2.1.1). At this 3-4 wells of a 48-well plate with organoids, cultured for 5-7 days, were frozen in FBS supplemented with 10% DMSO. After thawing, organoids were taken up in DMEM-F12, spun down (3 min, 1200 rpm), dissolved in a small volume of medium, mixed 1:1 with Matrigel and seeded again as domes in 3-4 wells, overlaying them with full organoid medium as described above.

6.2.2 Production of WNT3A and DKK1

6.2.2.1 Production of Control and WNT3A conditioned media

Control or WNT3A expressing L cells were cultured as described above to ~80% confluency in DMEM++ medium and split 1:5 on ∅10 cm dishes. After 3 days, the medium was collected from the plates and dead cells or fragments removed by centrifugation for 5 min at 2,000 xg. The supernatant was transferred to and stored in glass bottles at 4 °C. Control and WNT3A conditioned media (CM) were applied 1:5 in this study.

6.2.2.2 Production of DKK1 conditioned medium and DKK1 purification

About 80% confluent HEK293T cells were split 1:5 on ∅10 cm dishes in DMEM++ medium and transiently transfected with *pCS-FLAG-DKK1* by the calcium-phosphate transfection method the next day. In detail, 15 µg of FLAG-DKK1 plasmid per ∅10 cm dish were mixed with 500 µl of 250 mM $CaCl_2$ in H_2O and added dropwise to 500 µl 2XHBS. The transfection reaction was mixed, incubated for 20 min at RT and distributed dropwise over the cells. 7 h after the transfection, the medium was changed to prevent cell death due to a long exposure with the calcium-phosphate mix. The first fraction of the CM was collected 1 day after the transfection, medium was replaced by fresh medium and additional fractions harvested on succeeding days as indicated. For collection, the medium was centrifuged to remove dead cells and fragments (5 min, 2,000 rpm), the pellet discarded, and the supernatant (= DKK1 CM) stored at 4 °C.

The most potent fractions were collected on day 3 and 4 after transfection. Thus, medium collected 3 days after transfection was used in a dilution of 1:5 for all experiments included in this study unless otherwise specified. Control CM was obtained from untransfected HEK293T cells, that were cultured in a similar way as the HEK293T cells used for the production of the DKK1 CM, and applied in a dilution of 1:5.

For the MS experiment, FLAG-DKK1 CM was purified prior to its application using anti-FLAG M2 antibody-conjugated agarose beads (Sigma-Aldrich). In detail, anti-FLAG beads were placed into a column, washed with filtered TBS (flow < 1 ml/min), resuspended in TBS and

incubated with FLAG-DKK1 CM under rotation at 4 °C for 2 h. The bead-DKK1-mix was added to the column, flow adjusted to ~1 ml/min and the flow through saved to validate the efficiency of the FLAG-DKK1 binding to the beads in TOPflash assays later. The column was washed with filtered TBS (flow < 1 ml/min) and eluted 4 times with 100 µg/ml FLAG peptide in TBS and 2 times with 0.1 M Glycine-HCl pH 3.5. The pH was neutralized with Borate buffer, pH 8. The column was recalibrated with filtered TBS and stored for later use at 4 °C. Purified DKK1 was stored at –80 °C and used 1:50 in SILAC-MS experiments.

6.2.3 Cell cycle synchronization

To synchronize cells in mitosis, cells were arrested in G1/S phase by treating them for 24 h with 2 mM thymidine, washed three times with medium to remove thymidine and released in full culture medium. After 5 h, 2 µM dimethylenastron (DME) was added for 4 h to synchronize cells in prometaphase. Treatments were applied during the incubation with DME for 1.5 h or as described in the experimental procedures.

6.2.4 DNA transfection

For overexpression analyses, somatic and cancer cell lines were transfected with X-tremeGENE 9 DNA Transfection Reagent (Roche) for 24-48 h according to manufacturer instructions one day after seeding. In this, 50-100 ng DNA/well of a 96-well plate, 250-800 ng DNA/well of a 12-well plate or 500 ng/well of a 6-well plate were transfected, using a ratio of 3 µl X-tremeGENE 9 per 1 µg DNA in 100 µl serum-free Opti-MEM medium (Gibco).
HiPSCs were transfected with Lipofectamine 3000 Transfection Reagent (Thermo Fisher Scientific), using 1.5 µl Lipofectamine 3000 Reagent and 2 µl P3000 Reagent per 1 µg DNA in a total of 100 µl Opti-MEM. For transfections in 96-well formats or 10-well imaging plates, 100 ng DNA/well were applied.

6.2.4.1 Plasmids and expression constructs

The following plasmids were employed: FLAG-GSK3B, FLAG-CTNNB1, FLAG-DVL1, FLAG-mDvl2, FLAG-DVL3, FLAG-CK1E, LRP6, mFzd8, AXIN1, MYC-DVL2, pCS2+, pCS-FLAG-DKK1, TOPflash and Renilla plasmids were kind gifts from C. Niehrs (DKFZ Heidelberg). EGFP-KIF2A (#52401), 3xFLAG-DVL2 (#24802), FLAG-AXIN1 (#109370) and FLAG-betaTrCP (#10865) plasmids were purchased from Addgene. The EGFP-EB3 plasmid was a kind gift from H. Bastians (Georg-August-University Göttingen).
The phospho-inactive KIF2A mutant (KIF2A S100A) was generated by Gibson assembly. A KIF2A fragment including the S100 site with an alanine instead of the serine was inserted into

a linearized KIF2A plasmid to replace the normal sequence and ends were ligated again to form a circular DNA plasmid (done by Ana Garcia del Arco).

In the KIF2A truncation mutants, one domain of KIF2A or all domains except for the N domain were removed by PCR amplification and consecutive blunt-end ligation. To receive KIF2A WT and S100A constructs that are resistant to siRNA-mediated knockdown, every third base of the triplets included in the siKIF2A binding site were replaced, while still encoding the original amino acids, as illustrated in Figure 11A. The modified sequence was integrated in the KIF2A plasmids by PCR and blunt-end cloning (done with Anja Ciprianidis).

The primers for the generation of all constructs are given in Table 3.

Sequence of oligonucleotide including the S100A mutation (in vitro synthesized by Sigma-Aldrich)
AGAGATTGACCTGGAGAGCATCTTTTCACTTAACCCTGACCTTGTTCCTGATGAAGAA ATTGAACCCAGTCCAGAAACACCTCCACCTCCAGCATCCTCAGCCAAAGTAAACAAA ATTGTAAAGAATCGACGGACTGTAGCTGCTATTAAGAATGACCCTCCTTCAAGAGATA ATAGAGTGGTTGGTTCAGCACGTGCACGGCCCAGTCAATTTCCTGAACAGTCTTCCT CTGCACAACAGAATGGTAGTGTTTCAGATATATCTCCAGTTCAAGCTGCA AAAAAGGAAT

Table 3. PCR primers employed for the generation of KIF2A constructs used in this work.

Construct	**Forward primer**	**Reverse primer**
Linearized KIF2A plasmid	TTGGACCCCCTTCACGTAGA	TTGCCTTTTGTATCTCCAT
KIF2A-S100A insert	TGGAGATACAAAAGGCAAAGAGATTGACCTGGAGAGCA	TACGTGAAGGGGGTCCAAATTCCTTTTTTGCAGCTTGAACTG
KIF2A-ΔN (Δ1-153)	CCCCCTTCACGTAGAAAATCTAATTGTG	CATAGAATTCGAAGCTTGAGCTCG
KIF2A2-ΔNECK (Δ154-221)	CATAGGATATGTGTGTGTGTAAGAAAACG	TGAAGGGGGTCCAAATTCCTTT
KIF2A2-ΔMOTOR (Δ222-542)	ACATTAAGATATGCAAATAGGGTC	TTCATCAATAGGATCTGCTGTTG
KIF2A2-ΔSTALK (Δ543-706)	TAAGTCGACGGTACCGC	ATTAAGAGTATTTTCACAGGATGCCATTCC
KIF2A-N (Δ154-706)	TAAGTCGACGGTACCGC	TGAAGGGGGTCCAAATTCCTTT
siKIF2A-resistant KIF2A (wildtype and S100A)	TGGAACAGAAAATAGACATTTTAACTGAACTG	GGATGGCCTCAAGTTGTGTAGCATATGAATC

6.2.5 RNA interference

Stocks of 20 μM siRNA (Table 4) were prepared by resuspending lyophilized siRNA in RNase-free 1X siRNA buffer and stored at –20 °C. RPE1 cells were transfected with 50 nM siRNA and HeLa cells with 30 nM siRNA using Lipofectamine RNAiMAX Transfection Reagent (Thermo Fisher Scientific) according to manufacturer's instructions for 48 h one day after seeding. The siRNAs that were applied are summarized in Table 4.

Table 4. SiRNAs used in this work.

siRNA	Sequence (5'-3')	Supplier	Notes
siControl #1	–	Sigma-Aldrich, MISSION siRNA Universal Negative Control #1 (SIC001)	Used for imaging experiments within this work
siControl #2	–	Horizon Discovery, siGENOME Non-Targeting siRNA #5 (D-001210-05-20)	Used for Western blots withing this work
siKIF2A #1	GAAGCUAUUCUU GAGCAAA	Sigma-Aldrich, MISSION Pre-designed siRNA (SASI_Hs02_00319 177)	Used for all experiments in this work, where "siKIF2A" is indicated
siKIF2A #2	GGAAUG GCAUCCUGUGAA A	Gift from H. Bastians (Georg-August-University Göttingen)	Used in Jang et al., 2008 and others [186,193,200]
siKIF2A #3	GGCAAAGAGAUU GACCUGG	Gift from H. Bastians (Georg-August-University Göttingen)	Used in Ganem & Compton, 2004 and others[177,179,181,284]; Note: was indicated to cause off-target effects[195]
siKIF2C	GCAAUAAACCCAG AACUCU	Sigma-Aldrich, MISSION Pre-designed siRNA (SASI_Hs01_00111 628)	
siLRP5/6	CCAAUACCAUCAA CGUCCA (LRP5) CUAUGACCUCAG CAUUGAU (LRP)	Sigma-Aldrich, MISSION Pre-designed siRNA (1:1 mix of SASI_ Hs01_00086821 and SASI_Hs01_ 00039493)	Used for all experiments in this work, where indicated

siDVL1-3	GUCUGGAGUAGG GAUCUAA (DVL1) CUAGUCAACCUG UCUCUCA (DVL2) GCUACUACAUCU UCGGUGA (DVL3)	Sigma-Aldrich, MISSION Pre-designed siRNA (1:1:1 mix of SASI_ Hs01_00142403, SASI_Hs01_001424 04 and SASI_Hs01_ 0004203)	Used for all experiments in this work, where indicated

6.2.6 Wnt reporter assay (TOPflash)

HEK293T, RPE1 or HeLa cells were seeded into 96-well plates and transfected with X-tremeGENE 9 DNA Transfection Reagent (Roche) as described above (see 6.2.4). HEK293T cells were transfected with 50 ng DNA per well, including 5 ng TOPflash luciferase plasmid and 3 ng Renilla luciferase plasmid. RPE1 cells were transfected with 50 ng DNA per well, including 5 ng TOPflash luciferase and 1 ng Renilla luciferase. HeLa cells were transfected with a total of 100 ng DNA per well, including 30 ng TOPflash luciferase, 20 ng Renilla luciferase and optional 25 ng MYC-DVL2 or all components of the LRP6 signalosome, comprising 25 ng MYC-DVL2, 21.875 ng LRP6, 1.875 ng Fzd8 and 1.25 ng AXIN1. HiPSCs were seeded into 96-well plates and transfected with Lipofectamine 3000 Transfection Reagent (Thermo Fisher) using 100 ng DNA in total, including 30 ng TOPflash luciferase plasmid and 25 ng Renilla luciferase plasmid. All DNA reactions were filled up to 50 ng or 100 ng respectively with empty vector (pCS2+). Treatments were added one day after the transfection as indicated and applied overnight. Where no concentrations are given, Control CM, WNT3A CM and DKK1 CM were applied 1:5 and RSPO3 CM 1:50. Two days after transfection, cells were lysed with commercial 1X Passive Lysis Buffer (Promega) or home-made passive lysis buffer for 15 min at 4 °C on a shaker and analyzed using the Dual-Luciferase Reporter Assay System from Promega or home-made P/Rluc solutions with a Tecan Microplate Reader (Tecan Infinite M1000) (buffer and solutions are described under 6.1.2.3). At this, firstly 50 μl of the solution containing the Firefly substrate was added to each well and secondly 50 μl of the Renilla solution, which was each followed by recording the induced luciferase signal with the Tecan Reader. Of note, the addition of the Firefly luciferase substrate to the transfected cells induces a peak in signal activity that decreases and stabilizes after 1-2 min. Based on that, an incubation step of 1 min was added after adding the solution and before read-out.

For the downstream analysis, TOPflash signals were normalized to the Renilla reporter signal and Wnt activity was calculated and displayed relative to the control condition.

6.2.7 Gel electrophoresis and Western blot (WB)

HEK293T, RPE1 or HeLa cells were seeded in 6-well plates and transfected with siRNA for 48 h (see section 6.2.5), transfected with DNA for 24 h (section 6.2.4) and/or treated with Control CM (1:5), DKK1 CM (1:5), WNT3A CM (1:5) and the GSK3 inhibitor BIO (1 μM, Sigma-Aldrich) for 1.5 h, as indicated in the figures. Cells were harvested in ice-cold DPBS on ice by scraping them from the bottom of the wells and spun down (3 min, 2,000 rpm, 4 °C). For each sample, 2 confluent wells of a 6-well plate were combined. The pellets were lysed using 10-times their volume of full lysis buffer or cytoplasmic lysis buffer (compositions described in 6.1.2.4) for 5-10 min on ice, resuspended and centrifuged (5 min, 13,000 rpm, 4 °C). The supernatant was mixed 1:4 with NuPAGE loading buffer containing DTT and incubated for 5 min at 65 °C. NuPAGE Bis-Tris mini gels with 8% bis-acrylamide were prepared as depicted below (Table 5), using glass plates, 10-well or 15-well combs and gel casting stands from Bio-Rad.

Table 5. Preparation of 8% NuPAGE Bis-Tris gel with 4% stacking gel (recipe for 2 gels).

Component	Separating gel (8%)	Stacking gel (4%)
40% Bis-acrylamide (4°C)	2 ml	0.5 ml
1.25 Bis-Tris pH 6.8 (4°C)	2.857 ml	1.429 ml
dH_2O (RT)	5.143 ml	3.071 ml
TEMED (4°C)	10 μl	5 μl
10% APS (–20°C)	100 μl	50 μl
Final volume	10 ml	5 ml

5 μl PageRuler Prestained Protein Ladder (Thermo Fisher Scientific) and 15 μl of each sample were loaded per well of a 10-well gel, whereas 3 μl ladder and 10 μl sample were loaded per well when using 15-well gels. The gels were run using NuPAGE MOPS SDS running buffer (see 6.1.2.5) and Bio-Rad Mini-PROTEAN mini-gel chambers and PowerPac HC high-current power supplies for 10 min at 80 V until the loading front reached the separating gel. Afterwards the gel was run for another ~50 min at 150 V until the samples reached the end of the gel. Gels were transferred into nitrocellulose membranes by semi-dry blotting using a Trans-Blot SD semi-dry transfer cell (Bio-Rad) for 30 min. For this, gels and membranes were briefly incubated in NuPAGE transfer buffer (consult 6.1.2.5 for recipe) and stacked as follows: extra thick blotting paper (bottom), membrane, gel, extra thick blotting paper (top). After transfer, the membranes were blocked for 45 min in TBST blocking buffer containing either 5% BSA (Figure 1C,E and 2F) or 5% milk (Figure 3E, 5B, 6C, 7A) and incubated with primary antibodies

diluted in the respective blocking buffer at 4 °C overnight. The next day, membranes were washed 3 times for 5 min with TBST and incubated with secondary antibodies conjugated with horseradish peroxidase (HRP) at RT for 1 h. All washing and incubation steps were carried out at horizontal oscillation. Membranes were washed again 3 times á 5 min with TBST and analyzed with a chemiluminescence imager (Intas Science Imaging) using home-made enhanced chemiluminescent substrate (ECL) solutions for highly expressed proteins (6.1.2.5) or Clarity Max Western ECL Substrate (Bio-Rad) for weakly expressed proteins and IPs. The antibodies and respective dilutions used for the Western blot analyses are given in Table 6.

Table 6. Antibodies used for Western blot experiments in this work.

Primary antibodies			
Target	**Species**	**Supplier**	**Dilution**
α-tubulin	Mouse	Sigma-Aldrich, T9026	1:6000
α-tubulin (for IP analysis)	Rabbit	Sigma-Aldrich, SAB4500087	1:1000
β-catenin	Mouse	BD Bioscience, 610153	1:2000
CDK1	Mouse	Cell Signaling, 9116	1:1000
DVL1/2/3	Rabbit	Merck Millipore, ABD122	1:1000
FLAG M2	Mouse	Sigma-Aldrich, F1804	1:5000
GFP	Rabbit	Abcam, ab290	1:2000
KIF2A (for IP analysis)	Rabbit	Novus Biologicals, NB500-180	1:10000
KIF2A	Mouse	Santa Cruz, sc-271471	1:300
LRP6	Rabbit	Cell Signaling, 2560	1:1000
PLK1 (for IP analysis)	Rabbit	Bethyl Laboratories, A300-251A	1:1000
RANBP2	Mouse	Santa Cruz, sc-74518	1:500

Secondary antibodies			
Target	**Species**	**Supplier**	**Dilution**
Mouse IgG HRP conjugate	Goat	Sigma-Aldrich, AP308P	1:5000
Rabbit IgG HRP conjugate	Goat	Sigma-Aldrich, AP307P	1:5000

6.2.8 Immunoprecipitation (IP)

HeLa cells were seeded in 6-well plates, transfected with siRNA for 48 h (section 6.2.5), synchronized in mitosis (section 6.2.3) and treated with Control CM (1:5), DKK1 CM (1:5) or PLK1 inhibitor BI-2536 (1 μM, Selleckchem) for 1.5 h before harvesting as indicated.

To determine the endogenous interactions of PLK1 with KIF2A, PLK1 was immunoprecipitated and both KIF2A and PLK1 protein levels were analyzed by Western blotting. As a rule of thumb, for each sample containing ~1 mg protein lysate, 20 μl agarose beads and 5 μg antibody were used for the immunoprecipitation (IP). In detail, one day before the IP, protein G agarose (Roche) was washed 3 times by adding equal volumes of IP lysis buffer to the beads, spinning down (30 sec, 500-1,000 rpm, 4 °C) and discarding the buffer. and 20 μl of bead sediment (corresponding to 40 μl original agarose bead slurry) were mixed with 20 μl filtered IP lysis buffer including 5% BSA per sample. 5 μg of mouse anti-PLK1 antibody (25 μl of 200 μg/ml stock) was added to the mix and incubated in rotation at 4 °C overnight. The next day, cells were harvested in DPBS on ice as described above for Western blots (section 6.2.7). For each sample, 4 confluent wells of a 6-well plate were combined. The pellets were lysed with 1 ml IP lysis buffer (see 6.1.2.4) for 15 min on ice. In general, a protein concentration of 0.5-5 mg protein per ml is recommended for an efficient IP. Cells were resuspended again and centrifuged (15 min, 12,000 rpm, 4 °C). The supernatant was pre-cleaned with 20 μl washed agarose beads (40 μl beads diluted 1:1 in IP lysis buffer) in rotation at 4 °C for 1 h. The beads were removed by centrifugation (5 min, 12,000 rpm, 4 °C) and supernatant transferred into a new tube. A small volume of each lysate (about 1/13 of each sample) was saved for the “input”, mixed 1:4 with NuPAGE loading buffer containing 50 mM DTT and heated for 10 min at 70 °C.

The agarose beads, that were incubated with the PLK1 antibody overnight, were spun down (30 sec, 1,000 rpm, 4 °C), taken up 1:1 in IP lysis buffer and added to the lysates (40 μl bead-lysis buffer-mix per sample). The samples were incubated with the antibody-beads in rotation at 4 °C for 4 h. Afterwards, beads were washed 3 times with IP lysis buffer supplemented with 10 μM MG132. Proteins were eluted using 100 μl 1X NuPAGE loading buffer with 12.5 mM DTT and boiled for 10 min at 70 °C. After letting them cool down and spinning them briefly down, the samples and their inputs were loaded on 8% NuPAGE Bis-Tris gels and analyzed by Western blotting as described above (section 6.2.7). In so doing, rabbit anti-PLK1 (Bethyl Laboratories), rabbit anti-KIF2A (Novus Biologicals) and rabbit anti-α-tubulin (Sigma-Aldrich), in combination with goat anti-Rabbit IgG HRP conjugate (Sigma-Aldrich), were used for the analysis (for details on the antibodies, please consult Table 6).

6.2.9 Phosphoproteomics (SILAC-MS)

For the stable isotope labeling by amino acids in cell culture, coupled with mass spectrometry (SILAC-MS), RPE1 cells were synchronized in mitosis as described in section 6.2.3 and treated with home-made SILAC labelled Control, WNT3A or DKK1 medium for 1.5 h before harvesting (production described under 6.2.2). In this, SILAC Control medium contained medium isotopes (Arg6, Lys4), WNT3A medium light isotopes (Arg0, Lys0) and DKK1 medium heavy isotopes (Arg10, Lys8) (Cambridge Isotope Laboratories)[280]. After harvesting, the cells of each condition were lysed and samples prepared for phosphopeptide-MS analysis. In this process, the full lysates were cleaned, combined, digested into peptides, enriched for phosphopeptides, fractionated, and peptides analyzed for their phospho-site occupancy in a mass spectrometer. In parallel, the lysates were enriched and analyzed for ubiquitinated peptides, however the ubiquitination data was put aside for this study. The exact procedures of the phospho-MS analysis can be found in Bufe et al., 2021[285].

The downstream analysis of the MS data was performed by me using Microsoft Excel and the *GOrilla* software. Firstly, all proteins that were detected in only one experiment were removed. The log2 values of the independent datasets were calculated and mapped against each other to assure the reproducibility of the two performed experiments. To explore possible overlaps between the Wnt inhibition and activation scenario, the average changes in phosphopeptide counts, each for the DKK1/Control (H/M) and Control/WNT3A (M/L) ratios, were mapped against each other and compared. As there were only 4 proteins that were contrary regulated by WNT3A and DKK1, I focused in the further course of the analysis only on the phosphoproteins that were regulated by DKK1. Therefore, the detected phosphoproteins for the DKK1/Control condition were narrowed down to the significantly regulated proteins. In this I defined all proteins that were 2-fold up- or downregulated as significantly changing (H/M >2 or <0.5). I manually curated the received list by removing proteins that appeared multiple times. With the extracted list I performed a gene ontology enrichment analysis of functional protein groups using the *GOrilla* software, applying all proteins detected in the phospho-MS screen as the genetic background[281,282].

6.2.10 Immunofluorescence (IF)

RPE1 or HeLa cells were seeded in 12-well plates on Ø 15 mm coverslips and transfected with siRNA for 48 h (see 6.2.5), transfected with DNA for 24 h (see 6.2.4) and treated for 1.5 h as indicated in the figures and described above. Cells were fixed with 2% paraformaldehyde (PFA) in PBS for 10 min at RT. After this step, the plate was either stored at 4 °C in PBS for later staining or cells were stained directly for the indicated protein(s) and DAPI at RT. At this,

cells were opened with 0.01% Triton X-100 in PBS for 10 min at horizontal oscillation and blocked with 2% horse serum in 0.1% Triton X-100 in PBS for 20 min. Subsequently, cells were incubated with primary antibodies, diluted in blocking buffer as indicated in Table 7, for 3 h. Afterwards, they were washed 3 times for 5 min in horizontal oscillation with 0.01% Triton X-100 in PBS and incubated for 1 h with Alexa Fluor secondary antibodies diluted 1:500 and 1 μg/ml DAPI in bocking buffer. Finally, cells were washed twice with 0.01% Triton X-100 in PBS and once with PBS for 5 min at horizontal oscillation. For mounting, coverslips were rinsed in H_2O, mounted with mounting medium (Fluoromount, Sigma-Aldrich), dried overnight, sealed with nail polish, and stored at 4 °C in the dark until imaging.

Table 7. Antibodies used for immunofluorescence experiments in this work.

Primary antibodies			
Target	**Species**	**Supplier**	**Dilution**
α-tubulin	Mouse	Sigma-Aldrich, T9026	1:250
α-tubulin	Rabbit	Sigma-Aldrich, SAB4500087	1:500
FLAG M2	Mouse	Sigma-Aldrich, F1804	1:500
KIF2A	Mouse	Santa Cruz, sc-271471	1:50
Pericentrin	Rabbit	Abcam, ab4448	1:1000

Secondary antibodies			
Target	**Species**	**Supplier**	**Dilution**
Mouse AF488	Donkey	Thermo Fisher, A21202	1:500
Rabbit AF488	Donkey	Thermo Fisher, A21206	1:500
Mouse AF594	Donkey	Thermo Fisher, A21203	1:500
Rabbit AF594	Donkey	Thermo Fisher, A21207	1:500

Coverslips were imaged with a Nikon Eclipse Ti microscope (Nikon) using a 60X objective with oil immersion (Nikon) and the NIS Elements software. The data were analyzed using Fiji (ImageJ2). To assess KIF2A levels at the spindle poles, a threshold for the KIF2A signal was set to only detect KIF2A located at the poles. The intensities of KIF2A are displayed relative to the control condition. To determine chromosome congression and alignment in mitosis, the length of the forming metaphase plate was divided by its width towards the spindle poles. Cells for which not both poles were distinctively visible, correlating with tilted cells, which was visualized by pericentrin stainings, were excluded from the analyses. The localization of the overexpressed KIF2A mutants in DVL2 puncta in interphase (Figure 5C,D) was quantified by

the number of cells possessing KIF2A and DVL2 in puncta relative to cells showing DVL2 alone in puncta. Colocalization of KIF2A with PLK1 in DVL interphase puncta (Figure 6D,E) was recorded by the number of puncta per cell that comprised KIF2A and PLK1 relative to the total area of the cell. Notably, there were little cells that included KIF2A or PLK1 only. Most cells did show either both KIF2A and PLK1 in puncta or none.

6.2.11 Proximity ligation assay (PLA)

HeLa cells were seeded in 12-well plates with coverslips and transfected or treated as indicated and described in the section above (see 6.2.10). Cells were fixed with 2% PFA for 10 min and opened with 0.01% Triton X-100 for 10 min at horizontal oscillation and RT. To quantify the proximity and possible interaction of proteins proximity ligation assays (PLAs) were performed using the Duolink In Situ Red Starter Kit Mouse/Rabbit from Sigma-Aldrich following the manufacturer's instructions. After mounting, the coverslips were sealed with nail polish and stored at –20 °C in the dark until imaging. Note: 1) The Duolink mounting medium contains DAPI already, thus no DAPI has to be added during the procedure. 2) The Duolink mounting medium does not solidify, therefore caution should be taken when storing and imaging the coverslips to not move the coverslips accidently. Surrounding the coverslip with nail polish helps to prevent the moving and drying out of the sample.

For the overexpression PLAs, *EGFP-KIF2A* and a *FLAG*-tagged Wnt pathway component were overexpressed in equal amounts and the interactions analyzed using rabbit anti-GFP (Abcam) and mouse anti-FLAG M2 (Sigma-Aldrich) antibodies. Endogenous interactions were investigated by using mouse anti-KIF2A (Santa Cruz), rabbit anti-DVL (Merck Millipore) and rabbit anti-PLK1 (Abcam) in PLA experiments. Details on the used antibodies are given in Table 8.

Table 8. Antibodies used for proximity ligation assays (PLA) in this work.

Primary antibodies			
Target	**Species**	**Supplier**	**Dilution**
DVL1/2/3	Rabbit	Merck Millipore, ABD122	1:500
FLAG M2	Mouse	Sigma-Aldrich, F1804	1:800
GFP	Rabbit	Abcam, ab290	1:800
KIF2A	Mouse	Santa Cruz, sc-271471	1:50
PLK1	Rabbit	Abcam, ab14209	1:250

Coverslips were imaged with a Nikon Eclipse Ti microscope (Nikon) using a 60X objective with oil immersion (Nikon) and the NIS Elements software. The data were analyzed using Fiji (ImageJ2). At this, for the overexpression PLAs, the number of PLA complexes (Figure 4B,C) or PLA mean fluorescence intensity (Figure 4F) per cell were quantified and divided by the corrected total cell fluorescence (CTCF) of the EGFP-KIF2A signal of the respective cell to normalize for the transfection efficiency. The CTCF corresponds to the integrated density of the GFP signal minus the area of the selected cell multiplied by the average mean fluorescence of the background (Formula: CTCF = IntDent – (Area x Mean background)). For the endogenous PLAs (Figure 4H, 6B), the number of PLA complexes per cell were quantified and divided by the cell area. For all experiments the obtained values were calculated and plotted relative to the control condition.

6.2.12 Analysis of bipolar spindle maintenance and centrosome amplification

The involvement of KIF2A in bipolar spindle maintenance and centrosomes amplification was tested as previously described by Tanenbaum et al., 2009[195].

In detail, HeLa cells were seeded in 12-well plates with coverslips and transfected with 30 nM siRNA against KIF2A, LRP5/6, DVL1-3 or KIF2C (MCAK) as described under 6.2.5. The latter protein is known to contribute to spindle bipolarity and hence served as a positive control for the experiment[195]. The next day, cells were treated with 2.5 mM thymidine for 24 h to synchronize them in G1/S, released for 7.5 h in DMEM++ medium and synchronized with 5 μM MG132 for 2.5 h in metaphase. During metaphase EG5 (KIF11) was inhibited with 2 μM DME for 1.5 h. Cells were fixed with 2% PFA, opened with 0.01% Triton X-100 and stained with mouse anti-α-tubulin (Sigma Aldrich), rabbit anti-Pericentrin (Abcam) and DAPI as described above (section 6.2.10).

Coverslips were imaged with a Nikon Eclipse Ti microscope (Nikon) using a 60X objective with oil immersion (Nikon) and the NIS Elements software. The data were analyzed using Fiji (ImageJ2). The occurrence of cells with monopolar versus bipolar spindles as well as the centrosome number per cell was quantified and displayed relative to the total number of cells analyzed. Note: The inhibition of EG5 (KIF11), which is important for centrosome separation and the formation of a bipolar spindle, causes monopolar spindles in prophase[157,195]. Contrasting this, in metaphase, EG5 inhibition does not affect bipolarity, unless a protein required for bipolar spindle maintenance is lost simultaneously, leading to the formation of monopolar spindles.

6.2.13 Karyotype analysis

RPE1 cells were seeded in 6-well plates and transfected with 10 nM siRNA against KIF2A, LRP5/6 or scrambled (siControl #2) every 5 days throughout 30 days (as described in 6.2.5). The karyotype of the cells was analyzed by the Bastians laboratory as described previously[52]. In so doing, cells were treated with 2 μM DME for 4 h before harvesting to enrich the culture for mitotic cells. Afterwards, cells were collected, spun down (5 min, 1,000 rpm), washed with PBS, mixed carefully with prewarmed hypotonic solution (40% DMEM-F12 without penicillin-streptomycin or FBS + 60% H_2O) and incubated at RT for 15 min. Cells were fixed in Carnoy's solution (3:1 solution of methanol:glacial acetic acid) by mixing them with the fixative, centrifugating them (5 min, 1,000 rpm) and recovering the pellet, which was repeated 3 times. Finally, the pellet was resuspended in acetic acid and cell suspension dropped onto pre-cooled (4 °C), wet glass slides to break the cells and spread chromosomes. Spreads were incubated on a wet tissue at 42 °C for 5-10 min and dried at RT. The slides were stained with 8% Giemsa staining solution, dried and mounted with Euparal mounting medium. Chromosome spreads were imaged and chromosome numbers counted manually to determine the karyotype (done by the Bastians laboratory).

6.2.14 Live cell imaging

6.2.14.1 Live cell imaging of 2D cell lines

HeLa-Kyoto cells stably expressing *EGFP-α-tubulin* and *H2B-mCherry*, HeLa-Kyoto cells stably expressing *EB3-EGFP* or wildtype hiPSCs were seeded in 10-well CELLview slides (Greiner Bio-One) and transfected with 30 nM siRNA for 48 h (see 6.2.5) and/or transfected with 100 ng plasmid DNA per well for 24 h (6.2.4) as indicated. Treatments with CM were applied either directly before starting the imaging (for HeLa-Kyoto cells) or overnight (for hiPSCs). The DNA of HeLa-Kyoto EB3-EGFP and hiPS cells was labelled 1 h prior and during the live cell imaging experiment with 500 nM SiR-DNA (Spirochrome AG, SC007). The used concentration of SiR-DNA did not cause any mitotic delays or aberrations as validated in preliminary experiments with HeLa-Kyoto and hiPS cells (data not shown). During the imaging, HeLa-Kyoto cells were cultured in DMEM medium with HEPES and no phenol red (Gibco), supplemented with 10% FBS (Gibco), 1% penicillin-streptomycin (Gibco) and 1% sodium pyruvate (100 mM) (Gibco), to prevent background signals and scattering due to the red pH indicator. HiPSCs were imaged in fresh Essential 8 medium (Thermo Scientific), supplemented with 1% penicillin-streptomycin (Gibco). The live cell imaging was performed at the Nikon Imaging Center (University Heidelberg) using an automated Nikon Eclipse Ti2 inverted microscope, which was equipped with a 40X objective with water immersion (Nikon

Apo LWD 40X NA 1.15 λS), a water suspensor to ensure regular water supply to maintain the immersion, and a NEO sCMOS camera (Andor). Live cells were recorded every 10 min for up to 16 h (for HeLa-Kyoto EGFP-α-tubulin/H2B-mCherry) or every 5 min for 5 h (HeLa-Kyoto EB3-EGFP and hiPSCs) in a preheated chamber (STXG-WSKM Stage Top Incubator, Tokai Hit) at 37 °C and 5% CO_2. In detail, for each condition 8 positions (2 wells with each 4 positions) were pre-selected and 5 z-stacks with 2 μM (HeLa-Kyoto EGFP-α-tubulin/H2B-mCherry) or 1 μM (HeLa-Kyoto EB3-EGFP, hiPSCs) distance, using the lowest exposure times possible to still see the signal well (~100-300 ms) and 2x2 binning, were acquired. The image acquisition was controlled with the NIS Elements 5.1 software. The downstream analysis of the images was done with Fiji (ImageJ2). For HeLa-Kyoto EGFP-α-tubulin/H2B-mCherry, in Figure 8, the lengths of the different mitotic phases were quantified as indicated in the figure and two dominant phenotypes were registered, namely chromosome misalignments and multipolar (predominantly tripolar) spindles. In the following experiment (Figure 9) the time the cells needed to progress from nuclear envelope breakdown (NEB) to anaphase entry and all phenotypic aberrations, that were noticed from the beginning until the end of the imaging, were recorded by screening through the z-stacks and time series. At this, both chromosome misalignments and multipolar spindles in metaphase, anaphase lagging chromosomes or bridges as well as the fate of the cells, namely the division into 3 or more daughter cells (“>2 daughter cells”), binuclearity, micronuclei or apoptosis, were noted. For both experiments, only cells that showed stable transfection with both EGFP-α-tubulin and H2B-mCherry were considered.

When analyzing the HeLa-Kyoto EB3-EGFP and hiPSCs, the mitotic timing from NEB until anaphase entry and the number of chromosome alignment defects in metaphase were recorded. Prior to the analysis, the z-stacks, displaying the metaphases of the cells most clearly, were selected and maximum intensity projections performed. Subsequently, mitotic phenotypes were recorded and categorized into 4 groups, including I) cells with a normal metaphase, II) cells showing “mild misalignment”, which was characterized by errors or delays in the alignment of all chromosomes in a thin metaphase plate, reflected by a clearly wider chromosome spread of the plate towards the poles, before anaphase III) cells characterized by “severe misalignment”, displaying one or more chromosomes clearly detached from the metaphase plate and IV) cells that ended up with “misalignment + arrest”, which showed mostly severe chromosome misalignments and were arrested for longer than 75 min in mitosis, often undergoing mitotic failure. For all experiments the recorded mitotic defects were plotted relative to the total number of metaphase cells analyzed.

6.2.14.2 Live cell imaging of 3D intestinal organoids

Mouse intestinal organoids stably expressing *H2B-EGFP* were seeded as domes in 10-well CELLview slides (Greiner Bio-One) and cultured in WENR medium (see section 6.2.1.2) after splitting to enrich for stem cells and create cyst-like shapes, which facilitate the imaging. The next day, for two wells each, the medium was replaced by full WENR medium, EN medium (WENR without WNT and RSPO) or EN medium supplemented with DKK1 6 h prior to imaging as indicated. The intestinal organoids were analyzed by confocal live cell imaging, which was performed at the Nikon Imaging Center (University Heidelberg) using an automated Nikon Eclipse Ti2, which was equipped with a Crest X-Light V3 spinning disk system (Nikon), a 40X water immersion objective (Nikon Apo LWD 40X NA 1.15 λS), a water suspensor to ensure regular water supply for the immersion and an Iris 15 sCMOS camera (Teledyne Photometrics). Prior to imaging, 4 organoids per well were defined to be monitored over the course of the experiment. At this, small, round, single organoids showing moderate brightness were preferentially selected. During the live imaging 5 z-stacks with 1 μM distance, using the lowest exposure time possible, were recorded every 5 min for 5 h in a preheated chamber (Tokai Hit) at 37 °C and 5% CO_2 using the spinning disk unit of the system, which was controlled by the NIS Elements 5.1 software. The images were analyzed using Fiji (ImageJ2). At this, anaphase bridges, lagging chromosomes and multipolar spindles were quantified by screening through the z-stacks and time series. The defects were plotted relative to the total number of mitotic cells analyzed.

6.2.15 Microtubule plus-end tracking

Microtubule plus-end assembly rates were determined by tracking EGFP-EB3 as previously described by the Bastians group[305].

Wildtype hiPSCs were seeded in 8-well microscopy chambers (μ-Slide 8 Well, ibiTreat Surface, Ibidi) and transfected with 300 ng EGFP-EB3 plasmid per well for 24 h (see 6.2.4) and treated with Control CM (1:5), DKK1 CM (1:5) and nucleosides (20 μM of each deoxyadenine, thymidine, deoxyguanosine and deoxycytidine (Santa Cruz)) overnight as indicated. The next day, 30 min before starting the imaging, cells were synchronized with 2 μM DME to ensure that all spindle MTs are recorded in the same mitotic phase. Note: As MTs are cold-sensitive, it is important to always preheat the medium before addition and to not keep the cells out of the incubator for too long or put them on any cold surface.

Live cell imaging was performed at the Nikon Imaging Center (University Heidelberg) using an automated Nikon Eclipse Ti2 inverted microscope, which was equipped with a 100X objective with oil immersion (Nikon Plan Fluor 100X NA 1.3) and a NEO sCMOS camera

(Andor). Single EGFP-EB3-positive spindles with moderate brightness were selected and 4 z-stacks with 0.4 μM distance recorded every 2 seconds over 30-45 seconds in a preheated chamber (STXG-WSKM Stage Top Incubator, Tokai Hit) at 37 °C and 5% CO_2. At this, low exposure times (200 ms), 2x2 binning and a manual 1.5X magnification were used. The microscope was controlled by the NIS Elements 5.1 software. For the downstream analysis, images were deconvolved using NIS Elements 5.1 (automatic deconvolution) and further processed via Fiji (ImageJ2). At this, maximum intensity projections of all z-stacks were performed and EGFP-EB3 comets tracked by the "Manual Tracking" plugin embedded in Fiji. The average assembly rates (μm/min) were calculated based on at least two values for each individual MT and ≥ 30 MTs per spindle, which were randomly selected.

6.2.16 Statistical analysis

The raw data were imported, analyzed, and organized in Microsoft Excel for Mac (version 16.56) and subsequently transferred to GraphPad Prism 9 for macOS (version 9.2.0) for statistical analysis and plotting. The data are displayed as mean values +/– standard deviation (SD) or as the ratio of cells showing a phenotype in comparison to the total number of cells that were analyzed (given as percentage (%)). The statistical significance of the results was tested by unpaired t tests (for comparisons of two groups) or ordinary one-way ANOVA analysis with Tukey's correction (for more than two groups) using GraphPad Prism 9. The significance is indicated as * = $P < 0.05$, ** = $P < 0.01$, *** = $P < 0.001$, or ns = not significant in the figures.

6.2.17 Image processing and creation of figures

The raw images were imported into Fiji (ImageJ version 2.1.0) and analyzed as indicated above. Exemplary images were selected, cropped to the region of interest and channels adjusted to enable better visualization. Changes in contrast or brightness were equally applied to all images of the data set and across the entire images. The analyzed data was plotted using GraphPad Prism 9 for macOS (version 9.2.0). Schemes were created with BioRender.com. The elements of the final figures were combined and arranged in Microsoft PowerPoint for Mac (version 16.56) and exported as PNG files.

7. References

1 Nusse, R. & Clevers, H. Wnt/beta-Catenin Signaling, Disease, and Emerging Therapeutic Modalities. *Cell* **169**, 985-999, doi:10.1016/j.cell.2017.05.016 (2017).

2 Steinhart, Z. & Angers, S. Wnt signaling in development and tissue homeostasis. *Development* **145**, doi:10.1242/dev.146589 (2018).

3 Yang, Y. & Mlodzik, M. Wnt-Frizzled/planar cell polarity signaling: cellular orientation by facing the wind (Wnt). *Annu Rev Cell Dev Biol* **31**, 623-646, doi:10.1146/annurev-cellbio-100814-125315 (2015).

4 Nichols, S. A., Dirks, W., Pearse, J. S. & King, N. Early evolution of animal cell signaling and adhesion genes. *Proc Natl Acad Sci U S A* **103**, 12451-12456, doi:10.1073/pnas.0604065103 (2006).

5 Hobmayer, B. *et al.* WNT signalling molecules act in axis formation in the diploblastic metazoan Hydra. *Nature* **407**, 186-189, doi:10.1038/35025063 (2000).

6 Noordermeer, J., Klingensmith, J., Perrimon, N. & Nusse, R. dishevelled and armadillo act in the wingless signalling pathway in Drosophila. *Nature* **367**, 80-83, doi:10.1038/367080a0 (1994).

7 Sidow, A. Diversification of the Wnt gene family on the ancestral lineage of vertebrates. *Proc Natl Acad Sci U S A* **89**, 5098-5102, doi:10.1073/pnas.89.11.5098 (1992).

8 Prud'homme, B., Lartillot, N., Balavoine, G., Adoutte, A. & Vervoort, M. Phylogenetic analysis of the Wnt gene family. Insights from lophotrochozoan members. *Curr Biol* **12**, 1395, doi:10.1016/s0960-9822(02)01068-0 (2002).

9 Najdi, R. *et al.* A uniform human Wnt expression library reveals a shared secretory pathway and unique signaling activities. *Differentiation* **84**, 203-213, doi:10.1016/j.diff.2012.06.004 (2012).

10 Grumolato, L. *et al.* Canonical and noncanonical Wnts use a common mechanism to activate completely unrelated coreceptors. *Genes Dev* **24**, 2517-2530, doi:10.1101/gad.1957710 (2010).

11 Torres, M. A. *et al.* Activities of the Wnt-1 class of secreted signaling factors are antagonized by the Wnt-5A class and by a dominant negative cadherin in early Xenopus development. *J Cell Biol* **133**, 1123-1137, doi:10.1083/jcb.133.5.1123 (1996).

12 Kuhl, M. *et al.* Antagonistic regulation of convergent extension movements in Xenopus by Wnt/beta-catenin and Wnt/Ca2+ signaling. *Mech Dev* **106**, 61-76, doi:10.1016/s0925-4773(01)00416-6 (2001).

13 Sato, A., Yamamoto, H., Sakane, H., Koyama, H. & Kikuchi, A. Wnt5a regulates distinct signalling pathways by binding to Frizzled2. *EMBO J* **29**, 41-54, doi:10.1038/emboj.2009.322 (2010).

14 Paclikova, P. *et al.* Roles of individual human Dishevelled paralogs in the Wnt signalling pathways. *Cell Signal* **85**, 110058, doi:10.1016/j.cellsig.2021.110058 (2021).

15 Niehrs, C. The complex world of WNT receptor signalling. *Nat Rev Mol Cell Biol* **13**, 767-779, doi:10.1038/nrm3470 (2012).

16 van Amerongen, R. & Nusse, R. Towards an integrated view of Wnt signaling in development. *Development* **136**, 3205-3214, doi:10.1242/dev.033910 (2009).

17 Mikels, A. J. & Nusse, R. Purified Wnt5a protein activates or inhibits beta-catenin-TCF signaling depending on receptor context. *PLoS Biol* **4**, e115, doi:10.1371/journal.pbio.0040115 (2006).

18 Slusarski, D. C., Corces, V. G. & Moon, R. T. Interaction of Wnt and a Frizzled homologue triggers G-protein-linked phosphatidylinositol signalling. *Nature* **390**, 410-413, doi:10.1038/37138 (1997).

19 Clevers, H., Loh, K. M. & Nusse, R. Stem cell signaling. An integral program for tissue renewal and regeneration: Wnt signaling and stem cell control. *Science* **346**, 1248012, doi:10.1126/science.1248012 (2014).

20 Behrens, J. *et al.* Functional interaction of an axin homolog, conductin, with beta-catenin, APC, and GSK3beta. *Science* **280**, 596-599, doi:10.1126/science.280.5363.596 (1998).
21 Zeng, L. *et al.* The mouse Fused locus encodes Axin, an inhibitor of the Wnt signaling pathway that regulates embryonic axis formation. *Cell* **90**, 181-192, doi:10.1016/s0092-8674(00)80324-4 (1997).
22 Liu, C. *et al.* Control of beta-catenin phosphorylation/degradation by a dual-kinase mechanism. *Cell* **108**, 837-847 (2002).
23 Aberle, H., Bauer, A., Stappert, J., Kispert, A. & Kemler, R. beta-catenin is a target for the ubiquitin-proteasome pathway. *Embo j* **16**, 3797-3804, doi:10.1093/emboj/16.13.3797 (1997).
24 Bhanot, P. *et al.* A new member of the frizzled family from Drosophila functions as a Wingless receptor. *Nature* **382**, 225-230, doi:10.1038/382225a0 (1996).
25 Tamai, K. *et al.* LDL-receptor-related proteins in Wnt signal transduction. *Nature* **407**, 530-535, doi:10.1038/35035117 (2000).
26 Theisen, H. *et al.* dishevelled is required during wingless signaling to establish both cell polarity and cell identity. *Development* **120**, 347-360 (1994).
27 Zeng, X. *et al.* A dual-kinase mechanism for Wnt co-receptor phosphorylation and activation. *Nature* **438**, 873-877, doi:10.1038/nature04185 (2005).
28 Davidson, G. *et al.* Casein kinase 1 gamma couples Wnt receptor activation to cytoplasmic signal transduction. *Nature* **438**, 867-872, doi:10.1038/nature04170 (2005).
29 Davidson, G. *et al.* Cell cycle control of wnt receptor activation. *Dev Cell* **17**, 788-799, doi:10.1016/j.devcel.2009.11.006 (2009).
30 Piao, S. *et al.* Direct inhibition of GSK3beta by the phosphorylated cytoplasmic domain of LRP6 in Wnt/beta-catenin signaling. *PLoS One* **3**, e4046, doi:10.1371/journal.pone.0004046 (2008).
31 Bilic, J. *et al.* Wnt induces LRP6 signalosomes and promotes dishevelled-dependent LRP6 phosphorylation. *Science* **316**, 1619-1622, doi:10.1126/science.1137065 (2007).
32 Taelman, V. F. *et al.* Wnt signaling requires sequestration of glycogen synthase kinase 3 inside multivesicular endosomes. *Cell* **143**, 1136-1148, doi:10.1016/j.cell.2010.11.034 (2010).
33 Cruciat, C. M. *et al.* Requirement of prorenin receptor and vacuolar H+-ATPase-mediated acidification for Wnt signaling. *Science* **327**, 459-463, doi:10.1126/science.1179802 (2010).
34 Yamamoto, H., Komekado, H. & Kikuchi, A. Caveolin is necessary for Wnt-3a-dependent internalization of LRP6 and accumulation of beta-catenin. *Dev Cell* **11**, 213-223, doi:10.1016/j.devcel.2006.07.003 (2006).
35 Kim, S. E. *et al.* Wnt stabilization of beta-catenin reveals principles for morphogen receptor-scaffold assemblies. *Science* **340**, 867-870, doi:10.1126/science.1232389 (2013).
36 Molenaar, M. *et al.* XTcf-3 transcription factor mediates beta-catenin-induced axis formation in Xenopus embryos. *Cell* **86**, 391-399, doi:10.1016/s0092-8674(00)80112-9 (1996).
37 Behrens, J. *et al.* Functional interaction of beta-catenin with the transcription factor LEF-1. *Nature* **382**, 638-642, doi:10.1038/382638a0 (1996).
38 Tetsu, O. & McCormick, F. Beta-catenin regulates expression of cyclin D1 in colon carcinoma cells. *Nature* **398**, 422-426, doi:10.1038/18884 (1999).
39 He, T. C. *et al.* Identification of c-MYC as a target of the APC pathway. *Science* **281**, 1509-1512, doi:10.1126/science.281.5382.1509 (1998).

40 Jho, E. H. *et al.* Wnt/beta-catenin/Tcf signaling induces the transcription of Axin2, a negative regulator of the signaling pathway. *Mol Cell Biol* **22**, 1172-1183, doi:10.1128/MCB.22.4.1172-1183.2002 (2002).
41 Daniels, D. L. & Weis, W. I. Beta-catenin directly displaces Groucho/TLE repressors from Tcf/Lef in Wnt-mediated transcription activation. *Nat Struct Mol Biol* **12**, 364-371, doi:10.1038/nsmb912 (2005).
42 Cruciat, C. M. & Niehrs, C. Secreted and transmembrane wnt inhibitors and activators. *Cold Spring Harb Perspect Biol* **5**, a015081, doi:10.1101/cshperspect.a015081 (2013).
43 Mao, B. *et al.* LDL-receptor-related protein 6 is a receptor for Dickkopf proteins. *Nature* **411**, 321-325, doi:10.1038/35077108 (2001).
44 Glinka, A. *et al.* Dickkopf-1 is a member of a new family of secreted proteins and functions in head induction. *Nature* **391**, 357-362, doi:10.1038/34848 (1998).
45 Mao, B. *et al.* Kremen proteins are Dickkopf receptors that regulate Wnt/beta-catenin signalling. *Nature* **417**, 664-667, doi:10.1038/nature756 (2002).
46 Yamamoto, H., Sakane, H., Yamamoto, H., Michiue, T. & Kikuchi, A. Wnt3a and Dkk1 regulate distinct internalization pathways of LRP6 to tune the activation of beta-catenin signaling. *Dev Cell* **15**, 37-48, doi:10.1016/j.devcel.2008.04.015 (2008).
47 Kim, N. G., Xu, C. & Gumbiner, B. M. Identification of targets of the Wnt pathway destruction complex in addition to beta-catenin. *Proc Natl Acad Sci U S A* **106**, 5165-5170, doi:10.1073/pnas.0810185106 (2009).
48 Xu, C., Kim, N. G. & Gumbiner, B. M. Regulation of protein stability by GSK3 mediated phosphorylation. *Cell Cycle* **8**, 4032-4039, doi:10.4161/cc.8.24.10111 (2009).
49 Acebron, S. P., Karaulanov, E., Berger, B. S., Huang, Y. L. & Niehrs, C. Mitotic wnt signaling promotes protein stabilization and regulates cell size. *Mol Cell* **54**, 663-674, doi:10.1016/j.molcel.2014.04.014 (2014).
50 Huang, Y. L., Anvarian, Z., Doderlein, G., Acebron, S. P. & Niehrs, C. Maternal Wnt/STOP signaling promotes cell division during early Xenopus embryogenesis. *Proc Natl Acad Sci U S A* **112**, 5732-5737, doi:10.1073/pnas.1423533112 (2015).
51 Da Silva, F. *et al.* Mitotic WNT signalling orchestrates neurogenesis in the developing neocortex. *EMBO J* **40**, e108041, doi:10.15252/embj.2021108041 (2021).
52 Stolz, A., Neufeld, K., Ertych, N. & Bastians, H. Wnt-mediated protein stabilization ensures proper mitotic microtubule assembly and chromosome segregation. *EMBO Rep* **16**, 490-499, doi:10.15252/embr.201439410 (2015).
53 Lin, Y. C. *et al.* Wnt10b-GSK3beta-dependent Wnt/STOP signaling prevents aneuploidy in human somatic cells. *Life Sci Alliance* **4**, doi:10.26508/lsa.202000855 (2021).
54 Madan, B. *et al.* Temporal dynamics of Wnt-dependent transcriptome reveal an oncogenic Wnt/MYC/ribosome axis. *J Clin Invest* **128**, 5620-5633, doi:10.1172/JCI122383 (2018).
55 Koch, S., Acebron, S. P., Herbst, J., Hatiboglu, G. & Niehrs, C. Post-transcriptional Wnt Signaling Governs Epididymal Sperm Maturation. *Cell* **163**, 1225-1236, doi:10.1016/j.cell.2015.10.029 (2015).
56 Chen, J. *et al.* CDK1-mediated BCL9 phosphorylation inhibits clathrin to promote mitotic Wnt signalling. *EMBO J* **37**, doi:10.15252/embj.201899395 (2018).
57 De, A. Wnt/Ca2+ signaling pathway: a brief overview. *Acta Biochim Biophys Sin (Shanghai)* **43**, 745-756, doi:10.1093/abbs/gmr079 (2011).
58 Sheldahl, L. C. *et al.* Dishevelled activates Ca2+ flux, PKC, and CamKII in vertebrate embryos. *J Cell Biol* **161**, 769-777, doi:10.1083/jcb.200211094 (2003).
59 Boutros, M., Paricio, N., Strutt, D. I. & Mlodzik, M. Dishevelled activates JNK and discriminates between JNK pathways in planar polarity and wingless signaling. *Cell* **94**, 109-118, doi:10.1016/s0092-8674(00)81226-x (1998).

60 Strutt, D. I., Weber, U. & Mlodzik, M. The role of RhoA in tissue polarity and Frizzled signalling. *Nature* **387**, 292-295, doi:10.1038/387292a0 (1997).
61 Winter, C. G. *et al.* Drosophila Rho-associated kinase (Drok) links Frizzled-mediated planar cell polarity signaling to the actin cytoskeleton. *Cell* **105**, 81-91, doi:10.1016/s0092-8674(01)00298-7 (2001).
62 Schlessinger, K., McManus, E. J. & Hall, A. Cdc42 and noncanonical Wnt signal transduction pathways cooperate to promote cell polarity. *J Cell Biol* **178**, 355-361, doi:10.1083/jcb.200701083 (2007).
63 Axelrod, J. D., Miller, J. R., Shulman, J. M., Moon, R. T. & Perrimon, N. Differential recruitment of Dishevelled provides signaling specificity in the planar cell polarity and Wingless signaling pathways. *Genes Dev* **12**, 2610-2622, doi:10.1101/gad.12.16.2610 (1998).
64 Westfall, T. A. *et al.* Wnt-5/pipetail functions in vertebrate axis formation as a negative regulator of Wnt/beta-catenin activity. *J Cell Biol* **162**, 889-898, doi:10.1083/jcb.200303107 (2003).
65 Martin, B. L. & Kimelman, D. Regulation of canonical Wnt signaling by Brachyury is essential for posterior mesoderm formation. *Dev Cell* **15**, 121-133, doi:10.1016/j.devcel.2008.04.013 (2008).
66 Lustig, B. *et al.* Negative feedback loop of Wnt signaling through upregulation of conductin/axin2 in colorectal and liver tumors. *Mol Cell Biol* **22**, 1184-1193 (2002).
67 Niida, A. *et al.* DKK1, a negative regulator of Wnt signaling, is a target of the beta-catenin/TCF pathway. *Oncogene* **23**, 8520-8526, doi:10.1038/sj.onc.1207892 (2004).
68 Yamaguchi, T. P., Bradley, A., McMahon, A. P. & Jones, S. A Wnt5a pathway underlies outgrowth of multiple structures in the vertebrate embryo. *Development* **126**, 1211-1223, doi:10.1242/dev.126.6.1211 (1999).
69 Gong, Y., Mo, C. & Fraser, S. E. Planar cell polarity signalling controls cell division orientation during zebrafish gastrulation. *Nature* **430**, 689-693, doi:10.1038/nature02796 (2004).
70 Voiculescu, O., Bertocchini, F., Wolpert, L., Keller, R. E. & Stern, C. D. The amniote primitive streak is defined by epithelial cell intercalation before gastrulation. *Nature* **449**, 1049-1052, doi:10.1038/nature06211 (2007).
71 Heisenberg, C. P. *et al.* Silberblick/Wnt11 mediates convergent extension movements during zebrafish gastrulation. *Nature* **405**, 76-81, doi:10.1038/35011068 (2000).
72 Wallingford, J. B. *et al.* Dishevelled controls cell polarity during Xenopus gastrulation. *Nature* **405**, 81-85, doi:10.1038/35011077 (2000).
73 Wallingford, J. B. & Harland, R. M. Xenopus Dishevelled signaling regulates both neural and mesodermal convergent extension: parallel forces elongating the body axis. *Development* **128**, 2581-2592 (2001).
74 Huelsken, J. *et al.* Requirement for beta-catenin in anterior-posterior axis formation in mice. *J Cell Biol* **148**, 567-578, doi:10.1083/jcb.148.3.567 (2000).
75 Sokol, S., Christian, J. L., Moon, R. T. & Melton, D. A. Injected Wnt RNA induces a complete body axis in Xenopus embryos. *Cell* **67**, 741-752, doi:10.1016/0092-8674(91)90069-b (1991).
76 Wray, J. *et al.* Inhibition of glycogen synthase kinase-3 alleviates Tcf3 repression of the pluripotency network and increases embryonic stem cell resistance to differentiation. *Nat Cell Biol* **13**, 838-845, doi:10.1038/ncb2267 (2011).
77 Yi, F. *et al.* Opposing effects of Tcf3 and Tcf1 control Wnt stimulation of embryonic stem cell self-renewal. *Nat Cell Biol* **13**, 762-770, doi:10.1038/ncb2283 (2011).
78 Sato, N., Meijer, L., Skaltsounis, L., Greengard, P. & Brivanlou, A. H. Maintenance of pluripotency in human and mouse embryonic stem cells through activation of Wnt signaling by a pharmacological GSK-3-specific inhibitor. *Nat Med* **10**, 55-63, doi:10.1038/nm979 (2004).

79 Augustin, I. *et al.* Autocrine Wnt regulates the survival and genomic stability of embryonic stem cells. *Sci Signal* **10**, doi:10.1126/scisignal.aah6829 (2017).
80 ten Berge, D. *et al.* Embryonic stem cells require Wnt proteins to prevent differentiation to epiblast stem cells. *Nat Cell Biol* **13**, 1070-1075, doi:10.1038/ncb2314 (2011).
81 Xu, Z. *et al.* Wnt/beta-catenin signaling promotes self-renewal and inhibits the primed state transition in naive human embryonic stem cells. *Proc Natl Acad Sci U S A* **113**, E6382-E6390, doi:10.1073/pnas.1613849113 (2016).
82 van de Wetering, M. *et al.* The beta-catenin/TCF-4 complex imposes a crypt progenitor phenotype on colorectal cancer cells. *Cell* **111**, 241-250, doi:10.1016/s0092-8674(02)01014-0 (2002).
83 Habib, S. J. *et al.* A localized Wnt signal orients asymmetric stem cell division in vitro. *Science* **339**, 1445-1448, doi:10.1126/science.1231077 (2013).
84 Lowndes, M., Rotherham, M., Price, J. C., El Haj, A. J. & Habib, S. J. Immobilized WNT Proteins Act as a Stem Cell Niche for Tissue Engineering. *Stem Cell Reports* **7**, 126-137, doi:10.1016/j.stemcr.2016.06.004 (2016).
85 Sato, T. *et al.* Single Lgr5 stem cells build crypt-villus structures in vitro without a mesenchymal niche. *Nature* **459**, 262-265, doi:10.1038/nature07935 (2009).
86 Barker, N. *et al.* Identification of stem cells in small intestine and colon by marker gene Lgr5. *Nature* **449**, 1003-1007, doi:10.1038/nature06196 (2007).
87 Kuhnert, F. *et al.* Essential requirement for Wnt signaling in proliferation of adult small intestine and colon revealed by adenoviral expression of Dickkopf-1. *Proc Natl Acad Sci U S A* **101**, 266-271, doi:10.1073/pnas.2536800100 (2004).
88 Farin, H. F. *et al.* Visualization of a short-range Wnt gradient in the intestinal stem-cell niche. *Nature* **530**, 340-343, doi:10.1038/nature16937 (2016).
89 Merenda, A., Fenderico, N. & Maurice, M. M. Wnt Signaling in 3D: Recent Advances in the Applications of Intestinal Organoids. *Trends Cell Biol* **30**, 60-73, doi:10.1016/j.tcb.2019.10.003 (2020).
90 Kim, K. A. *et al.* R-Spondin family members regulate the Wnt pathway by a common mechanism. *Mol Biol Cell* **19**, 2588-2596, doi:10.1091/mbc.E08-02-0187 (2008).
91 de Lau, W. *et al.* Lgr5 homologues associate with Wnt receptors and mediate R-spondin signalling. *Nature* **476**, 293-297, doi:10.1038/nature10337 (2011).
92 Korinek, V. *et al.* Depletion of epithelial stem-cell compartments in the small intestine of mice lacking Tcf-4. *Nat Genet* **19**, 379-383, doi:10.1038/1270 (1998).
93 Rippon, H. J. & Bishop, A. E. Embryonic stem cells. *Cell Prolif* **37**, 23-34, doi:10.1111/j.1365-2184.2004.00298.x (2004).
94 Takahashi, K. & Yamanaka, S. Induction of pluripotent stem cells from mouse embryonic and adult fibroblast cultures by defined factors. *Cell* **126**, 663-676, doi:10.1016/j.cell.2006.07.024 (2006).
95 Zhang, P. *et al.* Regulation of induced pluripotent stem (iPS) cell induction by Wnt/beta-catenin signaling. *J Biol Chem* **289**, 9221-9232, doi:10.1074/jbc.M113.542845 (2014).
96 Ueno, S. *et al.* Biphasic role for Wnt/beta-catenin signaling in cardiac specification in zebrafish and embryonic stem cells. *Proc Natl Acad Sci U S A* **104**, 9685-9690, doi:10.1073/pnas.0702859104 (2007).
97 Tzahor, E. Wnt/beta-catenin signaling and cardiogenesis: timing does matter. *Dev Cell* **13**, 10-13, doi:10.1016/j.devcel.2007.06.006 (2007).
98 Naito, A. T. *et al.* Developmental stage-specific biphasic roles of Wnt/beta-catenin signaling in cardiomyogenesis and hematopoiesis. *Proc Natl Acad Sci U S A* **103**, 19812-19817, doi:10.1073/pnas.0605768103 (2006).
99 Munji, R. N., Choe, Y., Li, G., Siegenthaler, J. A. & Pleasure, S. J. Wnt signaling regulates neuronal differentiation of cortical intermediate progenitors. *J Neurosci* **31**, 1676-1687, doi:10.1523/JNEUROSCI.5404-10.2011 (2011).

100 Draganova, K. *et al.* Wnt/beta-catenin signaling regulates sequential fate decisions of murine cortical precursor cells. *Stem Cells* **33**, 170-182, doi:10.1002/stem.1820 (2015).
101 Kalani, M. Y. *et al.* Wnt-mediated self-renewal of neural stem/progenitor cells. *Proc Natl Acad Sci U S A* **105**, 16970-16975, doi:10.1073/pnas.0808616105 (2008).
102 ten Berge, D., Brugmann, S. A., Helms, J. A. & Nusse, R. Wnt and FGF signals interact to coordinate growth with cell fate specification during limb development. *Development* **135**, 3247-3257, doi:10.1242/dev.023176 (2008).
103 Niehrs, C. & Acebron, S. P. Mitotic and mitogenic Wnt signalling. *EMBO J* **31**, 2705-2713, doi:10.1038/emboj.2012.124 (2012).
104 Gong, Y. *et al.* LDL receptor-related protein 5 (LRP5) affects bone accrual and eye development. *Cell* **107**, 513-523, doi:10.1016/s0092-8674(01)00571-2 (2001).
105 Mani, A. *et al.* LRP6 mutation in a family with early coronary disease and metabolic risk factors. *Science* **315**, 1278-1282, doi:10.1126/science.1136370 (2007).
106 Kyun, M. L. *et al.* Wnt3a Stimulation Promotes Primary Ciliogenesis through beta-Catenin Phosphorylation-Induced Reorganization of Centriolar Satellites. *Cell Rep* **30**, 1447-1462 e1445, doi:10.1016/j.celrep.2020.01.019 (2020).
107 Lee, K. H. *et al.* Identification of a novel Wnt5a-CK1varepsilon-Dvl2-Plk1-mediated primary cilia disassembly pathway. *EMBO J* **31**, 3104-3117, doi:10.1038/emboj.2012.144 (2012).
108 Sheng, X. *et al.* Vangl2 participates in the primary ciliary assembly under low fluid shear stress in hUVECs. *Cell Tissue Res* **387**, 95-109, doi:10.1007/s00441-021-03546-0 (2022).
109 Mitchison, H. M. & Valente, E. M. Motile and non-motile cilia in human pathology: from function to phenotypes. *J Pathol* **241**, 294-309, doi:10.1002/path.4843 (2017).
110 Seeley, E. S. & Nachury, M. V. The perennial organelle: assembly and disassembly of the primary cilium. *J Cell Sci* **123**, 511-518, doi:10.1242/jcs.061093 (2010).
111 Liu, H., Kiseleva, A. A. & Golemis, E. A. Ciliary signalling in cancer. *Nat Rev Cancer* **18**, 511-524, doi:10.1038/s41568-018-0023-6 (2018).
112 Miyamoto, T. *et al.* The Microtubule-Depolymerizing Activity of a Mitotic Kinesin Protein KIF2A Drives Primary Cilia Disassembly Coupled with Cell Proliferation. *Cell Rep* **10**, 664-673, doi:10.1016/j.celrep.2015.01.003 (2015).
113 Gerdes, J. M. *et al.* Disruption of the basal body compromises proteasomal function and perturbs intracellular Wnt response. *Nat Genet* **39**, 1350-1360, doi:10.1038/ng.2007.12 (2007).
114 Corbit, K. C. *et al.* Kif3a constrains beta-catenin-dependent Wnt signalling through dual ciliary and non-ciliary mechanisms. *Nat Cell Biol* **10**, 70-76, doi:10.1038/ncb1670 (2008).
115 McDermott, K. M., Liu, B. Y., Tlsty, T. D. & Pazour, G. J. Primary cilia regulate branching morphogenesis during mammary gland development. *Curr Biol* **20**, 731-737, doi:10.1016/j.cub.2010.02.048 (2010).
116 Hall, A. C., Lucas, F. R. & Salinas, P. C. Axonal remodeling and synaptic differentiation in the cerebellum is regulated by WNT-7a signaling. *Cell* **100**, 525-535, doi:10.1016/s0092-8674(00)80689-3 (2000).
117 Ciani, L., Krylova, O., Smalley, M. J., Dale, T. C. & Salinas, P. C. A divergent canonical WNT-signaling pathway regulates microtubule dynamics: dishevelled signals locally to stabilize microtubules. *J Cell Biol* **164**, 243-253, doi:10.1083/jcb.200309096 (2004).
118 Zhou, F. Q., Zhou, J., Dedhar, S., Wu, Y. H. & Snider, W. D. NGF-induced axon growth is mediated by localized inactivation of GSK-3beta and functions of the microtubule plus end binding protein APC. *Neuron* **42**, 897-912, doi:10.1016/j.neuron.2004.05.011 (2004).

119 Etienne-Manneville, S. & Hall, A. Cdc42 regulates GSK-3beta and adenomatous polyposis coli to control cell polarity. *Nature* **421**, 753-756, doi:10.1038/nature01423 (2003).
120 Otero, J. J., Fu, W., Kan, L., Cuadra, A. E. & Kessler, J. A. Beta-catenin signaling is required for neural differentiation of embryonic stem cells. *Development* **131**, 3545-3557, doi:10.1242/dev.01218 (2004).
121 Hirabayashi, Y. *et al.* The Wnt/beta-catenin pathway directs neuronal differentiation of cortical neural precursor cells. *Development* **131**, 2791-2801, doi:10.1242/dev.01165 (2004).
122 Lucas, F. R., Goold, R. G., Gordon-Weeks, P. R. & Salinas, P. C. Inhibition of GSK-3beta leading to the loss of phosphorylated MAP-1B is an early event in axonal remodelling induced by WNT-7a or lithium. *J Cell Sci* **111 (Pt 10)**, 1351-1361 (1998).
123 Sanchez, C., Perez, M. & Avila, J. GSK3beta-mediated phosphorylation of the microtubule-associated protein 2C (MAP2C) prevents microtubule bundling. *Eur J Cell Biol* **79**, 252-260, doi:10.1078/s0171-9335(04)70028-x (2000).
124 Lovestone, S., Hartley, C. L., Pearce, J. & Anderton, B. H. Phosphorylation of tau by glycogen synthase kinase-3 beta in intact mammalian cells: the effects on the organization and stability of microtubules. *Neuroscience* **73**, 1145-1157, doi:10.1016/0306-4522(96)00126-1 (1996).
125 Morfini, G., Szebenyi, G., Elluru, R., Ratner, N. & Brady, S. T. Glycogen synthase kinase 3 phosphorylates kinesin light chains and negatively regulates kinesin-based motility. *EMBO J* **21**, 281-293, doi:10.1093/emboj/21.3.281 (2002).
126 Shi, S. H., Cheng, T., Jan, L. Y. & Jan, Y. N. APC and GSK-3beta are involved in mPar3 targeting to the nascent axon and establishment of neuronal polarity. *Curr Biol* **14**, 2025-2032, doi:10.1016/j.cub.2004.11.009 (2004).
127 Chilov, D. *et al.* Phosphorylated beta-catenin localizes to centrosomes of neuronal progenitors and is required for cell polarity and neurogenesis in developing midbrain. *Dev Biol* **357**, 259-268, doi:10.1016/j.ydbio.2011.06.029 (2011).
128 Scali, C. *et al.* Inhibition of Wnt signaling, modulation of Tau phosphorylation and induction of neuronal cell death by DKK1. *Neurobiol Dis* **24**, 254-265, doi:10.1016/j.nbd.2006.06.016 (2006).
129 Rawal, N. *et al.* Parkin protects dopaminergic neurons from excessive Wnt/beta-catenin signaling. *Biochem Biophys Res Commun* **388**, 473-478, doi:10.1016/j.bbrc.2009.07.014 (2009).
130 Caricasole, A. *et al.* Induction of Dickkopf-1, a negative modulator of the Wnt pathway, is associated with neuronal degeneration in Alzheimer's brain. *J Neurosci* **24**, 6021-6027, doi:10.1523/JNEUROSCI.1381-04.2004 (2004).
131 Arellano, M. & Moreno, S. Regulation of CDK/cyclin complexes during the cell cycle. *Int J Biochem Cell Biol* **29**, 559-573, doi:10.1016/s1357-2725(96)00178-1 (1997).
132 Nigg, E. A. Mitotic kinases as regulators of cell division and its checkpoints. *Nat Rev Mol Cell Biol* **2**, 21-32, doi:10.1038/35048096 (2001).
133 Sherr, C. J. & Roberts, J. M. CDK inhibitors: positive and negative regulators of G1-phase progression. *Genes Dev* **13**, 1501-1512, doi:10.1101/gad.13.12.1501 (1999).
134 Weinberg, R. A. The retinoblastoma protein and cell cycle control. *Cell* **81**, 323-330, doi:10.1016/0092-8674(95)90385-2 (1995).
135 Meraldi, P., Lukas, J., Fry, A. M., Bartek, J. & Nigg, E. A. Centrosome duplication in mammalian somatic cells requires E2F and Cdk2-cyclin A. *Nat Cell Biol* **1**, 88-93, doi:10.1038/10054 (1999).
136 Strausfeld, U. *et al.* Dephosphorylation and activation of a p34cdc2/cyclin B complex in vitro by human CDC25 protein. *Nature* **351**, 242-245, doi:10.1038/351242a0 (1991).

137 Parker, L. L. & Piwnica-Worms, H. Inactivation of the p34cdc2-cyclin B complex by the human WEE1 tyrosine kinase. *Science* **257**, 1955-1957, doi:10.1126/science.1384126 (1992).
138 Mueller, P. R., Coleman, T. R., Kumagai, A. & Dunphy, W. G. Myt1: a membrane-associated inhibitory kinase that phosphorylates Cdc2 on both threonine-14 and tyrosine-15. *Science* **270**, 86-90, doi:10.1126/science.270.5233.86 (1995).
139 Mitra, J. & Enders, G. H. Cyclin A/Cdk2 complexes regulate activation of Cdk1 and Cdc25 phosphatases in human cells. *Oncogene* **23**, 3361-3367, doi:10.1038/sj.onc.1207446 (2004).
140 Gautier, J., Solomon, M. J., Booher, R. N., Bazan, J. F. & Kirschner, M. W. cdc25 is a specific tyrosine phosphatase that directly activates p34cdc2. *Cell* **67**, 197-211, doi:10.1016/0092-8674(91)90583-k (1991).
141 Gavet, O. & Pines, J. Progressive activation of CyclinB1-Cdk1 coordinates entry to mitosis. *Dev Cell* **18**, 533-543, doi:10.1016/j.devcel.2010.02.013 (2010).
142 Matthews, H. K., Bertoli, C. & de Bruin, R. A. M. Cell cycle control in cancer. *Nat Rev Mol Cell Biol* **23**, 74-88, doi:10.1038/s41580-021-00404-3 (2022).
143 Sanchez, Y. *et al.* Conservation of the Chk1 checkpoint pathway in mammals: linkage of DNA damage to Cdk regulation through Cdc25. *Science* **277**, 1497-1501, doi:10.1126/science.277.5331.1497 (1997).
144 Musacchio, A. & Salmon, E. D. The spindle-assembly checkpoint in space and time. *Nat Rev Mol Cell Biol* **8**, 379-393, doi:10.1038/nrm2163 (2007).
145 Kops, G. J., Weaver, B. A. & Cleveland, D. W. On the road to cancer: aneuploidy and the mitotic checkpoint. *Nat Rev Cancer* **5**, 773-785, doi:10.1038/nrc1714 (2005).
146 Heim, A., Rymarczyk, B. & Mayer, T. U. Regulation of Cell Division. *Adv Exp Med Biol* **953**, 83-116, doi:10.1007/978-3-319-46095-6_3 (2017).
147 Dephoure, N. *et al.* A quantitative atlas of mitotic phosphorylation. *Proc Natl Acad Sci U S A* **105**, 10762-10767, doi:10.1073/pnas.0805139105 (2008).
148 Olsen, J. V. *et al.* Quantitative phosphoproteomics reveals widespread full phosphorylation site occupancy during mitosis. *Sci Signal* **3**, ra3, doi:10.1126/scisignal.2000475 (2010).
149 Schmitz, M. H. *et al.* Live-cell imaging RNAi screen identifies PP2A-B55alpha and importin-beta1 as key mitotic exit regulators in human cells. *Nat Cell Biol* **12**, 886-893, doi:10.1038/ncb2092 (2010).
150 Wu, J. Q. *et al.* PP1-mediated dephosphorylation of phosphoproteins at mitotic exit is controlled by inhibitor-1 and PP1 phosphorylation. *Nat Cell Biol* **11**, 644-651, doi:10.1038/ncb1871 (2009).
151 McIntosh, J. R. Mitosis. *Cold Spring Harb Perspect Biol* **8**, doi:10.1101/cshperspect.a023218 (2016).
152 Goodson, H. V. & Jonasson, E. M. Microtubules and Microtubule-Associated Proteins. *Cold Spring Harb Perspect Biol* **10**, doi:10.1101/cshperspect.a022608 (2018).
153 Margolis, R. L. & Wilson, L. Opposite end assembly and disassembly of microtubules at steady state in vitro. *Cell* **13**, 1-8, doi:10.1016/0092-8674(78)90132-0 (1978).
154 Mitchison, T. & Kirschner, M. Dynamic instability of microtubule growth. *Nature* **312**, 237-242, doi:10.1038/312237a0 (1984).
155 Kollman, J. M., Merdes, A., Mourey, L. & Agard, D. A. Microtubule nucleation by gamma-tubulin complexes. *Nat Rev Mol Cell Biol* **12**, 709-721, doi:10.1038/nrm3209 (2011).
156 Civelekoglu-Scholey, G. & Scholey, J. M. Mitotic force generators and chromosome segregation. *Cell Mol Life Sci* **67**, 2231-2250, doi:10.1007/s00018-010-0326-6 (2010).
157 Smith, E. *et al.* Differential control of Eg5-dependent centrosome separation by Plk1 and Cdk1. *EMBO J* **30**, 2233-2245, doi:10.1038/emboj.2011.120 (2011).

158 Cowley, D. O. *et al.* Aurora-A kinase is essential for bipolar spindle formation and early development. *Mol Cell Biol* **29**, 1059-1071, doi:10.1128/MCB.01062-08 (2009).
159 Ubersax, J. A. *et al.* Targets of the cyclin-dependent kinase Cdk1. *Nature* **425**, 859-864, doi:10.1038/nature02062 (2003).
160 Maiato, H., Gomes, A. M., Sousa, F. & Barisic, M. Mechanisms of Chromosome Congression during Mitosis. *Biology (Basel)* **6**, doi:10.3390/biology6010013 (2017).
161 Hagting, A. *et al.* Human securin proteolysis is controlled by the spindle checkpoint and reveals when the APC/C switches from activation by Cdc20 to Cdh1. *J Cell Biol* **157**, 1125-1137, doi:10.1083/jcb.200111001 (2002).
162 Waizenegger, I. C., Hauf, S., Meinke, A. & Peters, J. M. Two distinct pathways remove mammalian cohesin from chromosome arms in prophase and from centromeres in anaphase. *Cell* **103**, 399-410, doi:10.1016/s0092-8674(00)00132-x (2000).
163 Clute, P. & Pines, J. Temporal and spatial control of cyclin B1 destruction in metaphase. *Nat Cell Biol* **1**, 82-87, doi:10.1038/10049 (1999).
164 Liu, D. *et al.* Regulated targeting of protein phosphatase 1 to the outer kinetochore by KNL1 opposes Aurora B kinase. *J Cell Biol* **188**, 809-820, doi:10.1083/jcb.201001006 (2010).
165 Rogers, G. C. *et al.* Two mitotic kinesins cooperate to drive sister chromatid separation during anaphase. *Nature* **427**, 364-370, doi:10.1038/nature02256 (2004).
166 Petronczki, M., Glotzer, M., Kraut, N. & Peters, J. M. Polo-like kinase 1 triggers the initiation of cytokinesis in human cells by promoting recruitment of the RhoGEF Ect2 to the central spindle. *Dev Cell* **12**, 713-725, doi:10.1016/j.devcel.2007.03.013 (2007).
167 Hirokawa, N., Niwa, S. & Tanaka, Y. Molecular motors in neurons: transport mechanisms and roles in brain function, development, and disease. *Neuron* **68**, 610-638, doi:10.1016/j.neuron.2010.09.039 (2010).
168 Hirokawa, N. Kinesin and dynein superfamily proteins and the mechanism of organelle transport. *Science* **279**, 519-526, doi:10.1126/science.279.5350.519 (1998).
169 Lawrence, C. J. *et al.* A standardized kinesin nomenclature. *J Cell Biol* **167**, 19-22, doi:10.1083/jcb.200408113 (2004).
170 Vale, R. D. & Fletterick, R. J. The design plan of kinesin motors. *Annu Rev Cell Dev Biol* **13**, 745-777, doi:10.1146/annurev.cellbio.13.1.745 (1997).
171 Walczak, C. E., Gayek, S. & Ohi, R. Microtubule-depolymerizing kinesins. *Annu Rev Cell Dev Biol* **29**, 417-441, doi:10.1146/annurev-cellbio-101512-122345 (2013).
172 Welburn, J. P. & Cheeseman, I. M. The microtubule-binding protein Cep170 promotes the targeting of the kinesin-13 depolymerase Kif2b to the mitotic spindle. *Mol Biol Cell* **23**, 4786-4795, doi:10.1091/mbc.E12-03-0214 (2012).
173 Romberg, L., Pierce, D. W. & Vale, R. D. Role of the kinesin neck region in processive microtubule-based motility. *J Cell Biol* **140**, 1407-1416, doi:10.1083/jcb.140.6.1407 (1998).
174 Ogawa, T., Nitta, R., Okada, Y. & Hirokawa, N. A common mechanism for microtubule destabilizers-M type kinesins stabilize curling of the protofilament using the class-specific neck and loops. *Cell* **116**, 591-602, doi:10.1016/s0092-8674(04)00129-1 (2004).
175 Trofimova, D. *et al.* Ternary complex of Kif2A-bound tandem tubulin heterodimers represents a kinesin-13-mediated microtubule depolymerization reaction intermediate. *Nat Commun* **9**, 2628, doi:10.1038/s41467-018-05025-7 (2018).
176 Yang, J. T., Laymon, R. A. & Goldstein, L. S. A three-domain structure of kinesin heavy chain revealed by DNA sequence and microtubule binding analyses. *Cell* **56**, 879-889, doi:10.1016/0092-8674(89)90692-2 (1989).
177 Steblyanko, Y. *et al.* Microtubule poleward flux in human cells is driven by the coordinated action of four kinesins. *EMBO J* **39**, e105432, doi:10.15252/embj.2020105432 (2020).

178 Kwon, H. J., Park, J. E., Song, H. & Jang, C. Y. DDA3 and Mdp3 modulate Kif2a recruitment onto the mitotic spindle to control minus-end spindle dynamics. *J Cell Sci* **129**, 2719-2725, doi:10.1242/jcs.180109 (2016).
179 Ganem, N. J., Upton, K. & Compton, D. A. Efficient mitosis in human cells lacking poleward microtubule flux. *Curr Biol* **15**, 1827-1832, doi:10.1016/j.cub.2005.08.065 (2005).
180 Gaetz, J. & Kapoor, T. M. Dynein/dynactin regulate metaphase spindle length by targeting depolymerizing activities to spindle poles. *J Cell Biol* **166**, 465-471, doi:10.1083/jcb.200404015 (2004).
181 Ganem, N. J. & Compton, D. A. The KinI kinesin Kif2a is required for bipolar spindle assembly through a functional relationship with MCAK. *J Cell Biol* **166**, 473-478, doi:10.1083/jcb.200404012 (2004).
182 Desai, A., Verma, S., Mitchison, T. J. & Walczak, C. E. Kin I kinesins are microtubule-destabilizing enzymes. *Cell* **96**, 69-78, doi:10.1016/s0092-8674(00)80960-5 (1999).
183 Zou, J., Hallen, M. A., Yankel, C. D. & Endow, S. A. A microtubule-destabilizing kinesin motor regulates spindle length and anchoring in oocytes. *J Cell Biol* **180**, 459-466, doi:10.1083/jcb.200711031 (2008).
184 Siddiqui, S. S. Metazoan motor models: kinesin superfamily in C. elegans. *Traffic* **3**, 20-28, doi:10.1034/j.1600-0854.2002.30104.x (2002).
185 Xu, R. *et al.* Mitosis-specific MRN complex promotes a mitotic signaling cascade to regulate spindle dynamics and chromosome segregation. *Proc Natl Acad Sci U S A* **115**, E10079-E10088, doi:10.1073/pnas.1806665115 (2018).
186 Ali, A., Veeranki, S. N., Chinchole, A. & Tyagi, S. MLL/WDR5 Complex Regulates Kif2A Localization to Ensure Chromosome Congression and Proper Spindle Assembly during Mitosis. *Dev Cell* **41**, 605-622 e607, doi:10.1016/j.devcel.2017.05.023 (2017).
187 Yi, Z. Y. *et al.* Kif2a regulates spindle organization and cell cycle progression in meiotic oocytes. *Sci Rep* **6**, 38574, doi:10.1038/srep38574 (2016).
188 Uehara, R. *et al.* Aurora B and Kif2A control microtubule length for assembly of a functional central spindle during anaphase. *J Cell Biol* **202**, 623-636, doi:10.1083/jcb.201302123 (2013).
189 Wilbur, J. D. & Heald, R. Mitotic spindle scaling during Xenopus development by kif2a and importin alpha. *Elife* **2**, e00290, doi:10.7554/eLife.00290 (2013).
190 Zhu, C. *et al.* Functional analysis of human microtubule-based motor proteins, the kinesins and dyneins, in mitosis/cytokinesis using RNA interference. *Mol Biol Cell* **16**, 3187-3199, doi:10.1091/mbc.e05-02-0167 (2005).
191 Ohi, R., Burbank, K., Liu, Q. & Mitchison, T. J. Nonredundant functions of Kinesin-13s during meiotic spindle assembly. *Curr Biol* **17**, 953-959, doi:10.1016/j.cub.2007.04.057 (2007).
192 Eagleson, G. *et al.* Kif2a depletion generates chromosome segregation and pole coalescence defects in animal caps and inhibits gastrulation of the Xenopus embryo. *Mol Biol Cell* **26**, 924-937, doi:10.1091/mbc.E13-12-0721 (2015).
193 Jang, C. Y. *et al.* DDA3 recruits microtubule depolymerase Kif2a to spindle poles and controls spindle dynamics and mitotic chromosome movement. *J Cell Biol* **181**, 255-267, doi:10.1083/jcb.200711032 (2008).
194 Chen, M. H. *et al.* KIF2A regulates the spindle assembly and the metaphase I-anaphase I transition in mouse oocyte. *Sci Rep* **6**, 39337, doi:10.1038/srep39337 (2016).
195 Tanenbaum, M. E. *et al.* Kif15 cooperates with eg5 to promote bipolar spindle assembly. *Curr Biol* **19**, 1703-1711, doi:10.1016/j.cub.2009.08.027 (2009).
196 Sun, M. *et al.* NuMA regulates mitotic spindle assembly, structural dynamics and function via phase separation. *Nat Commun* **12**, 7157, doi:10.1038/s41467-021-27528-6 (2021).

197 Merdes, A., Ramyar, K., Vechio, J. D. & Cleveland, D. W. A complex of NuMA and cytoplasmic dynein is essential for mitotic spindle assembly. *Cell* **87**, 447-458, doi:10.1016/s0092-8674(00)81365-3 (1996).
198 Lo, P. K. *et al.* Identification of a novel mouse p53 target gene DDA3. *Oncogene* **18**, 7765-7774, doi:10.1038/sj.onc.1203167 (1999).
199 Park, J. E., Song, H., Kwon, H. J. & Jang, C. Y. Ska1 cooperates with DDA3 for spindle dynamics and spindle attachment to kinetochore. *Biochem Biophys Res Commun* **470**, 586-592, doi:10.1016/j.bbrc.2016.01.101 (2016).
200 Jang, C. Y., Coppinger, J. A., Seki, A., Yates, J. R., 3rd & Fang, G. Plk1 and Aurora A regulate the depolymerase activity and the cellular localization of Kif2a. *J Cell Sci* **122**, 1334-1341, doi:10.1242/jcs.044321 (2009).
201 Santamaria, A. *et al.* The Plk1-dependent phosphoproteome of the early mitotic spindle. *Mol Cell Proteomics* **10**, M110 004457, doi:10.1074/mcp.M110.004457 (2011).
202 Knowlton, A. L., Vorozhko, V. V., Lan, W., Gorbsky, G. J. & Stukenberg, P. T. ICIS and Aurora B coregulate the microtubule depolymerase Kif2a. *Curr Biol* **19**, 758-763, doi:10.1016/j.cub.2009.03.018 (2009).
203 Watanabe, T. *et al.* TTBK2 with EB1/3 regulates microtubule dynamics in migrating cells through KIF2A phosphorylation. *J Cell Biol* **210**, 737-751, doi:10.1083/jcb.201412075 (2015).
204 Zhang, W. *et al.* Modeling microcephaly with cerebral organoids reveals a WDR62-CEP170-KIF2A pathway promoting cilium disassembly in neural progenitors. *Nat Commun* **10**, 2612, doi:10.1038/s41467-019-10497-2 (2019).
205 Broix, L. *et al.* Ciliogenesis and cell cycle alterations contribute to KIF2A-related malformations of cortical development. *Hum Mol Genet* **27**, 224-238, doi:10.1093/hmg/ddx384 (2018).
206 Homma, N. *et al.* KIF2A regulates the development of dentate granule cells and postnatal hippocampal wiring. *Elife* **7**, doi:10.7554/eLife.30935 (2018).
207 Homma, N. *et al.* Kinesin superfamily protein 2A (KIF2A) functions in suppression of collateral branch extension. *Cell* **114**, 229-239, doi:10.1016/s0092-8674(03)00522-1 (2003).
208 Ogawa, T. & Hirokawa, N. Microtubule Destabilizer KIF2A Undergoes Distinct Site-Specific Phosphorylation Cascades that Differentially Affect Neuronal Morphogenesis. *Cell Rep* **12**, 1774-1788, doi:10.1016/j.celrep.2015.08.018 (2015).
209 Noda, Y. *et al.* Phosphatidylinositol 4-phosphate 5-kinase alpha (PIPKalpha) regulates neuronal microtubule depolymerase kinesin, KIF2A and suppresses elongation of axon branches. *Proc Natl Acad Sci U S A* **109**, 1725-1730, doi:10.1073/pnas.1107808109 (2012).
210 Poirier, K. *et al.* Mutations in TUBG1, DYNC1H1, KIF5C and KIF2A cause malformations of cortical development and microcephaly. *Nat Genet* **45**, 639-647, doi:10.1038/ng.2613 (2013).
211 Cavallin, M. *et al.* Recurrent KIF2A mutations are responsible for classic lissencephaly. *Neurogenetics* **18**, 73-79, doi:10.1007/s10048-016-0499-8 (2017).
212 Li, X., Shu, K., Wang, Z. & Ding, D. Prognostic significance of KIF2A and KIF20A expression in human cancer: A systematic review and meta-analysis. *Medicine (Baltimore)* **98**, e18040, doi:10.1097/MD.0000000000018040 (2019).
213 Zhang, X. *et al.* Role of KIF2A in the progression and metastasis of human glioma. *Mol Med Rep* **13**, 1781-1787, doi:10.3892/mmr.2015.4700 (2016).
214 Wang, J. *et al.* KIF2A silencing inhibits the proliferation and migration of breast cancer cells and correlates with unfavorable prognosis in breast cancer. *BMC Cancer* **14**, 461, doi:10.1186/1471-2407-14-461 (2014).

215 Chen, J. *et al.* The molecular mechanism of kinesin family member 2A (KIF2A) underlying non-small cell lung cancer: the effect of its knockdown on malignant behaviors, stemness, chemosensitivity, and potential regulated signaling pathways. *Am J Transl Res* **14**, 68-85 (2022).
216 Botrugno, O. A. *et al.* Synergy between LRH-1 and beta-catenin induces G1 cyclin-mediated cell proliferation. *Mol Cell* **15**, 499-509, doi:10.1016/j.molcel.2004.07.009 (2004).
217 Surjit, M. & Lal, S. K. Glycogen synthase kinase-3 phosphorylates and regulates the stability of p27kip1 protein. *Cell Cycle* **6**, 580-588, doi:10.4161/cc.6.5.3899 (2007).
218 Yang, W. *et al.* Repression of transcription of the p27(Kip1) cyclin-dependent kinase inhibitor gene by c-Myc. *Oncogene* **20**, 1688-1702, doi:10.1038/sj.onc.1204245 (2001).
219 De Jaime-Soguero, A. *et al.* Wnt/Tcf1 pathway restricts embryonic stem cell cycle through activation of the Ink4/Arf locus. *PLoS Genet* **13**, e1006682, doi:10.1371/journal.pgen.1006682 (2017).
220 Aoki, K. *et al.* Chromosomal instability by beta-catenin/TCF transcription in APC or beta-catenin mutant cells. *Oncogene* **26**, 3511-3520, doi:10.1038/sj.onc.1210141 (2007).
221 Hlubek, F. *et al.* Securin (hPTTG1) expression is regulated by beta-catenin/TCF in human colorectal carcinoma. *Br J Cancer* **94**, 1672-1677, doi:10.1038/sj.bjc.6603155 (2006).
222 Hadjihannas, M. V., Bernkopf, D. B., Bruckner, M. & Behrens, J. Cell cycle control of Wnt/beta-catenin signalling by conductin/axin2 through CDC20. *EMBO Rep* **13**, 347-354, doi:10.1038/embor.2012.12 (2012).
223 Gottesfeld, J. M. & Forbes, D. J. Mitotic repression of the transcriptional machinery. *Trends Biochem Sci* **22**, 197-202, doi:10.1016/s0968-0004(97)01045-1 (1997).
224 Olmeda, D., Castel, S., Vilaro, S. & Cano, A. Beta-catenin regulation during the cell cycle: implications in G2/M and apoptosis. *Mol Biol Cell* **14**, 2844-2860, doi:10.1091/mbc.e03-01-0865 (2003).
225 Yang, Y., Topol, L., Lee, H. & Wu, J. Wnt5a and Wnt5b exhibit distinct activities in coordinating chondrocyte proliferation and differentiation. *Development* **130**, 1003-1015, doi:10.1242/dev.00324 (2003).
226 He, F. *et al.* Wnt5a regulates directional cell migration and cell proliferation via Ror2-mediated noncanonical pathway in mammalian palate development. *Development* **135**, 3871-3879, doi:10.1242/dev.025767 (2008).
227 Quesada-Hernandez, E. *et al.* Stereotypical cell division orientation controls neural rod midline formation in zebrafish. *Curr Biol* **20**, 1966-1972, doi:10.1016/j.cub.2010.10.009 (2010).
228 Segalen, M. *et al.* The Fz-Dsh planar cell polarity pathway induces oriented cell division via Mud/NuMA in Drosophila and zebrafish. *Dev Cell* **19**, 740-752, doi:10.1016/j.devcel.2010.10.004 (2010).
229 Lake, B. B. & Sokol, S. Y. Strabismus regulates asymmetric cell divisions and cell fate determination in the mouse brain. *J Cell Biol* **185**, 59-66, doi:10.1083/jcb.200807073 (2009).
230 Kang, T. *et al.* GSK-3 beta targets Cdc25A for ubiquitin-mediated proteolysis, and GSK-3 beta inactivation correlates with Cdc25A overproduction in human cancers. *Cancer Cell* **13**, 36-47, doi:10.1016/j.ccr.2007.12.002 (2008).
231 Kikuchi, K., Niikura, Y., Kitagawa, K. & Kikuchi, A. Dishevelled, a Wnt signalling component, is involved in mitotic progression in cooperation with Plk1. *EMBO J* **29**, 3470-3483, doi:10.1038/emboj.2010.221 (2010).
232 Kaplan, K. B. *et al.* A role for the Adenomatous Polyposis Coli protein in chromosome segregation. *Nat Cell Biol* **3**, 429-432, doi:10.1038/35070123 (2001).

233 Fodde, R. *et al.* Mutations in the APC tumour suppressor gene cause chromosomal instability. *Nat Cell Biol* **3**, 433-438, doi:10.1038/35070129 (2001).
234 Green, R. A. & Kaplan, K. B. Chromosome instability in colorectal tumor cells is associated with defects in microtubule plus-end attachments caused by a dominant mutation in APC. *J Cell Biol* **163**, 949-961, doi:10.1083/jcb.200307070 (2003).
235 Hadjihannas, M. V. *et al.* Aberrant Wnt/beta-catenin signaling can induce chromosomal instability in colon cancer. *Proc Natl Acad Sci U S A* **103**, 10747-10752, doi:10.1073/pnas.0604206103 (2006).
236 Tighe, A., Johnson, V. L. & Taylor, S. S. Truncating APC mutations have dominant effects on proliferation, spindle checkpoint control, survival and chromosome stability. *J Cell Sci* **117**, 6339-6353, doi:10.1242/jcs.01556 (2004).
237 Salinas, P. C. Modulation of the microtubule cytoskeleton: a role for a divergent canonical Wnt pathway. *Trends Cell Biol* **17**, 333-342, doi:10.1016/j.tcb.2007.07.003 (2007).
238 Cervenka, I. *et al.* Dishevelled is a NEK2 kinase substrate controlling dynamics of centrosomal linker proteins. *Proc Natl Acad Sci U S A* **113**, 9304-9309, doi:10.1073/pnas.1608783113 (2016).
239 Fumoto, K., Kadono, M., Izumi, N. & Kikuchi, A. Axin localizes to the centrosome and is involved in microtubule nucleation. *EMBO Rep* **10**, 606-613, doi:10.1038/embor.2009.45 (2009).
240 Kim, S. M. *et al.* Axin localizes to mitotic spindles and centrosomes in mitotic cells. *Exp Cell Res* **315**, 943-954, doi:10.1016/j.yexcr.2009.01.013 (2009).
241 Ruan, K. *et al.* PLK1 interacts and phosphorylates Axin that is essential for proper centrosome formation. *PLoS One* **7**, e49184, doi:10.1371/journal.pone.0049184 (2012).
242 Hadjihannas, M. V., Bruckner, M. & Behrens, J. Conductin/axin2 and Wnt signalling regulates centrosome cohesion. *EMBO Rep* **11**, 317-324, doi:10.1038/embor.2010.23 (2010).
243 Mogensen, M. M., Tucker, J. B., Mackie, J. B., Prescott, A. R. & Nathke, I. S. The adenomatous polyposis coli protein unambiguously localizes to microtubule plus ends and is involved in establishing parallel arrays of microtubule bundles in highly polarized epithelial cells. *J Cell Biol* **157**, 1041-1048, doi:10.1083/jcb.200203001 (2002).
244 Zumbrunn, J., Kinoshita, K., Hyman, A. A. & Nathke, I. S. Binding of the adenomatous polyposis coli protein to microtubules increases microtubule stability and is regulated by GSK3 beta phosphorylation. *Curr Biol* **11**, 44-49, doi:10.1016/s0960-9822(01)00002-1 (2001).
245 Green, R. A., Wollman, R. & Kaplan, K. B. APC and EB1 function together in mitosis to regulate spindle dynamics and chromosome alignment. *Mol Biol Cell* **16**, 4609-4622, doi:10.1091/mbc.e05-03-0259 (2005).
246 Dikovskaya, D. *et al.* Loss of APC induces polyploidy as a result of a combination of defects in mitosis and apoptosis. *J Cell Biol* **176**, 183-195, doi:10.1083/jcb.200610099 (2007).
247 Askham, J. M., Moncur, P., Markham, A. F. & Morrison, E. E. Regulation and function of the interaction between the APC tumour suppressor protein and EB1. *Oncogene* **19**, 1950-1958, doi:10.1038/sj.onc.1203498 (2000).
248 Nakamura, M., Zhou, X. Z. & Lu, K. P. Critical role for the EB1 and APC interaction in the regulation of microtubule polymerization. *Curr Biol* **11**, 1062-1067, doi:10.1016/s0960-9822(01)00297-4 (2001).
249 Mimori-Kiyosue, Y., Shiina, N. & Tsukita, S. Adenomatous polyposis coli (APC) protein moves along microtubules and concentrates at their growing ends in epithelial cells. *J Cell Biol* **148**, 505-518, doi:10.1083/jcb.148.3.505 (2000).

250 Zhang, J., Ahmad, S. & Mao, Y. BubR1 and APC/EB1 cooperate to maintain metaphase chromosome alignment. *J Cell Biol* **178**, 773-784, doi:10.1083/jcb.200702138 (2007).
251 Draviam, V. M., Shapiro, I., Aldridge, B. & Sorger, P. K. Misorientation and reduced stretching of aligned sister kinetochores promote chromosome missegregation in EB1- or APC-depleted cells. *EMBO J* **25**, 2814-2827, doi:10.1038/sj.emboj.7601168 (2006).
252 Wakefield, J. G., Stephens, D. J. & Tavare, J. M. A role for glycogen synthase kinase-3 in mitotic spindle dynamics and chromosome alignment. *J Cell Sci* **116**, 637-646, doi:10.1242/jcs.00273 (2003).
253 Tighe, A., Ray-Sinha, A., Staples, O. D. & Taylor, S. S. GSK-3 inhibitors induce chromosome instability. *BMC Cell Biol* **8**, 34, doi:10.1186/1471-2121-8-34 (2007).
254 Izumi, N., Fumoto, K., Izumi, S. & Kikuchi, A. GSK-3beta regulates proper mitotic spindle formation in cooperation with a component of the gamma-tubulin ring complex, GCP5. *J Biol Chem* **283**, 12981-12991, doi:10.1074/jbc.M710282200 (2008).
255 Fumoto, K., Hoogenraad, C. C. & Kikuchi, A. GSK-3beta-regulated interaction of BICD with dynein is involved in microtubule anchorage at centrosome. *EMBO J* **25**, 5670-5682, doi:10.1038/sj.emboj.7601459 (2006).
256 Ong Tone, S., Dayanandan, B., Fournier, A. E. & Mandato, C. A. GSK3 regulates mitotic chromosomal alignment through CRMP4. *PLoS One* **5**, e14345, doi:10.1371/journal.pone.0014345 (2010).
257 Rashid, M. S., Mazur, T., Ji, W., Liu, S. T. & Taylor, W. R. Analysis of the role of GSK3 in the mitotic checkpoint. *Sci Rep* **8**, 14259, doi:10.1038/s41598-018-32435-w (2018).
258 Kaplan, D. D., Meigs, T. E., Kelly, P. & Casey, P. J. Identification of a role for beta-catenin in the establishment of a bipolar mitotic spindle. *J Biol Chem* **279**, 10829-10832, doi:10.1074/jbc.C400035200 (2004).
259 Bahmanyar, S. *et al.* beta-Catenin is a Nek2 substrate involved in centrosome separation. *Genes Dev* **22**, 91-105, doi:10.1101/gad.1596308 (2008).
260 Huang, P., Senga, T. & Hamaguchi, M. A novel role of phospho-beta-catenin in microtubule regrowth at centrosome. *Oncogene* **26**, 4357-4371, doi:10.1038/sj.onc.1210217 (2007).
261 Louie, R. K. *et al.* Adenomatous polyposis coli and EB1 localize in close proximity of the mother centriole and EB1 is a functional component of centrosomes. *J Cell Sci* **117**, 1117-1128, doi:10.1242/jcs.00939 (2004).
262 Beamish, H. *et al.* Cyclin A/cdk2 regulates adenomatous polyposis coli-dependent mitotic spindle anchoring. *J Biol Chem* **284**, 29015-29023, doi:10.1074/jbc.M109.042820 (2009).
263 Lu, M. S. & Johnston, C. A. Molecular pathways regulating mitotic spindle orientation in animal cells. *Development* **140**, 1843-1856, doi:10.1242/dev.087627 (2013).
264 Walston, T. *et al.* Multiple Wnt signaling pathways converge to orient the mitotic spindle in early C. elegans embryos. *Dev Cell* **7**, 831-841, doi:10.1016/j.devcel.2004.10.008 (2004).
265 Sugioka, K., Mizumoto, K. & Sawa, H. Wnt regulates spindle asymmetry to generate asymmetric nuclear beta-catenin in C. elegans. *Cell* **146**, 942-954, doi:10.1016/j.cell.2011.07.043 (2011).
266 Gho, M. & Schweisguth, F. Frizzled signalling controls orientation of asymmetric sense organ precursor cell divisions in Drosophila. *Nature* **393**, 178-181, doi:10.1038/30265 (1998).
267 Yamashita, Y. M., Jones, D. L. & Fuller, M. T. Orientation of asymmetric stem cell division by the APC tumor suppressor and centrosome. *Science* **301**, 1547-1550, doi:10.1126/science.1087795 (2003).
268 Herman, M. A., Vassilieva, L. L., Horvitz, H. R., Shaw, J. E. & Herman, R. K. The C. elegans gene lin-44, which controls the polarity of certain asymmetric cell divisions,

encodes a Wnt protein and acts cell nonautonomously. *Cell* **83**, 101-110, doi:10.1016/0092-8674(95)90238-4 (1995).
269 Mimori-Kiyosue, Y., Shiina, N. & Tsukita, S. The dynamic behavior of the APC-binding protein EB1 on the distal ends of microtubules. *Curr Biol* **10**, 865-868, doi:10.1016/s0960-9822(00)00600-x (2000).
270 Su, L. K. *et al.* APC binds to the novel protein EB1. *Cancer Res* **55**, 2972-2977 (1995).
271 Munemitsu, S. *et al.* The APC gene product associates with microtubules in vivo and promotes their assembly in vitro. *Cancer Res* **54**, 3676-3681 (1994).
272 Trzepacz, C., Lowy, A. M., Kordich, J. J. & Groden, J. Phosphorylation of the tumor suppressor adenomatous polyposis coli (APC) by the cyclin-dependent kinase p34. *J Biol Chem* **272**, 21681-21684, doi:10.1074/jbc.272.35.21681 (1997).
273 Banks, J. D. & Heald, R. Adenomatous polyposis coli associates with the microtubule-destabilizing protein XMCAK. *Curr Biol* **14**, 2033-2038, doi:10.1016/j.cub.2004.10.049 (2004).
274 Kline-Smith, S. L., Khodjakov, A., Hergert, P. & Walczak, C. E. Depletion of centromeric MCAK leads to chromosome congression and segregation defects due to improper kinetochore attachments. *Mol Biol Cell* **15**, 1146-1159, doi:10.1091/mbc.e03-08-0581 (2004).
275 Radulescu, S. *et al.* Defining the role of APC in the mitotic spindle checkpoint in vivo: APC-deficient cells are resistant to Taxol. *Oncogene* **29**, 6418-6427, doi:10.1038/onc.2010.373 (2010).
276 Tighe, A., Johnson, V. L., Albertella, M. & Taylor, S. S. Aneuploid colon cancer cells have a robust spindle checkpoint. *EMBO Rep* **2**, 609-614, doi:10.1093/embo-reports/kve127 (2001).
277 Janssen, A., van der Burg, M., Szuhai, K., Kops, G. J. & Medema, R. H. Chromosome segregation errors as a cause of DNA damage and structural chromosome aberrations. *Science* **333**, 1895-1898, doi:10.1126/science.1210214 (2011).
278 Acebron, S. P. & Niehrs, C. beta-Catenin-Independent Roles of Wnt/LRP6 Signaling. *Trends Cell Biol* **26**, 956-967, doi:10.1016/j.tcb.2016.07.009 (2016).
279 Park, J., Cho, J., Kim, E. E. & Song, E. J. Deubiquitinating Enzymes: A Critical Regulator of Mitosis. *Int J Mol Sci* **20**, doi:10.3390/ijms20235997 (2019).
280 Ong, S. E. *et al.* Stable isotope labeling by amino acids in cell culture, SILAC, as a simple and accurate approach to expression proteomics. *Mol Cell Proteomics* **1**, 376-386, doi:10.1074/mcp.m200025-mcp200 (2002).
281 Eden, E., Lipson, D., Yogev, S. & Yakhini, Z. Discovering motifs in ranked lists of DNA sequences. *PLoS Comput Biol* **3**, e39, doi:10.1371/journal.pcbi.0030039 (2007).
282 Eden, E., Navon, R., Steinfeld, I., Lipson, D. & Yakhini, Z. GOrilla: a tool for discovery and visualization of enriched GO terms in ranked gene lists. *BMC Bioinformatics* **10**, 48, doi:10.1186/1471-2105-10-48 (2009).
283 Neumann, B. *et al.* Phenotypic profiling of the human genome by time-lapse microscopy reveals cell division genes. *Nature* **464**, 721-727, doi:10.1038/nature08869 (2010).
284 Manning, A. L. *et al.* The kinesin-13 proteins Kif2a, Kif2b, and Kif2c/MCAK have distinct roles during mitosis in human cells. *Mol Biol Cell* **18**, 2970-2979, doi:10.1091/mbc.e07-02-0110 (2007).
285 Bufe, A. *et al.* Wnt signaling recruits KIF2A to the spindle to ensure chromosome congression and alignment during mitosis. *Proc Natl Acad Sci U S A* **118**, doi:10.1073/pnas.2108145118 (2021).
286 Sigma-Aldrich, M. K. *How Proximity Ligation Assays (PLA) Work*, <https://www.sigmaaldrich.com/DE/de/technical-documents/technical-article/protein-biology/protein-and-nucleic-acid-interactions/how-pla-works> (2022).

287 Schwarz-Romond, T., Merrifield, C., Nichols, B. J. & Bienz, M. The Wnt signalling effector Dishevelled forms dynamic protein assemblies rather than stable associations with cytoplasmic vesicles. *J Cell Sci* **118**, 5269-5277, doi:10.1242/jcs.02646 (2005).
288 Lenart, P. *et al.* The small-molecule inhibitor BI 2536 reveals novel insights into mitotic roles of polo-like kinase 1. *Curr Biol* **17**, 304-315, doi:10.1016/j.cub.2006.12.046 (2007).
289 Nakajima, H., Toyoshima-Morimoto, F., Taniguchi, E. & Nishida, E. Identification of a consensus motif for Plk (Polo-like kinase) phosphorylation reveals Myt1 as a Plk1 substrate. *J Biol Chem* **278**, 25277-25280, doi:10.1074/jbc.C300126200 (2003).
290 de Carcer, G. *et al.* Plk1 overexpression induces chromosomal instability and suppresses tumor development. *Nat Commun* **9**, 3012, doi:10.1038/s41467-018-05429-5 (2018).
291 Wilhelm, T. *et al.* Mild replication stress causes chromosome mis-segregation via premature centriole disengagement. *Nat Commun* **10**, 3585, doi:10.1038/s41467-019-11584-0 (2019).
292 Rao, D. D., Vorhies, J. S., Senzer, N. & Nemunaitis, J. siRNA vs. shRNA: similarities and differences. *Adv Drug Deliv Rev* **61**, 746-759, doi:10.1016/j.addr.2009.04.004 (2009).
293 Vitre, B. D. & Cleveland, D. W. Centrosomes, chromosome instability (CIN) and aneuploidy. *Curr Opin Cell Biol* **24**, 809-815, doi:10.1016/j.ceb.2012.10.006 (2012).
294 Ganem, N. J., Godinho, S. A. & Pellman, D. A mechanism linking extra centrosomes to chromosomal instability. *Nature* **460**, 278-282, doi:10.1038/nature08136 (2009).
295 Thompson, S. L., Bakhoum, S. F. & Compton, D. A. Mechanisms of chromosomal instability. *Curr Biol* **20**, R285-295, doi:10.1016/j.cub.2010.01.034 (2010).
296 Fonseca, C. L. *et al.* Mitotic chromosome alignment ensures mitotic fidelity by promoting interchromosomal compaction during anaphase. *J Cell Biol* **218**, 1148-1163, doi:10.1083/jcb.201807228 (2019).
297 Blauwkamp, T. A., Nigam, S., Ardehali, R., Weissman, I. L. & Nusse, R. Endogenous Wnt signalling in human embryonic stem cells generates an equilibrium of distinct lineage-specified progenitors. *Nat Commun* **3**, 1070, doi:10.1038/ncomms2064 (2012).
298 Bakhoum, S. F., Thompson, S. L., Manning, A. L. & Compton, D. A. Genome stability is ensured by temporal control of kinetochore-microtubule dynamics. *Nat Cell Biol* **11**, 27-35, doi:10.1038/ncb1809 (2009).
299 Knouse, K. A., Lopez, K. E., Bachofner, M. & Amon, A. Chromosome Segregation Fidelity in Epithelia Requires Tissue Architecture. *Cell* **175**, 200-211 e213, doi:10.1016/j.cell.2018.07.042 (2018).
300 Burrell, R. A. *et al.* Replication stress links structural and numerical cancer chromosomal instability. *Nature* **494**, 492-496, doi:10.1038/nature11935 (2013).
301 Böhly, N., Kistner, M. & Bastians, H. Mild replication stress causes aneuploidy by deregulating microtubule dynamics in mitosis. *Cell Cycle* **18**, 2770-2783, doi:10.1080/15384101.2019.1658477 (2019).
302 Lamm, N. *et al.* Genomic Instability in Human Pluripotent Stem Cells Arises from Replicative Stress and Chromosome Condensation Defects. *Cell Stem Cell* **18**, 253-261, doi:10.1016/j.stem.2015.11.003 (2016).
303 Bester, A. C. *et al.* Nucleotide deficiency promotes genomic instability in early stages of cancer development. *Cell* **145**, 435-446, doi:10.1016/j.cell.2011.03.044 (2011).
304 Halliwell, J. A. *et al.* Nucleosides Rescue Replication-Mediated Genome Instability of Human Pluripotent Stem Cells. *Stem Cell Reports* **14**, 1009-1017, doi:10.1016/j.stemcr.2020.04.004 (2020).

305 Ertych, N. *et al.* Increased microtubule assembly rates influence chromosomal instability in colorectal cancer cells. *Nat Cell Biol* **16**, 779-791, doi:10.1038/ncb2994 (2014).
306 Meniel, V. *et al.* Apc and p53 interaction in DNA damage and genomic instability in hepatocytes. *Oncogene* **34**, 4118-4129, doi:10.1038/onc.2014.342 (2015).
307 Dawlaty, M. M. *et al.* Resolution of sister centromeres requires RanBP2-mediated SUMOylation of topoisomerase IIalpha. *Cell* **133**, 103-115, doi:10.1016/j.cell.2008.01.045 (2008).
308 Uemura, T. *et al.* DNA topoisomerase II is required for condensation and separation of mitotic chromosomes in S. pombe. *Cell* **50**, 917-925, doi:10.1016/0092-8674(87)90518-6 (1987).
309 Voets, E. & Wolthuis, R. M. MASTL is the human orthologue of Greatwall kinase that facilitates mitotic entry, anaphase and cytokinesis. *Cell Cycle* **9**, 3591-3601, doi:10.4161/cc.9.17.12832 (2010).
310 Vigneron, S. *et al.* Greatwall maintains mitosis through regulation of PP2A. *EMBO J* **28**, 2786-2793, doi:10.1038/emboj.2009.228 (2009).
311 Uppada, S. B. *et al.* MASTL induces Colon Cancer progression and Chemoresistance by promoting Wnt/beta-catenin signaling. *Mol Cancer* **17**, 111, doi:10.1186/s12943-018-0848-3 (2018).
312 Blom, N., Gammeltoft, S. & Brunak, S. Sequence and structure-based prediction of eukaryotic protein phosphorylation sites. *J Mol Biol* **294**, 1351-1362, doi:10.1006/jmbi.1999.3310 (1999).
313 Blom, N., Sicheritz-Ponten, T., Gupta, R., Gammeltoft, S. & Brunak, S. Prediction of post-translational glycosylation and phosphorylation of proteins from the amino acid sequence. *Proteomics* **4**, 1633-1649, doi:10.1002/pmic.200300771 (2004).
314 Kinexus, B. C. *PhosphoNET*, <http://www.phosphonet.ca> (2019).
315 Moores, C. A. *et al.* A mechanism for microtubule depolymerization by KinI kinesins. *Mol Cell* **9**, 903-909, doi:10.1016/s1097-2765(02)00503-8 (2002).
316 Kikuchi, K. *et al.* Map7/7D1 and Dvl form a feedback loop that facilitates microtubule remodeling and Wnt5a signaling. *EMBO Rep* **19**, doi:10.15252/embr.201745471 (2018).
317 Guillabert-Gourgues, A. *et al.* Kif26b controls endothelial cell polarity through the Dishevelled/Daam1-dependent planar cell polarity-signaling pathway. *Mol Biol Cell* **27**, 941-953, doi:10.1091/mbc.E14-08-1332 (2016).
318 Puri, D. *et al.* Wnt signaling establishes the microtubule polarity in neurons through regulation of Kinesin-13. *J Cell Biol* **220**, doi:10.1083/jcb.202005080 (2021).
319 Schwarz-Romond, T., Metcalfe, C. & Bienz, M. Dynamic recruitment of axin by Dishevelled protein assemblies. *J Cell Sci* **120**, 2402-2412, doi:10.1242/jcs.002956 (2007).
320 Kumari, A. *et al.* Microtubule-targeting agents impair kinesin-2-dependent nuclear transport of beta-catenin: Evidence of inhibition of Wnt/beta-catenin signaling as an important antitumor mechanism of microtubule-targeting agents. *FASEB J* **35**, e21539, doi:10.1096/fj.202002594R (2021).
321 Sun, D. *et al.* Regulation of neural stem cell proliferation and differentiation by Kinesin family member 2a. *PLoS One* **12**, e0179047, doi:10.1371/journal.pone.0179047 (2017).
322 Su, J. *et al.* Genomic Integrity Safeguards Self-Renewal in Embryonic Stem Cells. *Cell Rep* **28**, 1400-1409 e1404, doi:10.1016/j.celrep.2019.07.011 (2019).
323 Deng, X. *et al.* MiR-146b-5p promotes metastasis and induces epithelial-mesenchymal transition in thyroid cancer by targeting ZNRF3. *Cell Physiol Biochem* **35**, 71-82, doi:10.1159/000369676 (2015).

324 Koo, B. K. *et al.* Tumour suppressor RNF43 is a stem-cell E3 ligase that induces endocytosis of Wnt receptors. *Nature* **488**, 665-669, doi:10.1038/nature11308 (2012).
325 Xiong, X. *et al.* miR-937-5p targets SOX17 to modulate breast cancer cell cycle and cell proliferation through the Wnt signaling pathway. *Cell Signal* **77**, 109818, doi:10.1016/j.cellsig.2020.109818 (2021).
326 Fischer, M. M. *et al.* WNT antagonists exhibit unique combinatorial antitumor activity with taxanes by potentiating mitotic cell death. *Sci Adv* **3**, e1700090, doi:10.1126/sciadv.1700090 (2017).
327 Yu, J. M., Kim, J. H., Song, G. S. & Jung, J. S. Increase in proliferation and differentiation of neural progenitor cells isolated from postnatal and adult mice brain by Wnt-3a and Wnt-5a. *Mol Cell Biochem* **288**, 17-28, doi:10.1007/s11010-005-9113-3 (2006).
328 Lucas, F. R. & Salinas, P. C. WNT-7a induces axonal remodeling and increases synapsin I levels in cerebellar neurons. *Dev Biol* **192**, 31-44, doi:10.1006/dbio.1997.8734 (1997).
329 Simons, M. *et al.* Inversin, the gene product mutated in nephronophthisis type II, functions as a molecular switch between Wnt signaling pathways. *Nat Genet* **37**, 537-543, doi:10.1038/ng1552 (2005).
330 Kleber, M. & Sommer, L. Wnt signaling and the regulation of stem cell function. *Curr Opin Cell Biol* **16**, 681-687, doi:10.1016/j.ceb.2004.08.006 (2004).
331 Zeman, M. K. & Cimprich, K. A. Causes and consequences of replication stress. *Nat Cell Biol* **16**, 2-9, doi:10.1038/ncb2897 (2014).
332 Becker, K. A. *et al.* Self-renewal of human embryonic stem cells is supported by a shortened G1 cell cycle phase. *J Cell Physiol* **209**, 883-893, doi:10.1002/jcp.20776 (2006).
333 Vallabhaneni, H. *et al.* High Basal Levels of gammaH2AX in Human Induced Pluripotent Stem Cells Are Linked to Replication-Associated DNA Damage and Repair. *Stem Cells* **36**, 1501-1513, doi:10.1002/stem.2861 (2018).
334 Simara, P. *et al.* DNA double-strand breaks in human induced pluripotent stem cell reprogramming and long-term in vitro culturing. *Stem Cell Res Ther* **8**, 73, doi:10.1186/s13287-017-0522-5 (2017).
335 Hussein, S. M. *et al.* Copy number variation and selection during reprogramming to pluripotency. *Nature* **471**, 58-62, doi:10.1038/nature09871 (2011).
336 Laurent, L. C. *et al.* Dynamic changes in the copy number of pluripotency and cell proliferation genes in human ESCs and iPSCs during reprogramming and time in culture. *Cell Stem Cell* **8**, 106-118, doi:10.1016/j.stem.2010.12.003 (2011).
337 Mayshar, Y. *et al.* Identification and classification of chromosomal aberrations in human induced pluripotent stem cells. *Cell Stem Cell* **7**, 521-531, doi:10.1016/j.stem.2010.07.017 (2010).
338 Vafa, O. *et al.* c-Myc can induce DNA damage, increase reactive oxygen species, and mitigate p53 function: a mechanism for oncogene-induced genetic instability. *Mol Cell* **9**, 1031-1044, doi:10.1016/s1097-2765(02)00520-8 (2002).
339 Bartkova, J. *et al.* DNA damage response as a candidate anti-cancer barrier in early human tumorigenesis. *Nature* **434**, 864-870, doi:10.1038/nature03482 (2005).
340 Gregory, M. A., Qi, Y. & Hann, S. R. Phosphorylation by glycogen synthase kinase-3 controls c-myc proteolysis and subnuclear localization. *J Biol Chem* **278**, 51606-51612, doi:10.1074/jbc.M310722200 (2003).
341 Welcker, M. *et al.* Multisite phosphorylation by Cdk2 and GSK3 controls cyclin E degradation. *Mol Cell* **12**, 381-392, doi:10.1016/s1097-2765(03)00287-9 (2003).
342 Schwank, G., Andersson-Rolf, A., Koo, B. K., Sasaki, N. & Clevers, H. Generation of BAC transgenic epithelial organoids. *PLoS One* **8**, e76871, doi:10.1371/journal.pone.0076871 (2013).

343 Ahuja, A. K. *et al.* A short G1 phase imposes constitutive replication stress and fork remodelling in mouse embryonic stem cells. *Nat Commun* **7**, 10660, doi:10.1038/ncomms10660 (2016).
344 Cervantes, R. B., Stringer, J. R., Shao, C., Tischfield, J. A. & Stambrook, P. J. Embryonic stem cells and somatic cells differ in mutation frequency and type. *Proc Natl Acad Sci U S A* **99**, 3586-3590, doi:10.1073/pnas.062527199 (2002).
345 Blakemore, D. *et al.* MYBL2 and ATM suppress replication stress in pluripotent stem cells. *EMBO Rep*, e51120, doi:10.15252/embr.202051120 (2021).

8. Acknowledgements

First and foremost, I would like to thank my supervisor, Sergio P. Acebrón, for leading me through this project, supporting me from the beginning until the end, providing me with inspiration, bringing in new perspectives, helping me out when I was stuck, motivating me and being always accessible for my questions, doubts, and ideas. Without you and the supportive working atmosphere you created, I couldn't have made it through the PhD, completed my thesis and published such a nice paper!

Secondly, I thank my TAC members Thomas Holstein and Holger Bastians for introducing new ideas, points of view and approaches, disclosing ground for new discussions and leading my project forward. In the course if this, I thank especially Holger Bastians and his group for the great collaboration, input on our project, fruitful discussions, help with novel methods as well as his personal support and advice, whenever I faced uncertainty or questions.

Furthermore, I would like to thank Ulrike Engel and the whole Nikon Imaging Center for their great support and advice. Thanks to Ulrike for showing me all the equipment, elaborating the imaging procedures for my project, giving me advice whenever needed and staying with me until late at night in the microscope room to make the imaging running.

Moreover, I thank the whole Acébron Lab for their amazing mental and scientific support! Thanks to you, I enjoyed coming to the lab every day and knew that there was always somebody to raise me up and help me, when I was down. You made even the darkest days shine. Therefore, thank you for your advice and the fun, unforgettable moments we had during our lab outings, barbecues, coffee breaks or simply when hanging out in the lab. You are on fire! In line with this, I would like to thank the whole 6th floor. Thank you for the nice atmosphere, the lab breakfasts, the lunch breaks, the cake hours and that there was always a friendly face and ear around, to whom I could turn to, when I needed someone. The PhD would have only been half as fun as it was with you!

Finally, I would like to thank my whole family and my boyfriend for supporting me. Thank you to my parents and sister for always standing behind me, encouraging me and raising me up! Thank you to my grandparents for pushing me forward and motivating me! And a big thank you to my boyfriend for being there for me, calming me down, taking my mind off things and backing me up, whenever needed!

I owe all of you a lot for taking me through the last years and shaping me as the person I am. Without you, I wouldn't be where I am today!